EEG Topographic Changes in Opioid Use Disorder

by

Christopher Minnerly

A Thesis Submitted to the Faculty of

Charles E. Schmidt College of Medicine

In Partial Fulfillment of the Requirements for the Degree of

Master of Science

Florida Atlantic University

Boca Raton, FL

May 2020

EEG Topographic Changes in Opioid Use Disorder

by

Christopher Minnerly

This thesis was prepared under the direction of the candidate's thesis advisor, Dr. Rui Tao, Department of Biomedical Science, and has been approved by the members of his supervisory committee. It was submitted to the faculty of the Charles E. Schmidt College of Medicine and was accepted in partial fulfillment of the requirements for the degree of Master of Science.

SUPERVISORY COMMITTEE:

Rui Tao
Rui Tao (Apr 23, 2020)

Rui Tao, PhD
Thesis Advisor

Steven L. Bressler
Steven L. Bressler (Apr 28, 2020)

Steven Bressler, PhD

Howard M. Prentice
Howard M. Prentice (Apr 29, 2020)

Howard Prentice, PhD

Jangyenwu
Jangyenwu (Apr 29, 2020)

Jang-Yen Wu, PhD

Janet Robishaw
Janet Robishaw (May 3, 2020)

Janet Robishaw, PhD
Chair, Department of Biomedical Science

Phillip M. Boiselle
Phillip M. Boiselle (May 4, 2020)

Phillip M. Boiselle, MD
Dean, Charles E. Schmidt College of Medicine

Robert W. Stackman Jr., PhD
Dean, Graduate College

May 4th, 2020

Date

Acknowledgements

The authors would like to thank FHE Health (Deerfield Beach, FL) for granting permission to utilize their data for this study. We extend our gratitude to the following individuals in the NeuroRehabilitation department that collected and sorted the data, making our work much more streamlined: Dr. Karen Dodge; Dr. Nicholas Dogris; Dr. Rachael Bishop; Kara Harris; Charles Blackmon; Michele Stoehr; Leila Alami; and Amanda Nephew.

We additionally want to thank Dr. Ximena Levy for her knowledge and assistance in IRB procedures and Jeffrey Clark for his assistance in IT support, both of whom are staff at Florida Atlantic University.

Abstract

Author: Christopher Minnerly

Title: EEG Topographic Changes in Opioid Use Disorder

Thesis Advisor: Dr. Rui Tao, Ph.D

Institution: Florida Atlantic University

Degree: Master of Science

Year: 2020

The present study aimed at quantifying the topographic distribution of spectral power as measured with electroencephalogram (EEG) in patients with opioid use disorder (OUD) across five broad band frequencies (δ, θ, α, β, and γ). Through comparative groups of healthy controls, patients with methamphetamine use disorder, and patients with alcohol use disorder, it was determined that OUD EEG spectral power was globally increased in the δ frequency, and more region-specific in others (frontal lobes in θ and β frequencies). α frequency was reduced in occipital lobes in OUD. The observed changes are discussed in terms of the microcircuit-level changes in the cortex. Based on these findings, EEG may prove to be a valuable tool for diagnostic and prognostic evaluation of OUD.

EEG Topographic Changes in Opioid Use Disorder

Tables

Figures

Nomenclature

AMPA – α-amino-3-hydroxy-5-methyl-4-isoxazolepropionic acid glutamate receptor

AUD – alcohol use disorder

cAMP – cyclic adenosine monophosphate

CNS – central nervous system

DAT – dopamine transporter

DOR – delta opioid receptor

EEG – electroencephalography

FFT – fast Fourier transform

fMRI – functional magnetic resonance imaging

GABA – γ-aminobutyric acid

GCPR – G-coupled protein receptor

GDP – guanosine diphosphate

GIRK – G protein-coupled inwardly rectifying K^+ channel

GTP – guanosine triphosphate

OUD – opioid use disorder

KOR – kappa opioid receptor

MOR – mu opioid receptor

MUD – methamphetamine use disorder

NAC – nucleus accumbens

NMDA – *N*-methyl-D-aspartate glutamate receptor

ORL-1 – opioid receptor like-1

PAG – periaqueductal gray of the midbrain

PET – positron emission tomography

PNS – peripheral nervous system

RVM – rostral ventromedial nucleus of the medulla oblongata

SUD – substance use disorder

VMAT2 – vesicular monoamine transporter

VTA – ventral tegmental area

1. Introduction

1.1 History of opioids and synthetic opioids

Since opium was first extracted from the poppy plant (*Papaver somniferum*) in Mesopotamia (modern day Southwest Asia) and surrounding regions thousands of years ago, exogenous opioids have been used to treat pain in humans [see reviews; (Rosenblum et al., 2008; Askitopoulou, Ramoutsaki, & Konsolaki, 2002)]. During the early 19th century, morphine was extracted from opium and became the first commercially-available opioid for pain relief (Rosenblum et al., 2008). A few decades later, codeine was extracted from opium and was used as a cough suppressant (Rosenblum et al., 2008). By the late 19th century, on the search for new opioids to mass produce, chemists first synthesized diamorphine (heroin) (Jones et al., 2018). Since the start of the 20th century, other synthetic opioids have been created. In the United States (US), methadone, oxycodone, and hydrocodone are among the most abundantly distributed (Meldrum, 2016). Newly synthesized opioids, such as fentanyl and its analogs (Frisoni et al., 2018; Karila et al., 2018) have begun to flood the streets of the US and are causing deaths at alarming rates.

It isn't difficult to imagine the impact such synthetic opioids can have on the body, especially given that fentanyl is 50 times more potent than morphine (Vardanyan & Hruby, 2014). See Figure 1 for the chemical structure for some of the commonly abused opioids.

1.2 Rates of affliction in opioid use disorder

The opioid epidemic in the US has hit an all-time high in recent years, with rates of affliction exponentially increasing. In 2016, an estimated 12 million people used opioids for a variety of purposes and approximately 2.1 million of those individuals suffered from opioid use disorder (SAMSHA, 2017). By 2017, that number was closer to 2.4 million people in the US (NIDA, 2019). With nearly a 4-fold increase in unintentional opioid-related overdose deaths between 1999 and 2017 (Hedegaard, Warner, & Miniño, 2018), the opioid epidemic is projected to become progressively worse in the years to come (NIH, 2017).

Understanding how the brain is affected by opioid use is a crucial step in battling the opioid epidemic. Before opioid use disorder (OUD) is discussed, we must first discuss the pain response and the opioid systems of the body.

1.3 Pain Pathway

The perception of pain (nociception) involves various structures in the central (CNS) and peripheral nervous systems (PNS), including the thalamus, the periaqueductal gray of the midbrain (PAG), rostral ventromedial of the medulla oblongata (RVM), and the dorsal horn of the spinal cord, among others (Patestas & Gartner, 2016; Purves, Augustine, & Fitzpatrick, 2001).

Nociceptors are sensory neurons that are found throughout the body and have free nerve endings that are activated by noxious mechanical, chemical, or thermal stimuli (Al-Hasani & Bruchas, 2011; Purves, Augustine, & Fitzpatrick, 2001). A pain signal and its modulation are conducted via the ascending pathway and the descending pathway, respectively. The ascending or afferent pathway carries a pain signal along Aδ and C

axonal fibers towards the CNS (Patestas & Gartner, 2016; Purves, Augustine, & Fitzpatrick, 2001). Aδ fibers are myelinated and carry signals quickly, producing pain which is perceived as sharp or pricking (Patestas & Gartner, 2016; Purves, Augustine, & Fitzpatrick, 2001). C fibers are non-myelinated and conduct signals much more slowly, producing pain which is perceived as dull or aching (Patestas & Gartner, 2016; Purves, Augustine, & Fitzpatrick, 2001).

From the first order nociceptor, the signal is transduced via the dorsal root ganglion to the second order neurons of the dorsal horn of the spinal cord. Depending on the type of stimuli, the signal is conducted to respective layers of grey matter, called Rexed laminae (Rexed, 1954). Aδ and C fibers mostly innervate neurons in laminae I and II (Patestas & Gartner, 2016), which then transmit this information to laminae IV, V, and VI (Patestas & Gartner, 2016). From there, the signal decussates and crosses to the contralateral side of the spinal cord, ascending via the spinothalamic pathway or the spinoreticular pathway (Patestas & Gartner, 2016).

The spinothalamic pathway carries the signal to the RVM and then to the third order neurons of the ventral posterolateral nucleus of the thalamus (Patestas & Gartner, 2016). From the thalamus, the ipsilateral signal is then terminated in the primary somatosensory cortex (Patestas & Gartner, 2016). This pathway is responsible for the sensation and localization of pain (Patestas & Gartner, 2016).

The other ascending pathway, the spinoreticular pathway carries the signal from the spinal cord to the medullary-pontine reticular system and from there, to the intralaminar nuclei of the thalamus. This pathway is responsible for arousal/alerting of the pain and plays a role in the emotional response to the pain (Patestas & Gartner, 2016).

The descending or efferent pathway of the pain response carries signals from the cortex to the PAG, RVM, and locus coeruleus of the pons, which then activate opioid receptors in these target regions. The release and binding of endogenous opioids in this pathway cause an inhibitory response which is conducted to the dorsal horn of the spinal cord (Al-Hasani & Bruchas, 2011). The result is a reduced pain response or anti-nociception. See Figure 2 for a simplified diagram of the pain response.

In order to study opioids, scientists first had to understand the structures and functions of their natural receptors in the body. This understanding led to the discovery of the natural opioids produced by the body.

1.4 Opioid receptors

Opioid receptors are transmembrane G-coupled protein receptors (GCPRs), which are inhibitory (Dascal & Kahanovitch, 2015). The G protein is located on the intracellular side of the membrane, consisting of three subunits (α, β, and γ). In the inactive state, the G protein is located near the GCPR and has a molecule of guanosine diphosphate (GDP) bound to the α subunit (Dascal & Kahanovitch, 2015; Al-Hasani & Bruchas, 2011). When the ligand (opioid) binds to the extracellular surface of the receptor, a cascade of cellular changes occurs.

First, the GCPR undergoes a conformational change in which the receptor and the G protein briefly form a protein complex (Dascal & Kahanovitch, 2015; Al-Hasani & Bruchas, 2011). This activates the α subunit of the G protein, which dissociates its GDP molecule and binds a guanosine triphosphate (GTP) molecule. Next, the α subunit dissociates from the other two subunits and binds to adenylate cyclase, which in turn

inhibits production of cyclic adenosine monophosphate (cAMP), among other intracellular targets (Dascal & Kahanovitch, 2015; Al-Hasani & Bruchas, 2011).

The new β-γ dimer protein binds to various targets, such as phospholipases and protein kinases (Dascal & Kahanovitch, 2015; Al-Hasani & Bruchas, 2011). In addition, the β-γ dimer protein binds to G protein-coupled inwardly rectifying K^+ (GIRK) channels (Dascal & Kahanovitch, 2015; Al-Hasani & Bruchas, 2011). When these channels are activated, the efflux of K^+ out of the cell increases and in turn, the membrane potential becomes hyperpolarized (Dascal & Kahanovitch, 2015; Al-Hasani & Bruchas, 2011). This change in membrane potential reduces the influx of Ca^{2+}, which inhibits the release of neurotransmitters from the pre-synaptic neuron (Dascal & Kahanovitch, 2015; Al-Hasani & Bruchas, 2011). See Figure 3 for a simplified diagram of opioid receptors.

To date, four main types of opioid receptors have been identified in the human body: mu (MOR), kappa (KOR), delta (DOR), and opioid receptor like-1 (ORL-1) (Al-Hasani & Bruchas, 2011). The MOR is the main receptor subtype that is affected by opioids. Its activation is generally associated with analgesic effects, as well as euphoria and pleasure, which is believed to help create the addictive state of individuals who use opioids on a regular basis (Levashova & Myagkova, 2018; Al-Hasani & Bruchas, 2011). The DOR has been shown to produce similar effects of MOR agonism regarding modulation of the pain response (Al-Hasani & Bruchas, 2011) but with less impact on euphoria and systemic physiological changes, such as respiratory depression (Pradhan et al., 2011). The KOR is believed to be a regulatory opioid receptor subtype (Al-Hasani & Bruchas, 2011). Although KOR activation can provide some antinociceptive affects (Pradhan et al., 2011), during withdrawal, KOR activation can cause dysphoria and

anhedonia, among other “negative” side effects (Chavkin & Koob, 2016). The ORL-1 is the least understood opioid receptor subtype of the four. Since its discovery in the 1990s (Meunier et al., 1995; Reinscheid et al., 1995), it has been studied immensely. It is now believed to play a role in regulating opioid response, in that it blocks the anti-nociceptive properties of opioids and can even exacerbate the pain response (Levashova & Myagkova, 2018; Meunier et al., 1995).

The distribution of opioid receptors in the human body has been elucidated and confirmed using an absolute quantitative real-time polymerase chain reaction (Peng & Chang, 2012). MOR has been found in various structures throughout the body such as the cerebellum, nucleus accumbens, caudate nucleus, dorsal root ganglion, spinal cord, adrenal gland, pancreas, and small intestine (Peng & Chang, 2012). Likewise, KOR has been found in many of the same tissues (Peng & Chang, 2012). DOR on the other hand, is found not only in the tissues listed previously but also in the thymus, lung, and heart as well (Peng & Chang, 2012). ORL-1 receptors have been found in various structures of the brain, as well as the peripheral nervous system (Levashova & Myagkova, 2018; Meunier et al., 1995; Reinscheid et al., 1995).

1.5 Endogenous opioids in the human body

Along with the opioid receptors, various endogenous opioids have been identified in the human body. In general, endogenous MOR agonists are endorphins and endomorphines (Levashova & Myagkova, 2018). Endogenous DOR agonists are enkephalins (Levashova & Myagkova, 2018; Lay et al., 2016). Endogenous KOR agonists are dynorphins (Levashova & Myagkova, 2018; Chavkin & Koob, 2016).

Finally, the endogenous ORL-1 agonist is orphanin FQ/nociceptin (Meunier et al., 1995; Reinscheid et al., 1995).

1.6 Mesocorticolimbic pathway

Opioid use has been shown to affect the "natural reward" pathway in the brain, which comprises a circuit of the ventral tegmental area (VTA) of the midbrain and the ventral striatum (olfactory tubercle and nucleus accumbens), as well as the pre-frontal cortex (Russo & Nestler, 2013; Jalabert et al., 2011; Nestler & Malenka, 2004; Wise, 1996). The VTA contains various neuron subtypes including dopaminergic neurons, GABAergic interneurons, and glutamatergic neurons, whereas the nucleus accumbens contains GABAergic medium spiny neurons (Jalabert et al., 2011). In general, the VTA sends excitatory dopaminergic efferents to the nucleus accumbens and the pre-frontal cortex. The nucleus accumbens reciprocates with inhibitory GABAergic efferents back to the VTA (Russo & Nestler, 2013; Jalabert et al., 2011).

Although MORs can be found in both the VTA and ventral striatum (Charbogne et al., 2017; Madhavan, Bonci, & Whistler, 2010), they both play different roles in the formation and maintenance of addictive properties. Within the VTA, GABAergic interneurons project onto dopamine neurons and when opioids are introduced, binding to MORs disinhibits this GABAergic activity on the dopamine neurons (Johnson & North, 1992).

In chronic opioid use, however, the interneuron projections are potentiated, thus reducing dopaminergic afferents (Madhavan, Bonci, & Whistler, 2010). This pathway has been shown to be a primary mediator for opioid reward, analgesia, and opioid withdrawal (Heshmati & Russo, 2015; Russo & Nestler, 2013). On the other hand, the pathway from

the nucleus accumbens to the VTA has been shown to mediate motivation for opiates (Charbogne et al., 2017). This strong drive for opioids leads to a state of addiction, with physical dependence and mental disorders associated with it.

1.7 Diagnosis of opioid use disorder

Opioid use disorder (OUD), a complex mental disorder, is often diagnosed with psychiatric evaluation based on the fifth edition of the *Diagnostic and Statistical Manual of Mental Disorders* [DSM-5; (APA, 2013)]. Currently, OUD is diagnosed based on clinical criteria, such as cravings for opioids, physical dependence on opioids, and withdrawal symptoms without opioids (APA, 2013). However, new approaches to diagnosis are being sought due to poor patient reliability and lack of training from physicians (Wakeman et al., 2016; Rosenblatt et al., 2015). Unfortunately, patients often present with polysubstance abuse (Connor et al., 2014) or comorbid psychiatric illness (Brooner et al., 1997), making evaluations even more challenging.

1.8 Neuroimaging in opioid use disorder

Neuroimaging studies over several decades, have given us better insight to the functionality and connectivity of the areas of the brain being affected by substance abuse [see reviews; (Cabrera et al., 2016; Ieong & Yuan, 2017)]. Some of the leading methods include positron emission tomography [PET; (Gatley et al., 2005; Mena et al., 2005)], functional magnetic resonance imaging (fMRI), and electroencephalography [EEG; (Ieong & Yuan, 2017)]. Although each technique has its strengths, there are limitations to consider as well [see review; (Camprodon & Stern, 2013)]. PET and fMRI have high spatial resolution as compared to EEG, however, they lack in temporal resolution (Xue et al., 2010). EEG and fMRI are non-invasive, but PET requires the use of injecting a

radioactive isotope into the bloodstream during the recording process (Gatley et al., 2005). Perhaps the most important factors to consider, are the costs associated with each technique, as EEG is by far the most cost-effective (Camprodon & Stern, 2013). With many questions still unanswered about OUD and for the reasons mentioned above, EEG may be the most applicable neuroimaging technique to use in a clinical setting.

1.9 EEG theory

The human neocortex is organized into six distinct layers (*I-VI*) with functional neuronal circuit assemblies, referred to as cortical microcircuits (Nelson, 2002; Vegue, Perin, & Roxin, 2017). These microcircuits are composed of excitatory and inhibitory cells that work together to accomplish a myriad of cortical functions (Nelson, 2002; Vegue, Perin, & Roxin, 2017). In general, EEG utilizes electrodes placed on the scalp to record the activity being produced from the abundant pyramidal neurons in the cortex down to layers *III*, *IV*, and *V* (Hari & Parkkonen, 2015; Thompson & Thompson, 2015; Tatum, 2014). The post-synaptic potentials of dense collections of pyramidal neurons summate to produce the electrical field measured at the scalp (Tatum, 2014; Hari & Parkkonen, 2015; Thompson & Thompson, 2015). This is due to the changes in polarity created by the excitatory post-synaptic potentials of these pyramidal cells at the extracellular surface. The negative polarity (called a *sink*) is measured at the superficial end of the cell and the positive polarity (called a *source*) is measured at the deep end of the same cell (Tatum, 2014; Hari & Parkkonen, 2015; Thompson & Thompson, 2015). See Figure 4 to see the flow of current at an active synapse. The difference between the sink and the source at the active synapse creates the field potential measured as a dipole in the EEG recording. The received potentials are processed through an amplifier and

digitized to a computer screen using Fourier transforms to show the signals in real time (Tatum, 2014).

1.10 Oscillations in EEG

The interactions within the cortical microcircuits are responsible for the oscillations that EEG interprets. For example, if pyramidal neurons become activated, they summate to produce a large increase in excitation within the microcircuit. This in turn, activates GABAergic interneurons within the microcircuit, which inhibit many of the pyramidal neurons. The changes in excitation and inhibition are what create oscillations (Tatum, 2014; Kepecs & Fishell, 2014). These oscillations are measured as broad-range frequency bands, in hertz (Hz) or cycles per second. The five major frequency ranges are delta (1-4 Hz; δ), theta (4-8 Hz; θ), alpha (8-12 Hz; α), beta (12-30 Hz; β), and gamma (>30 Hz; γ). See Figure 5 for examples of these common waveforms.

1.11 Microcircuits

Although pyramidal cells are the main excitatory neurons found in the cortex (Jiang et al., 2015), the inhibitory interneurons that comprise a microcircuit have a variety of morphologies and functions that are designed to modulate the activity of the abundant pyramidal cells (Kepecs & Fishell, 2014). For instance, studies have shown there to be over a dozen distinct interneuron subtypes in the cortex (Markram et al., 2004; Jiang et al., 2015). The most common inhibitory interneuron types include cells that express and bind somatostatin (SOM), parvalbumin (PAL), and vasointestinal protein (VIP) (Markram et al., 2004). These cells are found in various layers of the cortex and interact with different regions of a given pyramidal cell (ie., dendrite vs. soma vs. axon) (Markram et al., 2004; Kepecs & Fishell, 2014). Additionally, microcircuits in a given

region of the cortex may vary greatly in the cytoarchitectural interactions therein. For example, the prefrontal cortex of the frontal lobe primarily contains PV- and SOM-expressing interneurons (Kvitsiani et al., 2013). The primary motor cortex also contains PV- and SOM-expressing interneurons (Yang, Murray, & Wang, 2016). The primary visual cortex of the occipital lobe (Ko et al., 2013; Pfeffer et al., 2013), as well as the auditory cortex of the temporal lobe (Blackwell & Geffen, 2017) contain cells that express all three major subtypes (PV, VIP, SOM). The connectivity and interactions of these cells differ in all the above-mentioned regions (Markram et al., 2004; Kepecs & Fishell, 2014; Jiang et al., 2015; Harquel et al., 2016). See Figure 6 for a typical microcircuit found in the brain.

1.12 EEG and opioid use disorder

OUD can be assessed with EEG, which reflects spatial and temporal activities of cortical microcircuits, consisting of pyramidal glutamatergic neurons, GABAergic interneurons, and subcortical inputs [(Rosch et al., 2018); also see a review by Cohen (Cohen, 2017)]. Opioids such as morphine and heroin, exert their neurological effects mainly through the activation of μ-opioid receptors that reside almost exclusively on GABAergic neurons (Taki et al., 2000; Huo et al., 2005). The μ-opioid receptors are functionally coupled with G protein-gated inwardly rectifying K^+ (GIRK) channels (Huo et al., 2005). When GIRK channels are activated, the GABAergic neurons become hyperpolarized and the net result is a decrease in amplitude of inhibitory postsynaptic potentials [IPSPs; (Svoboda & Lupica, 1998; Yokota et al., 2016)]. Thus, EEG activity is increased when GABAergic neurons in the cortical microcircuits are disinhibited with opioids (Louvel et al., 2001). Additionally, the underlying microcircuits receive afferent

innervations from neurons of deep brain nuclei, which are regulated by opioids on GABAergic neurons (Svingos et al., 2001). As a result, acute opioid administration causes a reduction of EEG spectral power at δ, θ, α, and β oscillations in drug-naïve humans (Graversen et al., 2010; Montandon et al., 2016) and in experimental rodents (Sun et al., 2006). However, long-term opioid administration causes an impairment of GIRK channels with the result of GABAergic hyperfunction (Chen et al., 2000; Meye et al., 2012). Furthermore, the impairment of GABAergic function is associated with opioid dependence (Assadi et al., 2003). See Figure 7 for the pharmacodynamics of opioid use in GABAergic cells.

1.13 EEG spectral analysis

An EEG power spectrum is the result of a Fourier-transformed frequency by voltage analysis (Tatum, 2014). EEG spectral power, including δ, θ, α, and β oscillations, have been found to be topographically altered across the frontal, central, temporal, parietal, and occipital cortices in individuals with OUD. For instance, Wang reported equal increases of δ, θ, α, and β powers in all 5 cortical regions (Wang et al., 2015). Motlagh showed that β oscillations, but not δ, θ, nor α, were increased in OUD patients (Motlagh et al., 2018). Thus, although there is no doubt that EEG spectra are altered or reorganized in one way or another following chronic use of opioids, it appears that there is no consensus of observations among investigators [see reviews; (Fingelkurts et al., 2006; Ieong & Yuan, 2017)].

1.14 Aims of the study

The goal of the present study is to quantitatively determine spectral power of EEG oscillations (e.g., δ, θ, α, β, and γ) in the frontal, central, temporal, parietal, and occipital

areas in individuals with OUD. As a means of evaluating if the observed changes are drug-specific, comparative groups of methamphetamine abusers, alcohol abusers, and healthy controls will be used. Spectral power changes (based on percentage) will be arbitrarily classified into four levels: high (>60%), medium (36-60%), low (16-35%), and no effect (<15%). Based on those power levels, the activity of δ, θ, α, β, and γ oscillations was topographically mapped in relation to the electrodes placed on the scalp. This approach of data analysis may be used to identify high-activity electrodes by which the mental status in patients with OUD is reliably assessed.

1.15 Methamphetamine use disorder and the dopaminergic system

As means of determining if the observed effects are specific to OUD, cases of methamphetamine use disorder (MUD) were used as a negative control. Pharmacologically, methamphetamine has been shown to act on several neurotransmitter systems (norepinephrine, serotonin, and dopamine) but here, the focus will be on the dopaminergic system. The dopaminergic system, which consists of five G protein-coupled receptor subtypes, is located throughout various regions of the cortex and sub-cortical regions (Park et al., 2011). Of the five dopamine receptor subtypes, D1 and D5 (D1-like class) are considering excitatory, while D2, D3, and D4 (D2-like class) are considered inhibitory (Vallone, Picetti, & Borrelli, 2000; Jackson, & Westlind-Danielsson, 1994). Methamphetamine has been reported to affect the dopamine transporter (McCann et al., 2008; Johanson et al., 2006) and the vesicular monoamine transporter (Sulzer et al., 2005), as well. The dopamine transporter (DAT) is a presynaptic membrane-bound protein that facilitates the reuptake of dopamine in the synaptic cleft (McCann et al., 2008; Johanson et al., 2006). The vesicular monoamine

transporter (VMAT2) is found inside the cell and facilitates the reuptake of catecholamines (such as dopamine) from the cytoplasm to the vesicles for repackaging (Sulzer et al., 2005; Fleckenstein & Hanson, 2003).

1.16 Mesocorticolimbic pathway revisited

D1 receptors are mostly found in the striatum; distributed throughout the caudate nucleus, putamen, olfactory bulb, and NAC (Lud Cadet et al., 2010). Among other areas, D2 receptors are also found throughout the striatum, as well as in the VTA (Beaulieu & Gainetdinov, 2011). DAT and VMAT2 are found throughout the same regions. Although mechanisms have not been fully elucidated, cell cultures studies have shown that methamphetamine causes the release of dopamine through DAT and VMAT2 systems (Pifl et al., 1995) and without them, dopamine release is reduced in rodents (Jones et al., 1998). Further, dependence on methamphetamine reduces DAT activity, shown by a reduction of the density of DAT in sub-cortical areas of the brain in humans (Volkow et al., 2001). Work by Park et al., (2011) revealed that genetic knock-out of MORs in mice, created a reduction in D1 receptor binding in the striatum, as well as a reduction of methamphetamine-related addictive behavior. This suggests methamphetamine may additionally act on the dopaminergic system via MORs (and possible other opioid receptors).

1.17 Methamphetamine and EEG

Given the differences in clinical presentation and the above-mentioned mechanisms of action, MUD should differ in terms of EEG activity as compared to OUD. One study utilized the dopamine receptor agonist, apomorphine to produce methamphetamine-like changes in EEG (Jang et al., 2009). As revealed therein, rats that

were treated acutely revealed a decrease in power in δ and β frequencies, especially in the frontal lobe (Jang et al., 2009) but, rats that were treated chronically revealed increases in power in the α and θ frequencies, especially in the frontal lobe (Jang et al., 2009).

As previously seen, MUD in humans has been linked to an increase in power in the δ and θ frequencies (Newton et al., 2003) and a decrease in α, β, and, γ frequencies (Zanettini et al., 2018).

1.18 Alcohol use disorder

Ethanol, referred to as *alcohol* here forward, is the psychoactive compound that has been used recreationally across cultures for thousands of years. The maladaptive over-consumption of alcohol leads to alcoholism and what is now referred to as alcohol use disorder [(AUD) DSM 5; APA, 2013]. Here, AUD cases were also used as a negative control to compare to the OUD group. Knowing the molecular mechanisms of AUD will help shed light onto the effects seen in the EEG.

1.19 Alcohol and glutamate

Studies suggest acute alcohol administration in the body reduces glutamate activity by antagonizing *N*-methyl-D-aspartate (NMDA) and α-amino-3-hydroxy-5-methyl-4-isoxazolepropionic acid (AMPA) receptors (Dildy-Mayfield & Harris, 1995), while chronic alcohol administration appears to do the opposite, upregulating glutamatergic activity via NMDA (Qiang & Ticku, 2005). Furthermore, NMDA receptors of parvalbumin-expressing interneurons are implicated in the modulation of alcohol dependence. When this receptor is lacking in this cell type, self-administration of alcohol is reduced in mice (Radke et al., 2017).

1.20 Alcohol and GABA

Alcohol has been found to affect GABAa receptors. When a ligand binds to the GABAa receptor, chloride is released and causes inhibition of the post-synaptic cell. Acute alcohol administration brings about agonistic properties of GABAa (see a review by Lobo & Harris, 2008). However, in the case of chronic alcohol administration, GABAa receptors appear to be downregulated in human subjects (Lewohl et al., 1997). The slow-acting, metabotropic GABAb receptor is also affected the same way as GABAa receptors, in which acute and chronic exposure increase and decrease inhibition, respectively (Federici et al., 2009; Frye et al., 1991).

1.21 Alcohol and dopamine

Like all substances of abuse, alcohol also affects the dopaminergic system in the brain. Acute alcohol administration leads to an increase in activation of the dopaminergic system in rats (see reviews by Koob & Volkow, 2010, 2016), while chronic alcohol exposure leads to a decrease in dopaminergic activation and an increase in DAT function in rats (Rothblat et al., 2001). Chronic alcohol exposure produced the same effects in humans, with a decrease in dopamine activation via D2 receptor hypofunction (Volkow et al., 2007).

1.22 Alcohol in EEG

In total, these combined effects should reveal that AUD facilitates excitatory activity in the brain. Thus, the power spectra of the alcohol-dependent group should be increased as compared to the healthy group. EEG studies of alcoholics have revealed inconsistent differences as compared to healthy control subjects. Some have reported decreased α power (Courtney & Polich, 2010), whereas others have reported increased β

power (Rangaswamy et al., 2002; Saletu-Zyhlarz et al., 2004) and decreased δ power (Saletu-Zyhlarz et al., 2004).

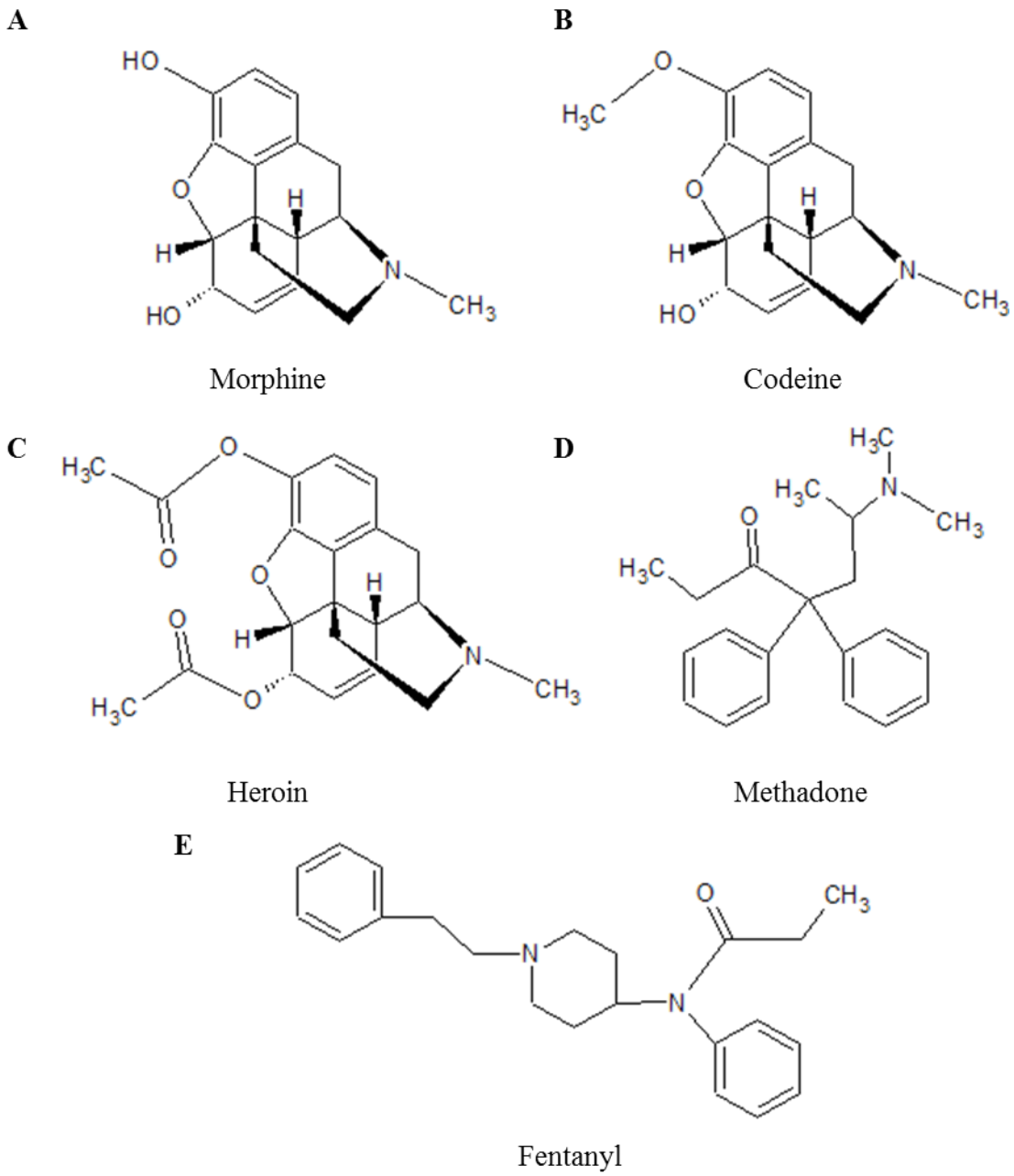

Figure 1: Chemical structures of common opioids. (A) The chemical structure for the naturally-occurring opioid, morphine. (B) The chemical structure for the naturally-occurring opioid, codeine. (C) The chemical structure for the synthetic opioid, diamorphine also known as heroin. (D) The chemical structure for the synthetic opioid, methadone. (E) The chemical structure for the synthetic opioid, fentanyl.

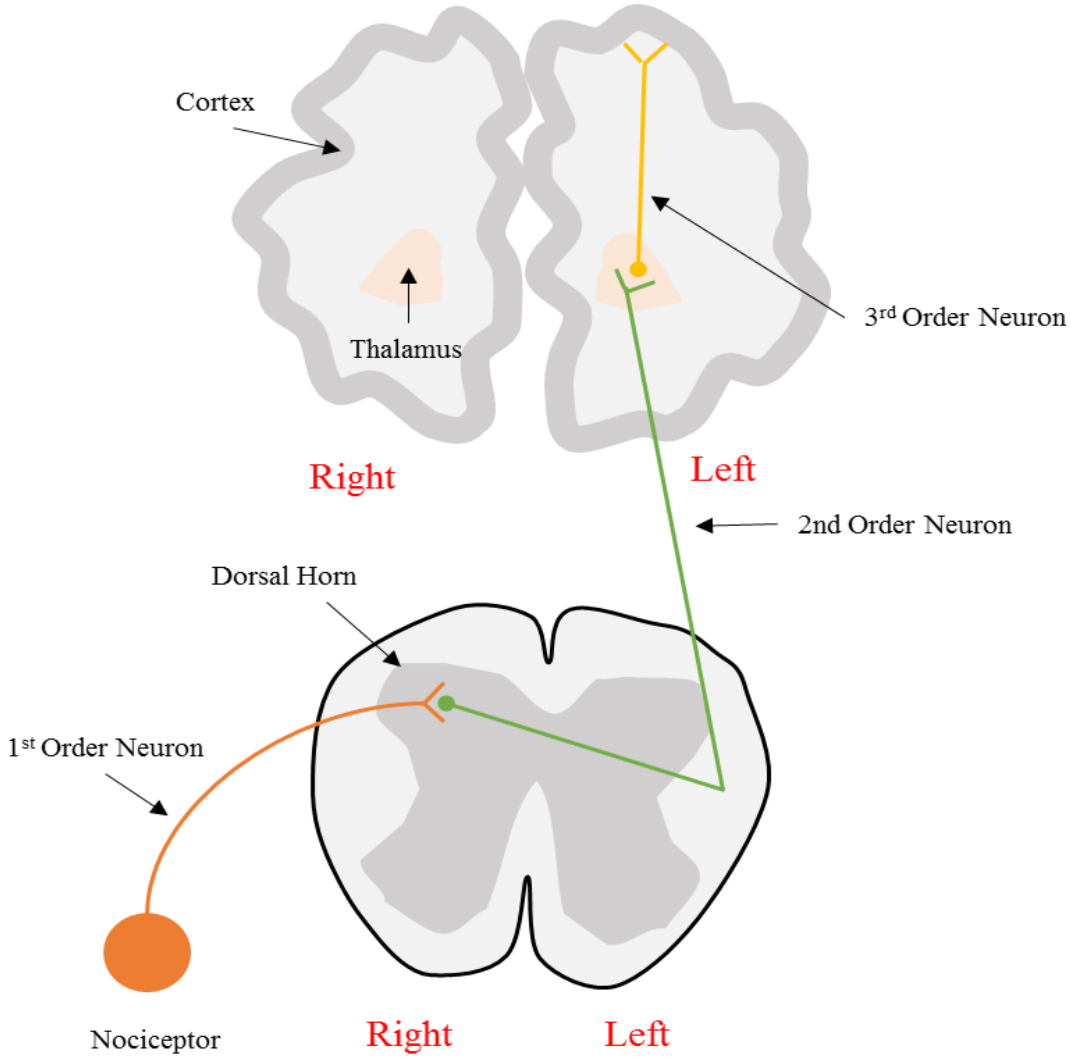

Figure 2: Simplified diagram of the ascending pain pathway. When a painful stimulus is detected by a nociceptor in the peripheral nervous system, the associated free nerve ending or 1st order neuron, sends a signal to the ipsilateral dorsal root ganglion in the dorsal horn of the spinal cord. Then, the signal is carried via the 2nd order neuron, decussating to the contralateral spinal cord, and ascending to the thalamus in the central nervous system. From the thalamus, a 3rd order neuron sends the signal to the somatosensory cortex of the brain, where the pain signal then gets processed further.

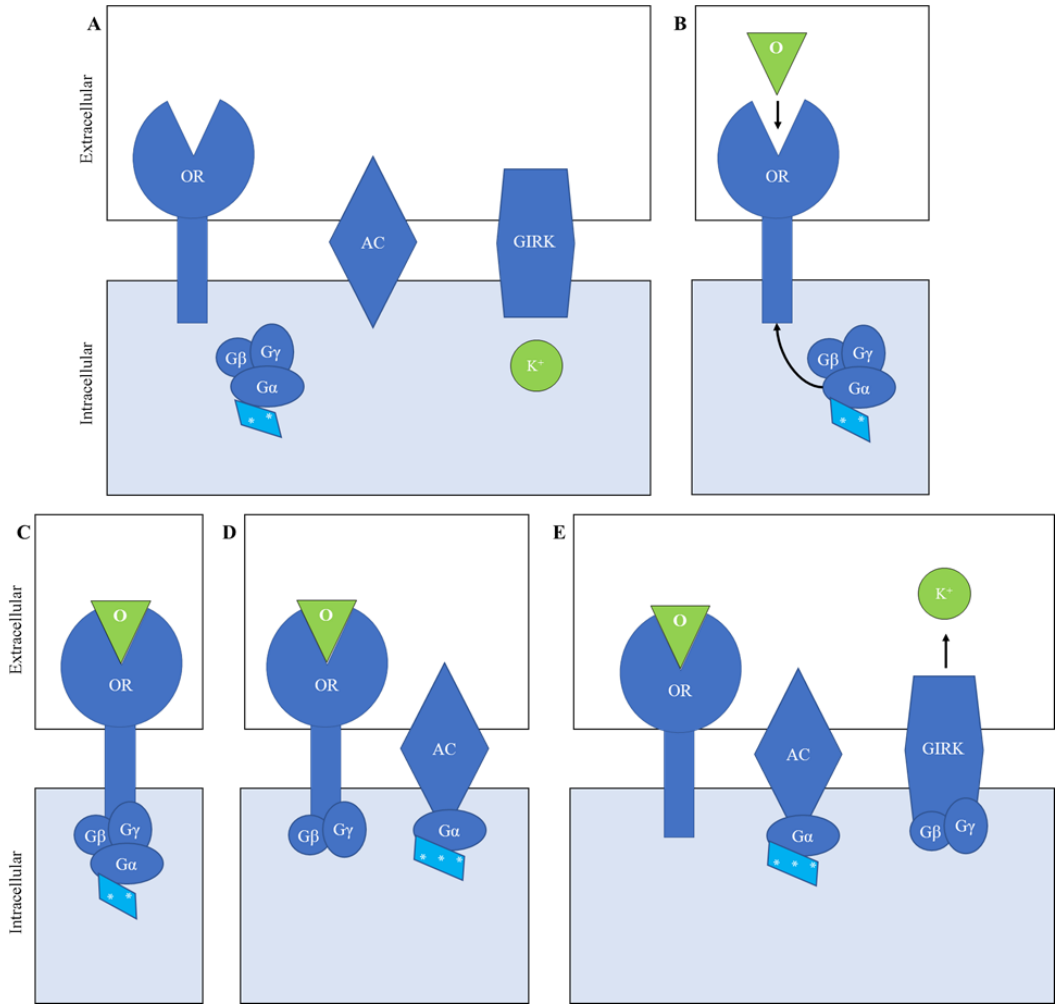

*Figure 3: Simplified diagram of a transmembrane-bound opioid receptor. (A) The opioid receptor in the inactive state. (B) The opioid receptor just before a ligand (opioid) binds to the extracellular surface. (C) With the ligand bound to the opioid receptor, the G protein complex binds to the intracellular surface of the opioid receptor. (D) The G protein undergoes a conformational change, with the alpha subunit dissociating from the beta and gamma subunits, and then binding to adenylate cyclase. (E) The beta and gamma subunits of the G protein dissociate from the opioid receptor and bind to a GIRK channel, resulting in K^+ efflux. Please note: OR, opioid receptor; O, opioid; AC, adenylate cyclase; GIRK, G protein-coupled inwardly rectifying K^+ channel; Gα, alpha subunit of G protein; Gβ, beta subunit of G protein; Gγ, gamma subunit of G protein; **, guanosine diphosphate (GDP); ***, guanosine triphosphate (GTP).*

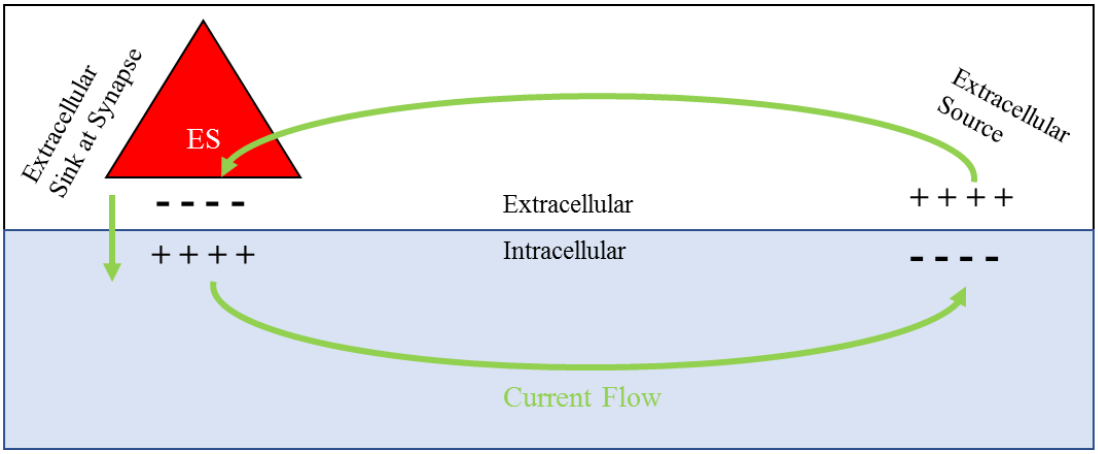

Figure 4: Simplified diagram of current flow at an active synapse in the cortex. The red triangle, labeled "ES" is an excitatory synapse on the extracellular surface. As this cell fires, current flows from the extracellular side to the intracellular side. This creates an extracellular sink at the site of the synapse. As the current flows down the membrane, the intracellular side becomes more negative, which in turn creates an extracellular source down the membrane.

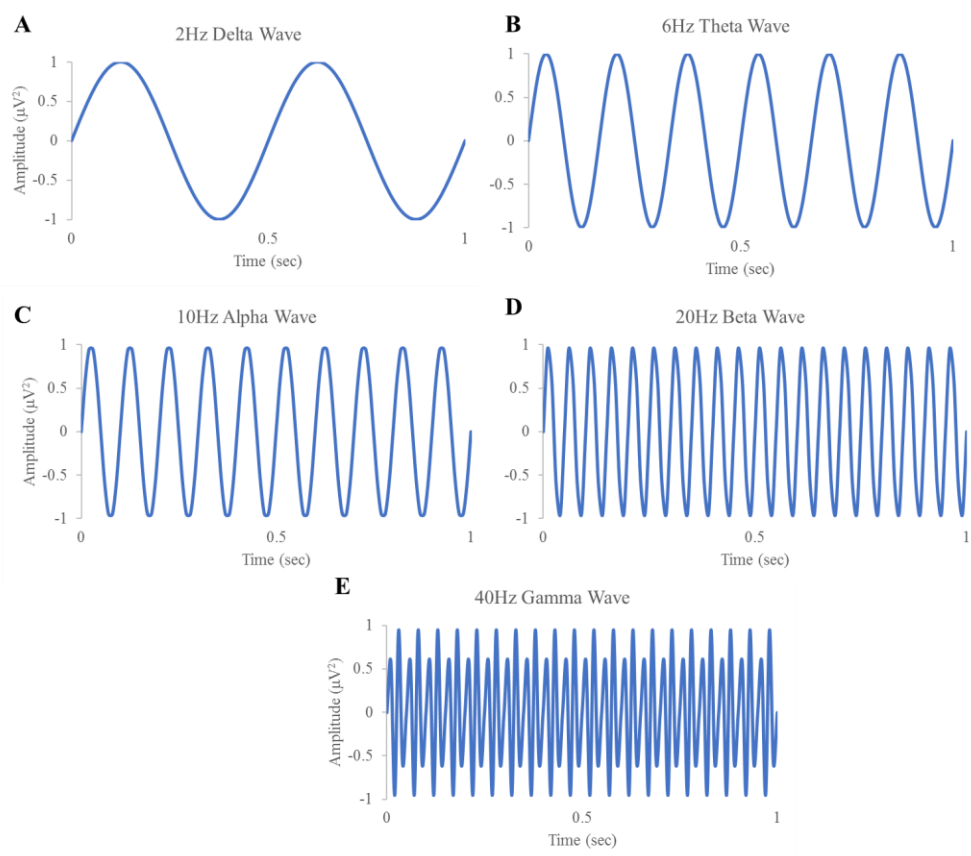

Figure 5: Idealized sinusoidal wave forms of various frequencies. (A) An example of a 2Hz delta frequency wave. (B) An example of a 6Hz theta frequency wave. (C) An example of a 10Hz alpha frequency wave. (D) An example of a 20Hz beta frequency wave. (E) An example of a 40Hz gamma frequency wave. The x-axes represent time in seconds and the y-axes represent amplitude in μV^2.

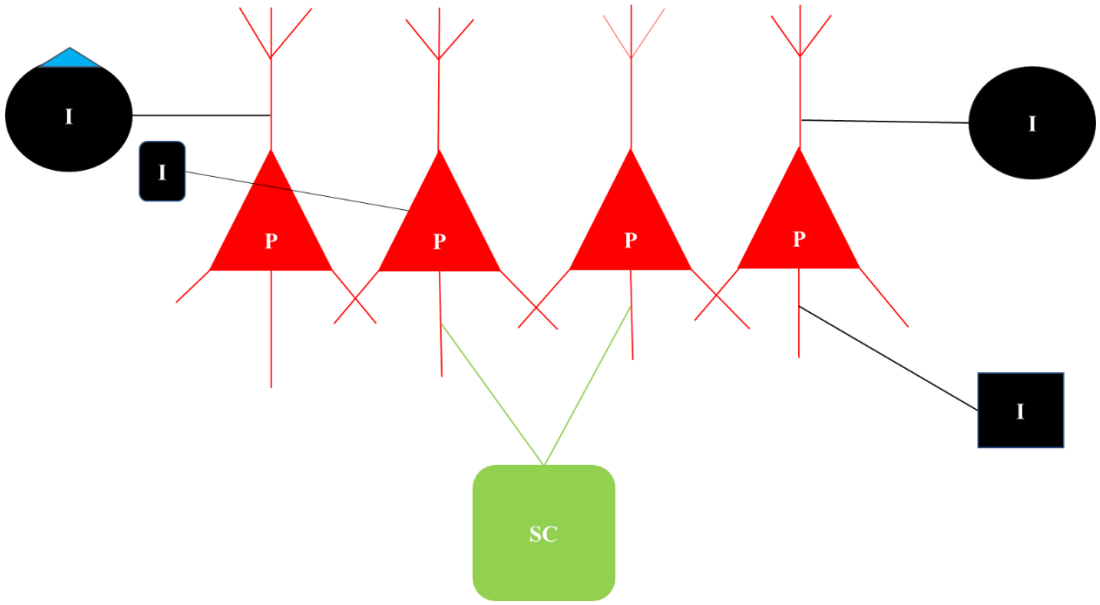

Figure 6: Simplified diagram of microcircuits in the brain. The red shapes labeled 'P' represent glutamatergic pyramidal cells in the cortex. The black shapes labeled 'I' represent γ-aminobutyric acid (GABAergic) interneuron neurons in the cortex. The green shape labeled 'SC' represent sub-cortical inputs, which may be excitatory or inhibitory.

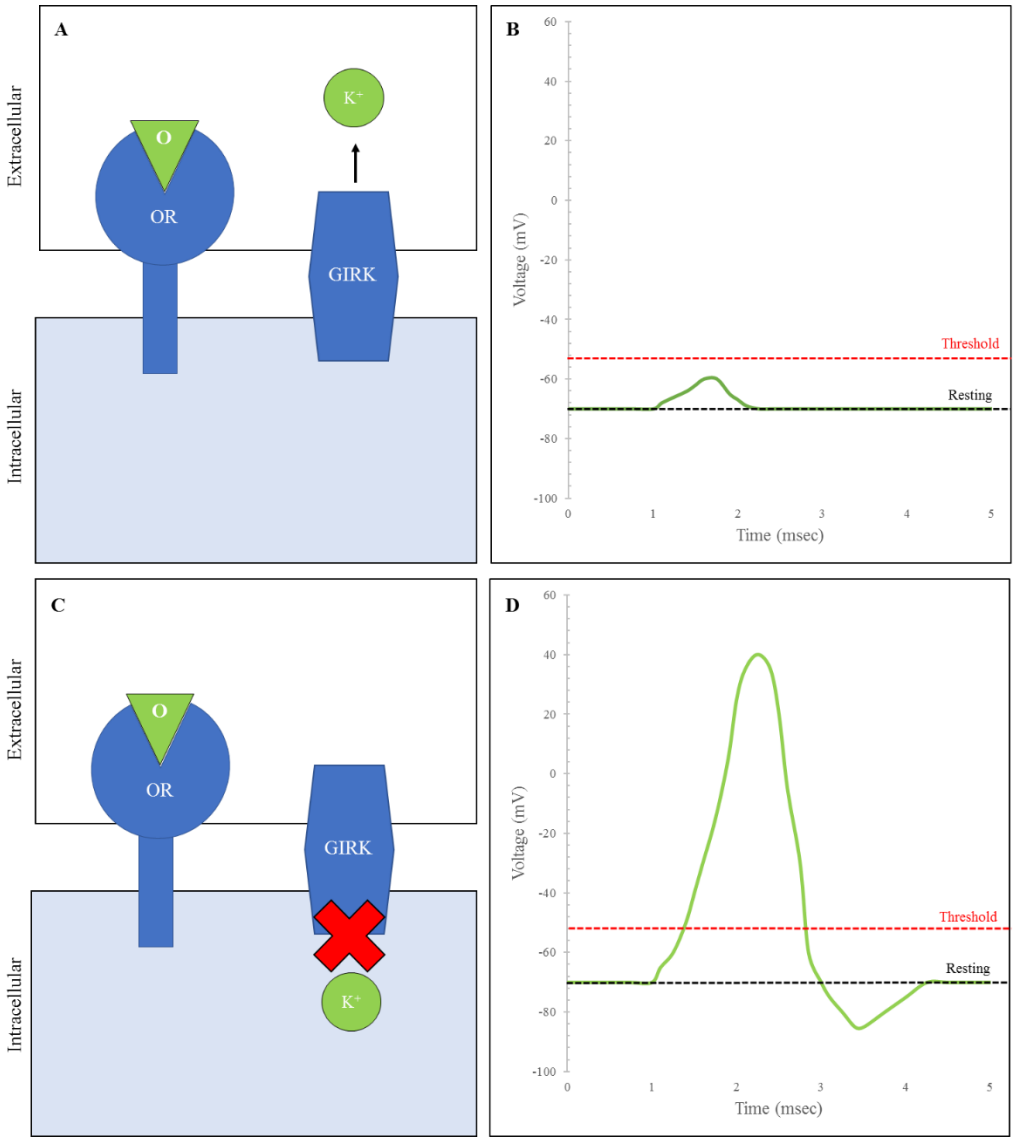

Figure 7: Opioid pharmacodynamics in GABAergic cells. (A) In acute opioid use, the GIRK channels are functional and K^+ effluxes out of the cell. (B) Due to the efflux of K^+, the membrane potential of the GABAergic cell is hyperpolarized, thus no action potential occurs. (C) In chronic opioid use, the GIRK channels are dysfunctional, so no K^+ efflux occurs. (D) With no efflux of K^+, the membrane potential of the GABAergic cell is polarized, thus an action potential occurs. Please note: OR, opioid receptor; O, opioid; GIRK, G protein-coupled inwardly rectifying K^+ channel; GABA, γ-aminobutyric acid.

2. Materials and methods

2.1 Study design

Data were obtained from an electronic medical database at a substance abuse treatment facility (FHE Health, Deerfield Beach, FL, USA), which had gathered ~1000 cases of information about patients' drug use history, DMS-5 diagnosis, and drug intoxication treatment. In addition, there were 20 cases obtained from healthy subjects from the staff with no substance abuse history. EEG data were tracked electronically, along with information about detox-related symptoms. Searches with opioid-related keywords (i.e., morphine, heroin, fentanyl, methadone or oxycodone) found 350 patients who had records of opioid use history. Approximately 450 patients had records of alcohol use history. Methamphetamine-related keywords (i.e., crystal meth, meth, ice) yielded approximately 100 records of methamphetamine use history, while the remaining cases were a mix of other substance use disorders.

Despite the plethora of data discovered, most of the patients in the database were identified as polysubstance users. Screening of all cases for polysubstance use; those with neurodegenerative diseases (e.g., Parkinson's, Alzheimer's); incomplete medical records; or low quality of EEG data were then excluded from the study. To the end, thirteen men and seven women identified as OUD were compared with 20 sex- and age-matched healthy controls. Eleven men and four women identified as MUD were compared to 20 sex- and age-matched controls. Fourteen males and six females identified as AUD were

compared to 20 sex- and age-matched controls. Table 1 shows the healthy control group medical information.

As shown in Table 2, OUD patients had at least a two-year history of opioid abuse (average of 7.2 years). As shown in Table 3, MUD patients had at least a one-year history of methamphetamine abuse (average of 5.0 years). As shown in Table 4, AUD patients had at least a two-year history of alcohol abuse (average of 8.6 years). As a standard procedure, detoxifications medications were prescribed prior to the time of EEG recordings while abstinent from other psychoactive substances for no more than one week (average of 2.4 days; 3.4 days; and 4.3 days; for OUD, MUD, AUD, respectively). No medication was reported while EEG was taken from the twenty healthy controls. Protocols of retrospective analysis of living subjects were approved by the institutional review board (IRB) from Florida Atlantic University (Boca Raton, FL, USA).

2.2 EEG data acquisition

EEG recordings were performed between 12:00 PM - 4:00 PM. Following instrumental calibration, a case (patient or healthy control) was seated in a comfortable chair in a dimmed recording room and the EEG procedures were orally instructed. A cap with 19 electrodes (Electro-Cap International, Eaton, OH, USA) was placed on the scalp. To reduce muscle artifacts in the EEG signal, the participant was instructed to assume a comfortable position and to avoid movement. Signals were collected with the band-pass filter of 1-100 Hz at a rate of 256 Hz, and amplified with Neurofield's Q20 amplifier (NeuroField Inc., Bishop, CA, USA) using NeuroGuide software (Applied Neuroscience Inc., Tampa, FL, USA). Each subject underwent 10 minutes of EEG recording with eyes closed. The equipment and materials used for the study can be seen in Figure 8.

2.3 EEG data analysis

EEG data were downloaded from the database as described previously. Raw data was edited using the editing tool within the NeuroGuide software to remove physical artifacts (including eye movement, jaw movement, and gross movement) and was then visually inspected. A 60-second epoch of quality data was gathered after removal of the aforementioned artifacts. Epoch selection was governed by reliability measures of the data within the NeuroGuide program. Test-retest values of 0.90 or greater are considered highly reliable and valid according to literature (Thatcher, 2010). Each epoch was subjected to EEG spectral power analysis, using a fast Fourier transform (FFT), and then extracted to Microsoft Excel for further data calculation. Powers of δ, θ, α, β or γ oscillations were individually sorted according to electrodes and averaged (mean ±SEM).

The relationship between 5 spectral powers and 19 electrodes were determined in distinct ways. First, the normal distribution of spectral powers (δ, θ, α, β, and γ) across different parts of the scalp was characterized. Specifically, in healthy controls, data obtained from different areas were compared, including the frontal versus rear components and the left versus right components. With such groundwork, we revealed differences in power levels between brain areas or lobes. Results of this analysis presented in Tables 5 & 6. Next, spectral powers of δ, θ, α, β, or γ oscillations at individual electrodes in patients with OUD, MUD, and AUD were compared with those of healthy controls, across all electrode sites (frontal: FP1, FP2, F3, F4, Fz, F7, F8; central: C3, Cz, C4; temporal: T3, T4, T5, T6; parietal: P3, P4, Pz; and occipital: O1, O2). To reveal topographic distribution of spectral power, percentage change was

arbitrarily categorized into four groups as follows: high >60%; medium 36-60%; low 16-36%; no change <15%. Results of the analyses presented in Figures 9-38.

2.4 Statistical analysis

All data are expressed as mean ± SEM and have been evaluated with repeated measures ANOVA between subjects (e.g., frontal *vs*. rear areas, patients *vs* healthy controls) followed by *post-hoc* Fisher test using StatView software 5.0 (SAS Institute Inc., Cary, NC, USA). Unpaired Student *t*-test was also utilized to determine statistical differences if appropriated. Significance was set at 0.05.

Table 1: Breakdown of information for healthy control group

Subject ID	Age (year)	Sex	Ethnicity[1]
C2	28	M	W
C3	24	F	W
C4	39	M	H
C5	23	F	W
C6	40	M	H
C7	38	F	W
C8	26	M	W
C9	21	F	W
C10	26	M	H
C11	60	M	W
C12	55	M	W
C13	26	M	W
C14	46	M	W
C15	50	M	W
C16	24	M	W
C17	37	F	W
C18	41	F	W
C19	30	M	W
C20	20	M	W
C21	21	F	W

[1]W denotes White; H, Hispanic. No medications were reported at time of recording. No health issues were reported at the time of recording. The group consisted of 20 total cases; 13 males, 7 females. Mean age of 34 years.

Table 2: Breakdown of medical information of patients with opioid use disorder

Subject ID	Age (year)	Sex	Ethnicity[1]	Drug[2]	Years on drug	Other health issues	Medications at the time of testing
O2	33	M	W	O, H	14	Bipolar disorder, unspecified	Buprenorphine
O3	29	M	W	H	6	N/A	Buprenorphine; Gabapentin
O6	31	F	W	H	5	N/A	Buprenorphine
O7	44	M	W	H	20	Hepatitis C	None
O8	22	F	W	H	4	Hepatitis C	Buprenorphine; Gabapentin; Quetiapine
O13	24	M	Hi	H	5	Hepatitis C	None
O14	30	M	W	O	3	N/A	Buprenorphine
O15	51	M	W	O	4	Essential hypertension	Buprenorphine; Hydroxyzine
O17	56	M	Hi	H	5	Mild intermittent asthma	Buprenorphine
O18	49	M	W	O	3	Essential hypertension	Buprenorphine; Metoprolol
O26	35	M	W	O, H	15	Psoriasis vulgaris	Buprenorphine
O27	45	F	W	O	10	Essential hypertension; Gastroesophageal reflux disease	Buprenorphine; Pantoprazole
O28	45	F	W	H	3	N/A	Buprenorphine; Gabapentin
O29	20	M	W	H	2	N/A	None
O30	40	M	W	O	12	N/A	Buprenorphine; Pantoprazole
O31	29	M	W	H	7	N/A	Buprenorphine; Gabapentin; Hydroxyzine
O33	25	F	W	H	4	N/A	Buprenorphine; Gabapentin; Hydroxyzine
O34	49	M	Hi	O	13	Gastro-esophageal reflux disease; Essential hypertension; Testicular hypofunction	Buprenorphine; Gabapentin; Hydroxyzine
O35	22	F	W	H	4	N/A	Buprenorphine
O26	19	F	W	H	4	N/A	Buprenorphine

[1]W denotes White; Hi, Hispanic.[2]M denotes morphine; H, heroin; O, oxycodone. The group consisted of 20 total cases; 13 males; 7 females. Mean age of 37 years.

Table 3: Breakdown of medical information of patients with methamphetamine use disorder

Subject ID	Age (year)	Sex	Ethnicity[1]	Years on drug	Other health issues	Medications at the time of testing
A2	39	M	W	5	N/A	Diazepam
A3	23	M	H	4	N/A	None
A6	38	M	B	7	Acute hepatitis C, without hepatic coma	Trazodone
A7	48	M	W	5	Essential hypertension	Hydroxyzine
A9	27	M	B	2	Gastro-esophageal reflux disease	Trazodone; Pantoprazole
A10	34	M	W	2	Gastro-esophageal reflux disease	Diazepam
A11	32	M	W	10	N/A	None
A13	25	F	H	2	Mild intermittent asthma	Albuterol
A14	32	M	W	5	Essential hypertension	Clonidine
A16	31	F	W	10	N/A	Trazodone
A17	30	F	W	10	N/A	None
A18	24	F	W	1	N/A	Hydroxyzine
A22	20	M	W	3	Myalgia	Hydroxyzine
A23	20	M	W	3	N/A	Trazodone
A24	20	M	W	3	N/A	Hydroxyzine; Mirtazapine

[1]W denotes White; H, Hispanic; B, Black. The group consisted of 15 total cases; 11 males, 4 females. Mean age of 30 years.

Table 4: Breakdown of medical information of patients with alcohol use disorder

Subject ID	Age (year)	Sex	Ethnicity[1]	Years on drug	Other health issues	Medications at the time of testing
A2	31	M	W	10	Essential hypertension	Gabapentin
A3	57	M	W	20	Essential hypertension; hyperlipidemia	Methocarbamol; Gabapentin; Losartan
A4	25	F	W	3	N/A	Olanzapine; Pantoprazole
A5	31	M	W	12	Gastro-esophageal reflux disease	Buspirone; Gabapentin; Pantoprazole
A8	49	F	W	20	N/A	Hydroxyzine; Diazepam; Gabapentin
A9	41	M	W	25	Essential hypertension	Diazepam; Gabapentin
A11	36	F	W	5	N/A	Diazepam; Gabapentin
A13	30	M	H	2	Mixed hyperlipidemia	Diazepam; Hydroxyzine
A15	23	M	W	3	N/A	Gabapentin
A16	32	M	W	8	N/A	Diazepam; Gabapentin
A18	37	F	W	3	Gastro-esophageal reflux disease	None
A19	54	M	W	25	Anemia	Diazepam; Carbamazepine
A20	23	M	W	5	N/A	None
A22	44	F	W	10	Essential hypertension	Diazepam; Gabapentin
A23	40	F	H	5	Essential hypertension	Lisinopril; Carvedilol; Pantoprazole
A24	28	M	W	5	N/A	Methocarbamol
A25	47	M	W	10	Type II diabetes; essential hypertension; myalgia	Atorvastatin; Pioglitazone; Canagliflozin
A26	55	M	W	10	Gastro-esophageal reflux disease	Levetiracetam; Diazepam
A27	46	M	W	3	Mild intermittent asthma; essential hypertension	Diazepam; Gabapentin
A28	42	M	W	10	N/A	None
A29	35	M	W	3	N/A	None
A30	32	M	H	5	Essential hypertension; asthma	Diazepam; Levetiracetam
A31	26	M	W	2	N/A	Gabapentin

[1]*W denotes White; H, Hispanic; B, Black. The group consisted of 23 total cases; 17 males, 6 females. Mean age of 38 years.*

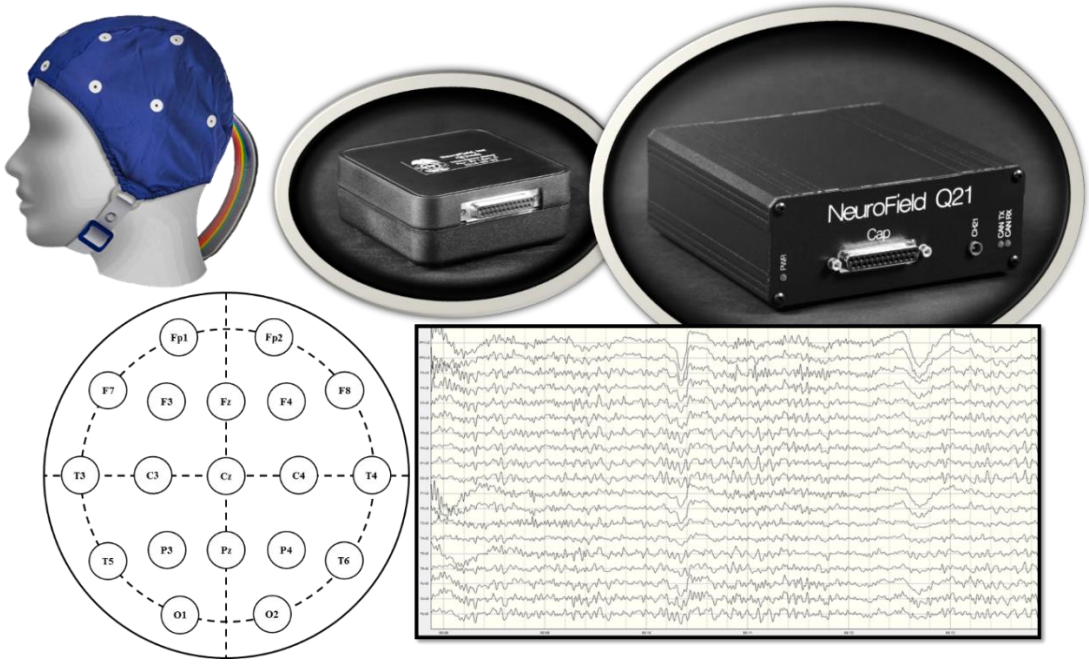

Figure 8: Materials used for the study. In the left corner of the top row is the 19-channel EEG cap (from Electro-Cap International, Inc. – Eaton, OH, USA) used for collecting data; in the middle and right of the top row are the QCheck electrode impedance monitor and Q21 amplifier, respectively (both from Neurofield, Inc. – Bishop, CA, USA); in the left corner of the bottom row is a diagram of the International 10-20 System to elaborate electrode placement across the scalp; and in the right corner of the bottom row is an example of a digitized EEG recording using Neuroguide software (Applied Neuroscience, Inc. – Largo, FL, USA).

3. Results

3.1 Results of normal distribution of spectral power across the cortex

First, analysis of the 20 healthy controls was completed in order to determine differences across the frontal (F; Fp1, Fp2, F3, F4, F7, F8, and Fz), central (C; C3, C4, Cz, T3, T4), and rear (R; T5, T6, P3, P4, Pz, O1, O2) regions. As shown in Table 5, the distribution of power levels revealed a pattern across the cortex in healthy controls. δ frequency power was significantly larger in the frontal region (F = 14.96) as compared to the rear region (R = 11.78, $p<0.01$). θ frequency power was significantly larger in the rear region (R = 10.62) as compared to the frontal region (F = 1.93, $p<0.01$). α frequency power and β frequency power were also significantly larger in the rear (α, R = 45.87; β, R = 12.68) than in the front (α, F = 15.38, $p<0.001$; β, F = 7.18, $p<0.001$). Additionally, the central region (α, C = 20.67; β, C = 8.93) in these two frequencies revealed power levels in between the frontal and rear regions, thus revealing a fluid distribution across the entire cortex. The γ frequency power revealed no significant difference between the frontal (F = 1.59) and rear regions (R = 1.73, $p=0.51$). Although not significant, the central region revealed the highest power levels across this frequency.

The analysis of left (Fp1, F3, F7, C3, T3, T5, P3, and O1) versus right (Fp2, F4, F8, C4, T4, T6, P4, and O2) hemispheres, as shown in Table 6, revealed no differences in power levels across any frequency in the cortex.

3.2 Results of opioid use disorder

3.2.1 δ Frequency power changes

Figure 9 displays the comparison of absolute δ frequency power between opioid use disorder and healthy controls and Figure 10 displays the percentage change between the two groups. Figure 9(A) shows significant increases in the frontal electrodes, F3, F4, and Fz, as compared to controls ($F(1,38)=5.036$, $p=0.0307$). These are marked by increases of 50%, 68%, and 58%, respectively (see Figure 10(F)). The remaining frontal electrodes, Fp1, Fp2, F7, and F8 were not significantly different. Figure 9(B) shows significant increases in the central electrodes, C3, C4, and Cz, as compared to controls ($F(1,38)=10.434$, $p=0.0026$). These are marked by increases of 60%, 60%, and 72%, respectively (Figure 10(F)). Figure 9(C) shows significant increases in the parietal electrodes, P3, P4, and Pz, as compared to controls ($F(1,38)=9.773$, $p=0.0034$). These are marked by increases of 53%, 51%, and 82%, respectively (Figure 10(F)). Figure 9(D) shows significant increases in the temporal electrodes, T3, T4, and T6, as compared to controls ($F(1,38)=6.846$, $p=0.0127$). These are marked by increases of 51%, 66%, and 58%, respectively (Figure 10(F)). The remaining temporal electrode, T5, was not significant. Lastly, Figure 9(E) shows significant increases in the occipital electrodes, O1 and O2, as compared to controls ($F(1,38)=9.773$, $p=0.0034$). These are marked by increases of 59% and 64%, respectively (see Figure 10(F)).

3.2.2 θ Frequency power changes

Figure 11 displays the comparison of absolute θ frequency power between opioid use disorder and healthy controls and Figure 12 displays the percentage change between the two groups. Figure 11(A) shows significant increases in the frontal electrodes, Fp1,

Fp2, F3, F4, F8, and Fz, as compared to controls (F(1,38)=7.560, p=0.0091). These are marked by increases of 51%, 42%, 52%, 57%, 44%, and 52%, respectively (see Figure 12(F)). The remaining frontal electrode, F7, was not significantly different compared to controls. Figure 11(B) shows significant increases in the central electrodes, C3, C4, and Cz, as compared to controls (F(1,38)=5.773, p=0.0213). These are marked by increases of 49%, 51%, and 53%, respectively (Figure 12(F)). Figure 11(C) shows the parietal electrodes, P3, P4, and Pz, as compared to controls (F(1,38)=2.446, p=0.1261). These are not significantly different (Figure 12(F)). Figure 11(D) shows the temporal electrodes, T3, T4, T5, and T6, as compared to controls (F(1,38)=1.590, p=0.2150). These are not significantly different (Figure 12(F)). Lastly, Figure 11(E) shows the occipital electrodes, O1 and O2, as compared to controls (F(1,38)=0.881, p=0.3538). These are not significantly different (see Figure 12(F)).

3.2.3 α Frequency power changes

Figure 13 displays the comparison of absolute α frequency power between opioid use disorder and healthy controls and Figure 14 displays the percentage change between the two groups. Figure 13(A) shows the frontal electrodes, Fp1, Fp2, F3, F4, F7, F8, and Fz, as compared to controls (F(1,38)=1.469, p=0.2330). These are not significantly different (see Figure 14(F)). Figure 13(B) shows the central electrodes, C3, C4, and Cz, as compared to controls (F(1,38)=1.802, p=0.1874). These are not significantly different (Figure 14(F)). Figure 13(C) shows significant decreases in the parietal electrodes, P4 and Pz, as compared to controls (F(1,38)=4.046, p=0.0417). These are marked by decreases of 54% in each (Figure 14(F)). The remaining parietal electrode, P3, was not significantly different. Figure 13(D) shows the temporal electrodes, T3, T4, T5, and T6,

as compared to controls (F(1,38)=2.145, p=0.1513). These are not significantly different (Figure 14(F)). Lastly, Figure 13(E) shows a significant decrease in the occipital electrode O2, as compared to controls (F(1,38)=3.883, p=0.0461). This is marked by a decrease of 69% (see Figure 14(F)). The remaining occipital electrode, O1, was not significantly different.

3.2.4 β Frequency power changes

Figure 15 displays the comparison of absolute β frequency power between opioid use disorder and healthy controls and Figure 16 displays the percentage change between the two groups. Figure 15(A) shows significant increases in the frontal electrodes, Fp1, F3, F4, F8, and Fz, as compared to controls (F(1,38)=4.795, p=0.0348). These are marked by increases of 44%, 45%, 42%, 34%, and 45%, respectively (see Figure 16(F)). The remaining frontal electrodes, Fp2 and F7 were not significantly different. Figure 15(B) shows the central electrodes, C3, C4, and Cz, as compared to controls (F(1,38)= 2.913, p=0.0961). These are not significantly different (Figure 16(F)). Figure 15(C) shows the parietal electrodes, P3, P4, and Pz, as compared to controls (F(1,38)=0.001, p=0.9812). These are not significantly different (Figure 16(F)). Figure 15(D) shows the temporal electrodes, T3, T4, T5, and T6, as compared to controls (F(1,38)=0.129, p=0.7210). These are not significantly different (Figure 16(F)). Lastly, Figure 15(E) shows the occipital electrodes, O1 and O2, as compared to controls (F(1,38)=1.028, p=0.3170). These are not significantly different (Figure 16(F)).

3.2.5 γ Frequency power changes

Figure 17 displays the comparison of absolute γ frequency power between opioid use disorder and healthy controls and Figure 18 displays the percentage change between

the two groups. Figure 17(A) shows the frontal electrodes, Fp1, Fp2, F3, F4, F7, F8, and Fz, as compared to controls ($F(1,38)=1.464$, $p=0.2337$). These are not significantly different (see Figure 18(F)). Figure 17(B) shows the central electrodes, C3, C4, and Cz, as compared to controls ($F(1,38)=1.115$, $p=0.2976$). These are not significantly different (Figure 18(F)). Figure 17(C) shows the parietal electrodes, P3, P4, and Pz, as compared to controls ($F(1,38)=0.005$, $p=0.9456$). These are not significantly different (Figure 18(F)). Figure 17(D) shows the temporal electrodes, T3, T4, T5, and T6, as compared to controls ($F(1,38)=1.132$, $p=0.2942$). These are not significantly different (Figure 18(F)). Lastly, Figure 17(E) shows the occipital electrodes, O1 and O2, as compared to controls ($F(1,38)=2.598$, $p=0.1152$). These are not significantly different (Figure 18(F)).

3.3 Results of methamphetamine use disorder

3.3.1 δ Frequency power changes

Figure 19 displays the comparison of absolute δ frequency power between methamphetamine use disorder and healthy controls and Figure 20 displays the percentage change between the two groups. Figure 19(A) shows the frontal electrodes, Fp1, Fp2, F3, F4, F7, F8, and Fz, as compared to controls ($F(1,33)=1.126$, $p=0.2963$). These are not significantly different (see Figure 10(F)). Figure 19(B) shows the central electrodes, C3, C4, and Cz, as compared to controls ($F(1,33)=2.438$, $p=0.1280$). These are not significantly different (Figure 20(F)). Figure 19(C) shows the parietal electrodes, P3, P4, and Pz, as compared to controls ($F(1,33)=0.950$, $p=0.3369$). These are not significantly different (Figure 20(F)). Figure 19(D) shows the temporal electrodes, T3, T4, T5, and T6, as compared to controls ($F(1,33)=1.460$, $p=0.2355$). These are not significantly different (Figure 20(F)). Lastly, Figure 19(E) shows the occipital electrodes,

O1 and O2, as compared to controls (F(1,33)=0.182, p=0.3741). These are not significantly different (see Figure 20(F)).

3.3.2 θ Frequency power changes

Figure 21 displays the comparison of absolute θ frequency power between methamphetamine use disorder and healthy controls and Figure 22 displays the percentage change between the two groups. Figure 21(A) shows the frontal electrodes, Fp1, Fp2, F3, F4, F7, F8, and Fz, as compared to controls (F(1,33)=1.159, p=0.2895). Although these were increased by upwards of 72% (Fp2), none were significant (see Figure 22(F)). Figure 21(B) shows the central electrodes, C3, C4, and Cz, as compared to controls (F(1,33)=0.523, p=0.4748). These are not significantly different (Figure 22(F)). Figure 21(C) shows the parietal electrodes, P3, P4, and Pz, as compared to controls (F(1,33)=0.024, p=0.8778). These are not significantly different (Figure 22(F)). Figure 21(D) shows the temporal electrodes, T3, T4, T5, and T6, as compared to controls (F(1,33)=0.001, p=0.9943). These are not significantly different (Figure 22(F)). Lastly, Figure 21(E) shows the occipital electrodes, O1 and O2, as compared to controls (F(1,33)=0.076, p=0.7847). These are not significantly different (see Figure 22(F)).

3.3.3 α Frequency power changes

Figure 23 displays the comparison of absolute α frequency power between methamphetamine use disorder and healthy controls and Figure 24 displays the percentage change between the two groups. Figure 23(A) shows significant decreases in the frontal electrodes, F3, F4, and Fz, as compared to controls (F(1,33)=3.655, p=0.0472). These were marked by reductions of 43%, 38%, and 41%, respectively. The remaining electrodes, Fp1, Fp2, F7, and F8 were not significantly different (see Figure

24(F)). Figure 23(B) shows the central electrodes, C3, C4, and Cz, as compared to controls ($F(1,33)=2.111$, $p=0.1557$). These are not significantly different (Figure 24(F)). Figure 23(C) shows the parietal electrodes, P3, P4, and Pz, as compared to controls ($F(1,33)=1.883$, $p=0.1792$). These are not significantly different (Figure 24(F)). Figure 23(D) shows the temporal electrodes, T3, T4, T5, and T6, as compared to controls ($F(1,33)=1.379$, $p=0.2486$). These are not significantly different (Figure 24(F)). Lastly, Figure 23(E) shows the occipital electrodes, O1 and O2, as compared to controls ($F(1,33)=1.965$, $p=0.1703$). These are not significantly different (see Figure 24(F)).

3.3.4 β Frequency power changes

Figure 25 displays the comparison of absolute β frequency power between methamphetamine use disorder and healthy controls and Figure 26 displays the percentage change between the two groups. Figure 25(A) shows the frontal electrodes, Fp1, Fp2, F3, F4, F7, F8, and Fz, as compared to controls ($F(1,33)=1.438$, $p=0.2390$). These are not significantly different (see Figure 26(F)). Figure 25(B) shows the central electrodes, C3, C4, and Cz, as compared to controls ($F(1,33)= 0.726$, $p=0.4005$). These are not significantly different (Figure 26(F)). Figure 25(C) shows the parietal electrodes, P3, P4, and Pz, as compared to controls ($F(1,33)=0.083$, $p=0.7757$). These are not significantly different (Figure 26(F)). Figure 25(D) shows the temporal electrodes, T3, T4, T5, and T6, as compared to controls ($F(1,33)=0.077$, $p=0.7833$). These are not significantly different (Figure 26(F)). Lastly, Figure 25(E) shows the occipital electrodes, O1 and O2, as compared to controls ($F(1,33)=0.348$, $p=0.5594$). These are not significantly different (Figure 26(F)).

3.3.5 γ Frequency power changes

Figure 27 displays the comparison of absolute γ frequency power between methamphetamine use disorder and healthy controls and Figure 28 displays the percentage change between the two groups. Figure 27(A) shows the frontal electrodes, Fp1, Fp2, F3, F4, F7, F8, and Fz, as compared to controls ($F(1,33)=1.124$, $p=0.2968$). These are not significantly different (see Figure 28(F)). Figure 27(B) shows the central electrodes, C3, C4, and Cz, as compared to controls ($F(1,33)=1.037$, $p=0.3159$). These are not significantly different (Figure 28(F)). Figure 27(C) shows a significant reduction in the parietal electrode, P4 as compared to controls ($F(1,33)=3.608$, $p=0.0437$). This was marked by a reduction of 27%. The remaining electrodes, P3 and Pz were not significantly different (Figure 28(F)). Figure 27(D) shows a significant reduction in the temporal electrode, T6, as compared to controls ($F(1,33)=3.846$, $p=0.0311$). This was marked by a reduction of 41%. The remaining electrodes, T3, T4, and T5, were not significantly different (Figure 28(F)). Lastly, Figure 27(E) shows the occipital electrodes, O1 and O2, as compared to controls ($F(1,33)=2.452$, $p=0.1269$). These are not significantly different (Figure 28(F)).

3.4 Results of alcohol use disorder

3.4.1 δ Frequency power changes

Figure 29 displays the comparison of absolute δ frequency power between alcohol use disorder and healthy controls and Figure 30 displays the percentage change between the two groups. Figure 29(A) shows significant decreases in the frontal electrodes, Fp1, Fp2, F3, F4, and F7 as compared to controls ($F(1,39)=3.962$, $p=0.0436$). These are marked by decreases of 30%, 33%, 29%, 22%, and 35%, respectively (see Figure 30(F)).

The remaining frontal electrodes, F8 and Fz, were not significantly different. Figure 29(B) shows significant decreases in the central electrodes, C3, C4, and Cz, as compared to controls ($F(1,39)=9.281$, $p=0.0041$). These are marked by decreases of 32%, 30%, and 27%, respectively (Figure 30(F)). Figure 29(C) shows significant decreases in the parietal electrodes, P3, P4, and Pz, as compared to controls ($F(1,39)=6.158$, $p=0.0175$). These are marked by decreases of 30%, 31%, and 25%, respectively (Figure 30(F)). Figure 29(D) shows significant decreases in the temporal electrodes, T3, T4, and T5, as compared to controls ($F(1,39)=6.852$, $p=0.0125$). These are marked by decreases of 38%, 27%, and 45%, respectively (Figure 30(F)). The remaining temporal electrode, T6, was not significantly different. Lastly, Figure 29(E) shows the occipital electrodes, O1 and O2, as compared to controls ($F(1,39)=1.727$, $p=0.1965$). These are not significantly different (see Figure 30(F)).

3.4.2 θ Frequency power changes

Figure 31 displays the comparison of absolute θ frequency power between alcohol use disorder and healthy controls and Figure 32 displays the percentage change between the two groups. Figure 31(A) shows significant decreases in the frontal electrodes, Fp1, Fp2, F3, F4, F7, and Fz, as compared to controls ($F(1,40)=5.489$, $p=0.0242$). These are marked by decreases of 30%, 32%, 35%, 30%, 31%, and 33%, respectively (see Figure 32(F)). The remaining frontal electrode, F8, was not significantly different compared to controls. Figure 31(B) shows significant decreases in the central electrodes, C3, C4, and Cz, as compared to controls ($F(1,40)=5.607$, $p=0.0228$). These are marked by decreases of 39%, 25%, and 37%, respectively (Figure 32(F)). Figure 31(C) shows significant decreases in the parietal electrodes, P3, P4, and Pz, as compared to controls

(F(1,40)=4.564, p=0.0388). These are marked by decreases of 41%, 37%, and 38%, respectively (Figure 32(F)). Figure 31(D) shows significant decreases in the temporal electrode, T3, as compared to controls (F(1,40)=4.708, p=0.0360). This is marked by a decrease of 43%. The remaining electrodes, T4, T5, and T6 are not significantly different (Figure 32(F)). Lastly, Figure 31(E) shows the occipital electrodes, O1 and O2, as compared to controls (F(1,40)=1.620, p=0.2104). These are not significantly different (see Figure 32(F)).

3.4.3 α Frequency power changes

Figure 33 displays the comparison of absolute α frequency power between alcohol use disorder and healthy controls and Figure 34 displays the percentage change between the two groups. Figure 33(A) shows significant decreases in the frontal electrodes, Fp1, Fp2, F3, F4, F7, F8, and Fz, as compared to controls (F(1,39)=6.112, p=0.0179). These are marked by decreases of 55%, 55%, 59%, 58%, 57%, 50%, and 58%, respectively (see Figure 34(F)). Figure 33(B) shows significant decreases in the central electrodes, C3, C4, and Cz, as compared to controls (F(1,39)=5.997, p=0.0189). These are marked by decreases of 66%, 63%, and 61%, respectively (Figure 34(F)). Figure 33(C) shows significant decreases in the parietal electrodes, P3, P4, and Pz, as compared to controls (F(1,39)=4.784, p=0.0348). These are marked by decreases of 65%, 63%, and 64%, respectively (Figure 34(F)). Figure 33(D) shows significant decreases in the temporal electrodes, T3 and T4, as compared to controls (F(1,39)=4.227, p=0.0465). These are marked by decreases of 67% and 54%, respectively (Figure 34(F)). The other electrodes, T5 and T6, are not significantly different. Lastly, Figure 33(E) shows a significant decrease in the occipital electrodes, O1 and O2, as compared to controls (F(1,39)=4.673,

p=0.0368). These are marked by decreases of 72% and 77%, respectively (see Figure 34(F)).

3.4.4 β Frequency power changes

Figure 35 displays the comparison of absolute β frequency power between alcohol use disorder and healthy controls and Figure 36 displays the percentage change between the two groups. Figure 35(A) shows the frontal electrodes, Fp1, Fp2, F3, F4, F7, F8, and Fz, as compared to controls (F(1,39)=0.303, p=0.5854). These are not significant (see Figure 36(F)). Figure 35(B) shows the central electrodes, C3, C4, and Cz, as compared to controls (F(1,39)= 0.0001, p=0.9989). These are not significantly different (Figure 36(F)). Figure 35(C) shows the parietal electrodes, P3, P4, and Pz, as compared to controls (F(1,39)=0.346, p=0.5596). These are not significantly different (Figure 36(F)). Figure 35(D) shows the temporal electrodes, T3, T4, T5, and T6, as compared to controls (F(1,39)=0.862, p=0.3588). These are not significantly different (Figure 36(F)). Lastly, Figure 35(E) shows the occipital electrodes, O1 and O2, as compared to controls (F(1,39)=0.051, p=0.8228). These are not significantly different (Figure 36(F)).

3.4.5 γ Frequency power changes

Figure 37 displays the comparison of absolute γ frequency power between alcohol use disorder and healthy controls and Figure 38 displays the percentage change between the two groups. Figure 37(A) shows the frontal electrodes, Fp1, Fp2, F3, F4, F7, F8, and Fz, as compared to controls (F(1,39)=1.871, p=0.1792). These are not significantly different (see Figure 38(F)). Figure 37(B) shows the central electrodes, C3, C4, and Cz, as compared to controls (F(1,39)=1.014, p=0.3202). These are not significantly different (Figure 38(F)). Figure 37(C) shows significant decreases in the parietal electrodes, P3,

P4, and Pz, as compared to controls (F(1,39)=8.025, p=0.0073). These are marked by decreases of 34%, 35%, and 23%, respectively (Figure 38(F)). Figure 17(D) shows significant decreases in the temporal electrodes, T3, T5, and T6, as compared to controls (F(1,39)=11.543, p=0.0016). These are marked by decreases of 63%, 29%, and 36%, respectively. The remaining electrode, T4, is not significantly different (Figure 38(F)). Lastly, Figure 37(E) shows significant decreases in the occipital electrodes, O1 and O2, as compared to controls (F(1,39)=4.895, p=0.0329). These are marked by decreases of 35% and 51%, respectively (Figure 38(F)).

3.5 Comparison of all groups

3.5.1 δ Frequency power changes

To get a better understanding of the differences between the groups, representatives of each group were chosen arbitrarily, and comparisons of each frequency are displayed. Figure 39 shows a δ frequency wave recorded in the F4 electrode, displaying an amplitude of 30 μV^2 and a time sequence of 6 seconds in each panel. As described previously, compared to a healthy control (A), an OUD patient (B) had a medium increase in amplitude, an AUD patient (C) had a low decrease in amplitude, and a MUD patient (D) had a low increase in amplitude.

3.5.1 θ Frequency power changes

Figure 40 shows a θ frequency wave recorded in the Cz electrode, displaying an amplitude of 20 μV^2 and a time sequence of 6 seconds in each panel. As described previously, compared to a healthy control (A), an OUD patient (B) had a medium increase in amplitude, an AUD patient (C) had a medium decrease in amplitude, and a MUD patient (D) had a medium increase in amplitude.

3.5.1 α Frequency power changes

Figure 41 shows an α frequency wave recorded in the O2 electrode, displaying an amplitude of 40 μV^2 and a time sequence of 6 seconds in each panel. As described previously, compared to a healthy control (A), an OUD patient (B) had a high decrease in amplitude, an AUD patient (C) had a high decrease in amplitude, and a MUD patient (D) had a medium decrease in amplitude.

3.5.1 β Frequency power changes

Figure 42 shows a β frequency wave recorded in the Fz electrode, displaying an amplitude of 20 μV^2 and a time sequence of 6 seconds in each panel. As described previously, compared to a healthy control (A), an OUD patient (B) had a medium increase in amplitude, an AUD patient (C) had no change in amplitude, and a MUD patient (D) had a low increase in amplitude.

3.5.1 γ Frequency power changes

Figure 43 shows a γ frequency wave recorded in the P4 electrode, displaying an amplitude of 10 μV^2 and a time sequence of 6 seconds in each panel. As described previously, compared to a healthy control (A), an OUD patient (B) had a low increase in amplitude, an AUD patient (C) had a low decrease in amplitude, and a MUD patient (D) had no change in amplitude.

Table 5: Comparative analysis of power levels as measured across the scalp in healthy controls

	Frontal (F; μV^2)[1]	Central (C; μV^2)	Rear (R; μV^2)	F/R Ratio	*P* Value[3]
δ[2]	14.49 ± 0.67	10.81 ± 0.54	11.79 ± 0.56	1.23	*P*<0.01
θ	7.92 ± 0.40	8.05 ± 0.61	10.63 ± 0.89	0.75	*P*<0.01
α	15.39 ± 1.36	20.67 ± 2.65	45.87 ± 5.63	0.34	*P*<0.001
β	7.18 ± 0.42	8.94 ± 0.65	12.68 ± 0.91	0.57	*P*<0.001
γ	1.59 ± 0.09	1.86 ± 0.19	1.73 ± 0.12	0.92	*P*>0.05

[1]Frontal (F; Fp1, Fp2, F3, F4, F7, F8, and Fz); Central (C; C3, C4, Cz, T3, T4); Rear (R; T5, T6, P3, P4, Pz, O1, O2). [2]δ (1-4 Hz); θ (4-8 Hz); α (8-12 Hz); β (12-30 Hz); γ (30-50 Hz). [3]Comparison between Frontal and Rear. Significance was determined by repeated measures ANOVA.

Table 6: Comparative analysis of power levels as measured at the left versus right scalp in healthy controls

	Left scalp (L; μV^2)[1]	Right scalp (R; μV^2)	L/R ratio	*P* Value[3]
δ^2	12.30 ± 0.56	12.28 ± 0.58	1.00	*P*>0.05
θ	8.59 ± 0.68	8.31 ± 0.54	1.03	*P*>0.05
α	26.46 ± 3.61	27.21 ± 3.69	0.97	*P*>0.05
β	9.33 ± 0.64	9.46 ± 0.66	0.99	*P*>0.05
γ	1.79 ± 0.13	1.75 ± 0.12	1.02	*P*>0.05

[1]Left (L; Fp1, F3, F7, C3, T3, T5, P3, and O1); Right (R; Fp2, F4, F8, C4, T4, T6, P4, and O2). [2]δ (1-4 Hz); θ (4-8 Hz); α (8-12 Hz); β (12-30 Hz); γ (30-50 Hz). [3]Comparison between Left and Right. Significance was determined by repeated measures ANOVA. The electrodes at midline (Fz, Cz, and Pz) were excluded from the data analysis.

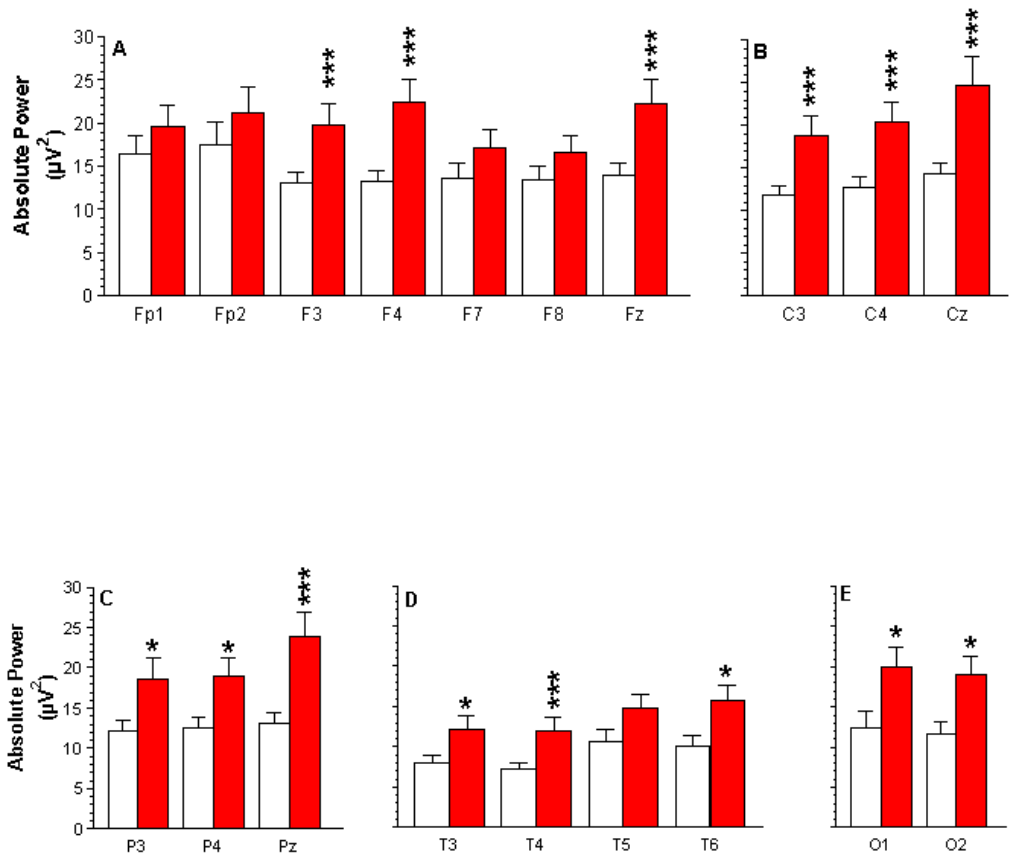

Figure 9: Absolute power of δ frequency in patients with opioid use disorder. (A) The δ power comparisons between opioid patients versus controls measured at the frontal electrodes, Fp1, Fp2, F3, F4, F7, F8, and Fz. (B) The δ power comparisons measured at the central electrodes, C3, C4, and Cz. (C) The δ power comparisons measured at the parietal electrodes, P3, P4, and Pz. (D) The δ power comparisons measured at the temporal electrodes, T3, T4, T5, and T6. (E) The δ power comparisons measured at the occipital electrodes, O1 and O2. Open columns denote the healthy control group and solid red columns denote the opioid group. All data are expressed in mean ± SEM. ∗P < 0.05, ∗∗∗P < 0.001 vs. healthy controls determined by repeated measures ANOVA followed by post hoc Fisher's test. NS, P > 0.05 vs. healthy control determined by repeated measures ANOVA.

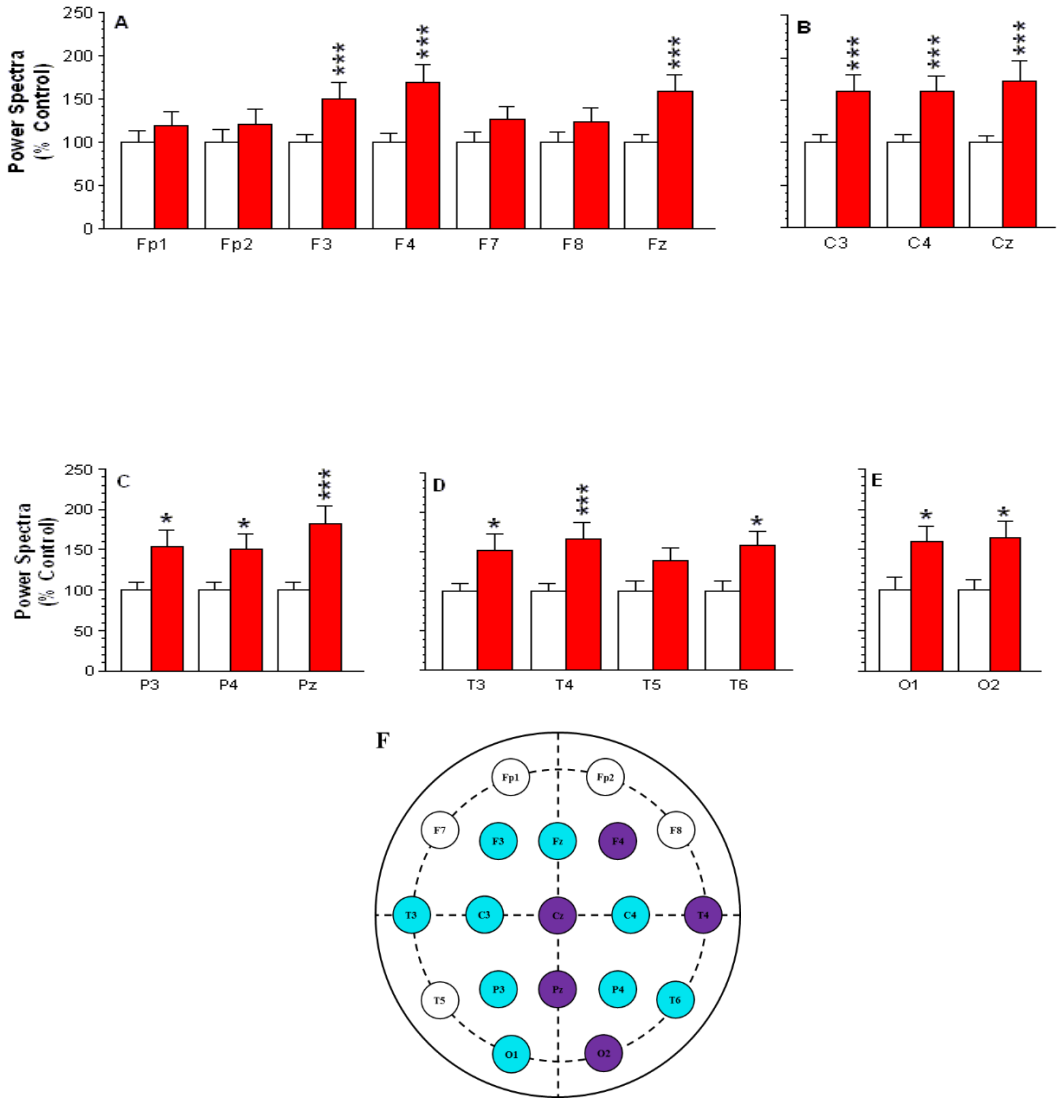

Figure 10: Topographic changes of δ power in patients with opioid use disorder. (A) The δ power percentage change measured at the frontal electrodes, Fp1, Fp2, F3, F4, F7, F8, and Fz. (B) The δ power percentage change measured at the central electrodes, C3, C4, and Cz. (C) The δ power percentage change measured at the parietal electrodes, P3, P4, and Pz. (D) The δ power percentage change measured at the temporal electrodes, T3, T4, T5, and T6. (E) The δ power percentage change measured at the occipital electrodes, O1 and O2. Open columns denote the healthy control group and solid red columns denote the opioid group. All data are expressed in mean ± SEM. ⁎P < 0.05, ⁎⁎⁎P < 0.001 vs. healthy controls determined by repeated measures ANOVA followed by post hoc Fisher's test. NS, P > 0.05 vs. healthy control determined by repeated measures ANOVA. (F) The topographic distribution of percentage power differences between opioid users and healthy controls. The blue electrodes represent medium increases (36-60%) in activity; the purple electrodes represent high increases (>60%) in activity; and the clear electrodes represent no change (<15%) in activity.

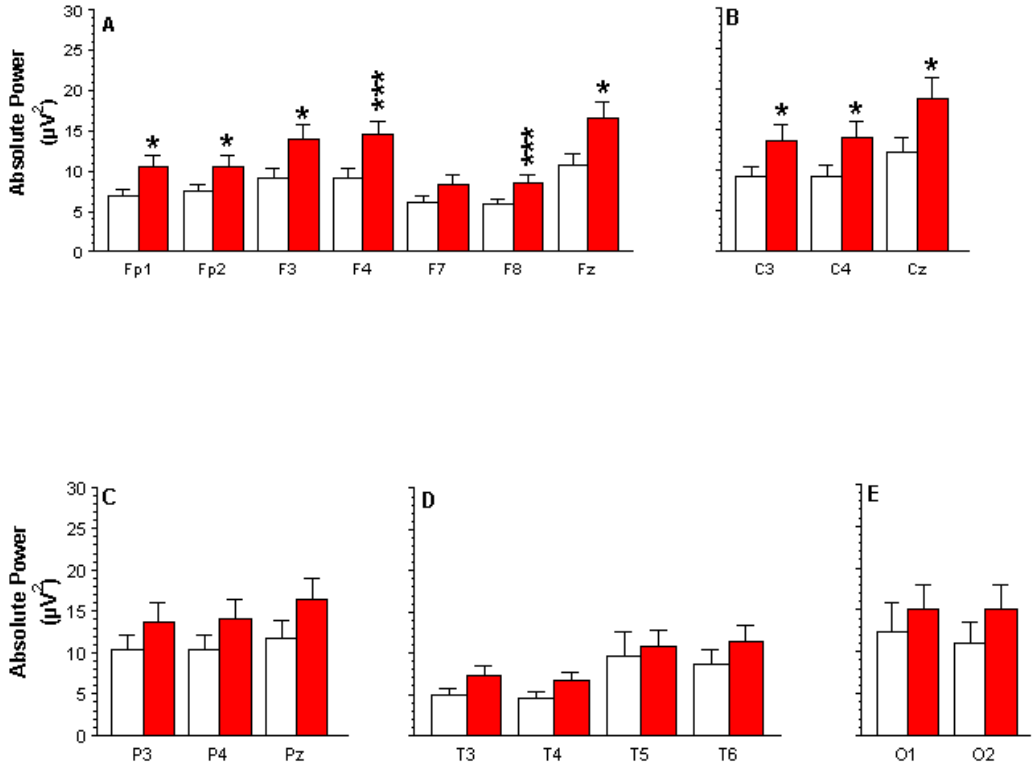

Figure 11: Absolute power of θ frequency in patients with opioid use disorder. (A) The θ power comparisons between opioid patients versus controls measured at the frontal electrodes, Fp1, Fp2, F3, F4, F7, F8, and Fz. (B) The θ power comparisons measured at the central electrodes, C3, C4, and Cz. (C) The θ power comparisons measured at the parietal electrodes, P3, P4, and Pz. (D) The θ power comparisons measured at the temporal electrodes, T3, T4, T5, and T6. (E) The θ power comparisons measured at the occipital electrodes, O1 and O2. Open columns denote the healthy control group and solid red columns denote the opioid group. All data are expressed in mean ± SEM. ∗P < 0.05, ∗∗∗P < 0.001 vs. healthy controls determined by repeated measures ANOVA followed by post hoc Fisher's test. NS, P > 0.05 vs. healthy control determined by repeated measures ANOVA.

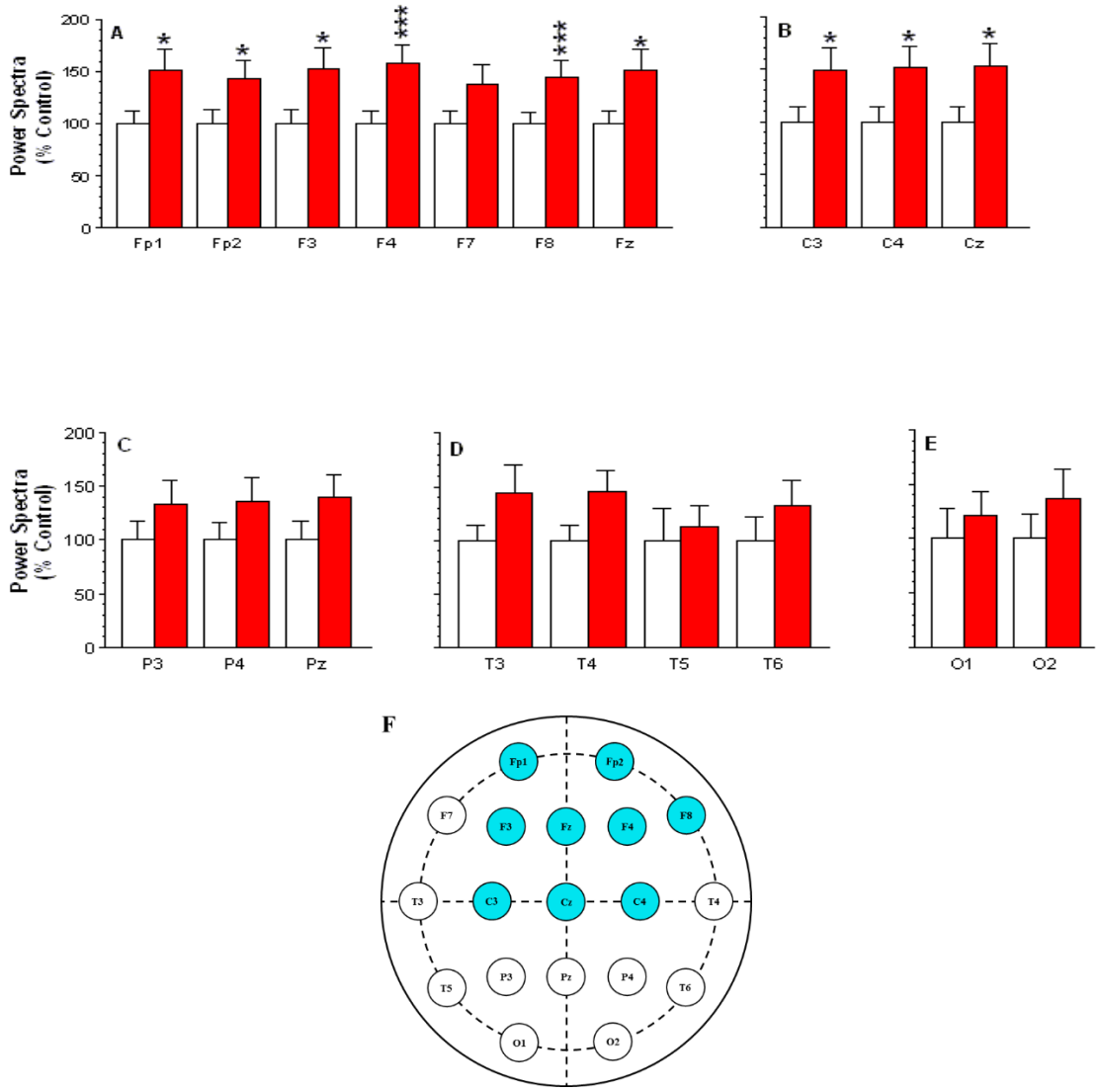

Figure 12: Topographic changes of θ power in patients with opioid use disorder. (A) The θ power percentage change measured at the frontal electrodes, Fp1, Fp2, F3, F4, F7, F8, and Fz. (B) The θ power percentage change measured at the central electrodes, C3, C4, and Cz. (C) The θ power percentage change measured at the parietal electrodes, P3, P4, and Pz. (D) The θ power percentage change measured at the temporal electrodes, T3, T4, T5, and T6. (E) The θ power percentage change measured at the occipital electrodes, O1 and O2. Open columns denote the healthy control group and solid red columns denote the opioid group. All data are expressed in mean ± SEM. ⁎P < 0.05, ⁎⁎⁎P < 0.001 vs. healthy controls determined by repeated measures ANOVA followed by post hoc Fisher's test. NS, P > 0.05 vs. healthy control determined by repeated measures ANOVA. (F) The topographic distribution of percentage power differences between opioid users and healthy controls. The blue electrodes represent medium increases (36-60%) in activity; and the clear electrodes represent no change (<15%) in activity.

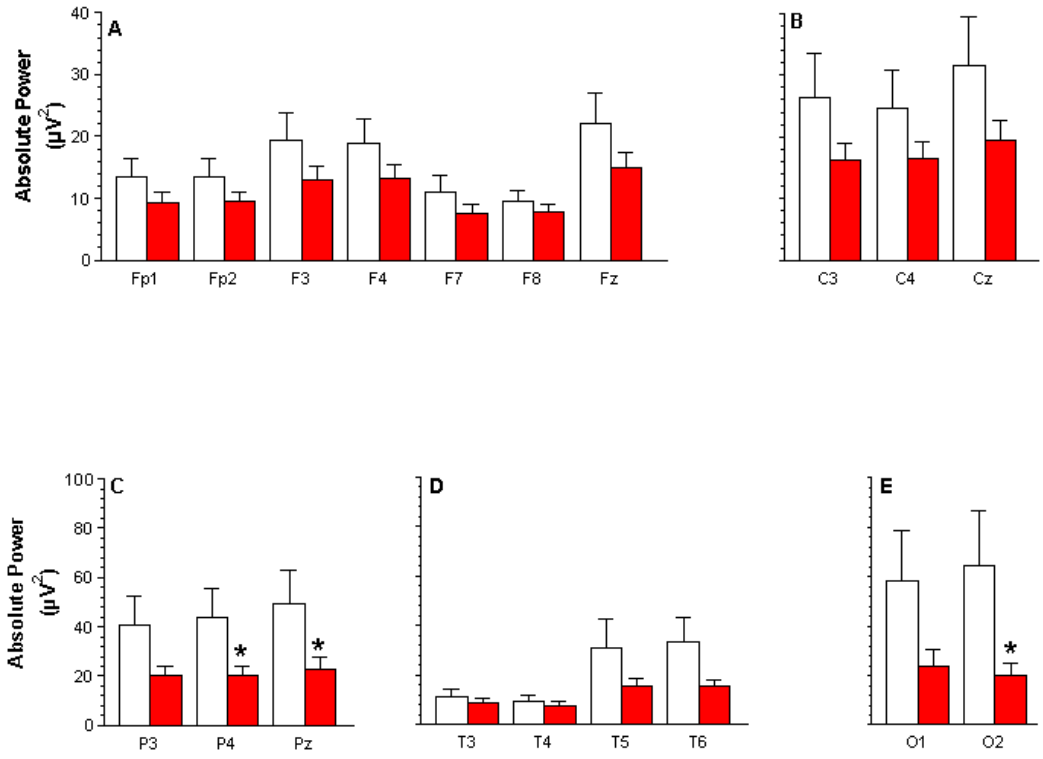

Figure 13: Absolute power of α frequency in patients with opioid use disorder. (A) The α power comparisons between opioid patients versus controls measured at the frontal electrodes, Fp1, Fp2, F3, F4, F7, F8, and Fz. (B) The α power comparisons measured at the central electrodes, C3, C4, and Cz. (C) The α power comparisons measured at the parietal electrodes, P3, P4, and Pz. (D) The α power comparisons measured at the temporal electrodes, T3, T4, T5, and T6. (E) The α power comparisons measured at the occipital electrodes, O1 and O2. Open columns denote the healthy control group and solid red columns denote the opioid group. All data are expressed in mean ± SEM. ∗P < 0.05 vs. healthy controls determined by repeated measures ANOVA followed by post hoc Fisher's test. NS, P > 0.05 vs. healthy control determined by repeated measures ANOVA.

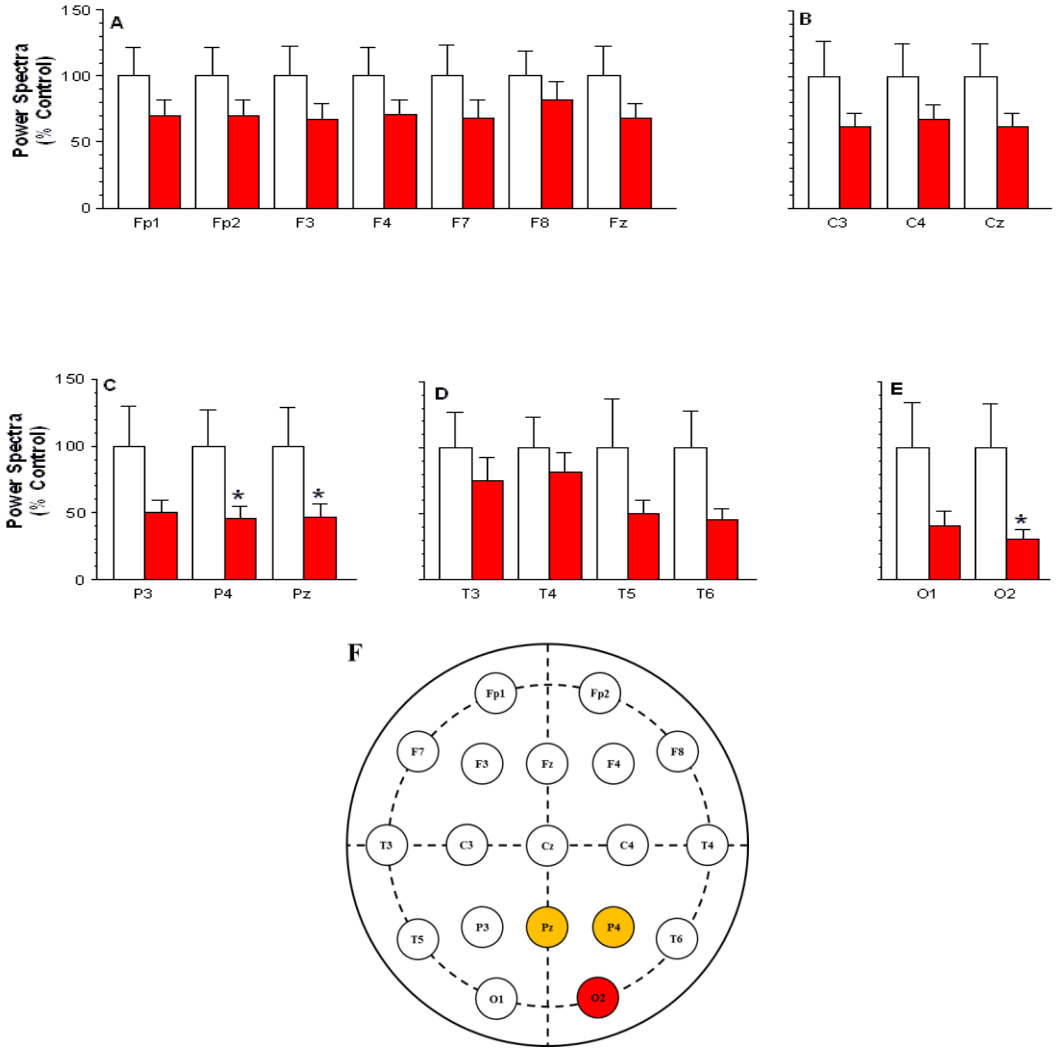

Figure 14: Topographic changes of α power in patients with opioid use disorder. (A) The α power percentage change measured at the frontal electrodes, Fp1, Fp2, F3, F4, F7, F8, and Fz. (B) The α power percentage change measured at the central electrodes, C3, C4, and Cz. (C) The α power percentage change measured at the parietal electrodes, P3, P4, and Pz. (D) The α power percentage change measured at the temporal electrodes, T3, T4, T5, and T6. (E) The α power percentage change measured at the occipital electrodes, O1 and O2. Open columns denote the healthy control group and solid red columns denote the opioid group. All data are expressed in mean ± SEM. ∗P < 0.05 vs. healthy controls determined by repeated measures ANOVA followed by post hoc Fisher's test. NS, P > 0.05 vs. healthy control determined by repeated measures ANOVA. (F) The topographic distribution of percentage power differences between opioid users and healthy controls. The orange electrodes represent medium decreases (36-60%) in activity; the red electrodes represent high decreases (>60%) in activity; and the clear electrodes represent no change (<15%) in activity.

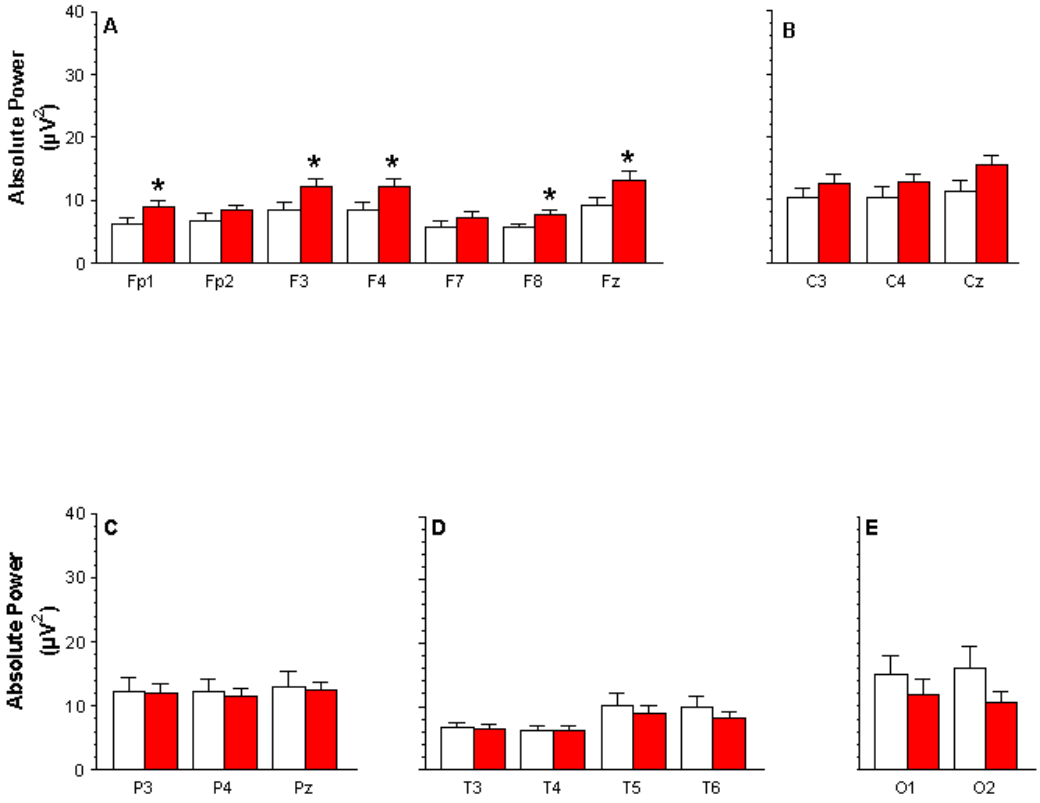

Figure 15: Absolute power of β frequency in patients with opioid use disorder. (A) The β power comparisons between opioid patients versus controls measured at the frontal electrodes, Fp1, Fp2, F3, F4, F7, F8, and Fz. (B) The β power comparisons measured at the central electrodes, C3, C4, and Cz. (C) The β power comparisons measured at the parietal electrodes, P3, P4, and Pz. (D) The β power comparisons measured at the temporal electrodes, T3, T4, T5, and T6. (E) The β power comparisons measured at the occipital electrodes, O1 and O2. Open columns denote the healthy control group and solid red columns denote the opioid group. All data are expressed in mean ± SEM. ∗P < 0.05 vs. healthy controls determined by repeated measures ANOVA followed by post hoc Fisher's test. NS, P > 0.05 vs. healthy control determined by repeated measures ANOVA.

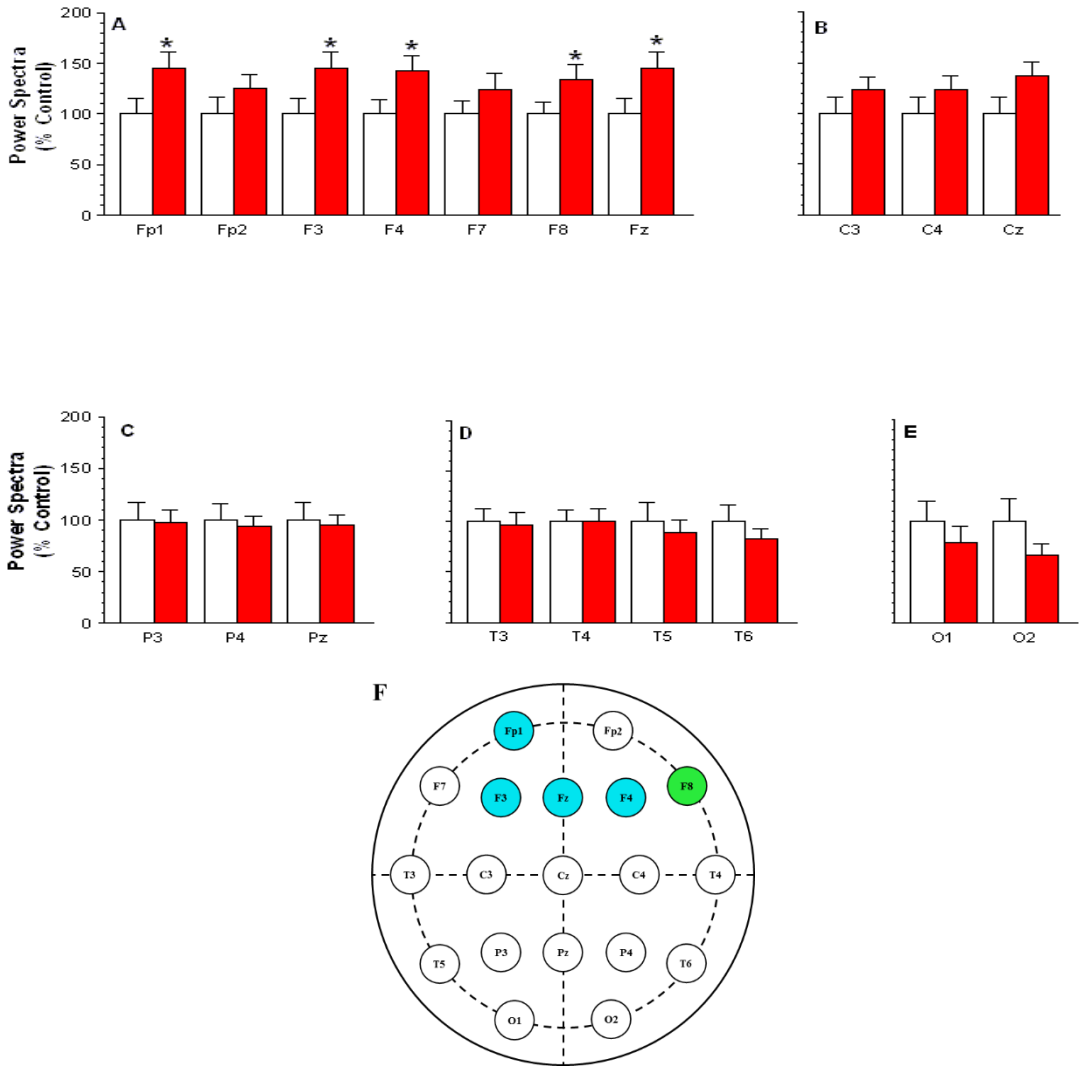

Figure 16: Topographic changes of β power in patients with opioid use disorder. (A) The β power percentage change measured at the frontal electrodes, Fp1, Fp2, F3, F4, F7, F8, and Fz. (B) The β power percentage change measured at the central electrodes, C3, C4, and Cz. (C) The β power percentage change measured at the parietal electrodes, P3, P4, and Pz. (D) The β power percentage change measured at the temporal electrodes, T3, T4, T5, and T6. (E) The β power percentage change measured at the occipital electrodes, O1 and O2. Open columns denote the healthy control group and solid red columns denote the opioid group. All data are expressed in mean ± SEM. ∗P < 0.05 vs. healthy controls determined by repeated measures ANOVA followed by post hoc Fisher's test. NS, P > 0.05 vs. healthy control determined by repeated measures ANOVA. (F) The topographic distribution of percentage power differences between opioid users and healthy controls. The green electrodes represent low increases (16-35%) in activity; blue electrodes represent medium increases (36-60%) in activity; and the clear electrodes represent no change (<15%) in activity.

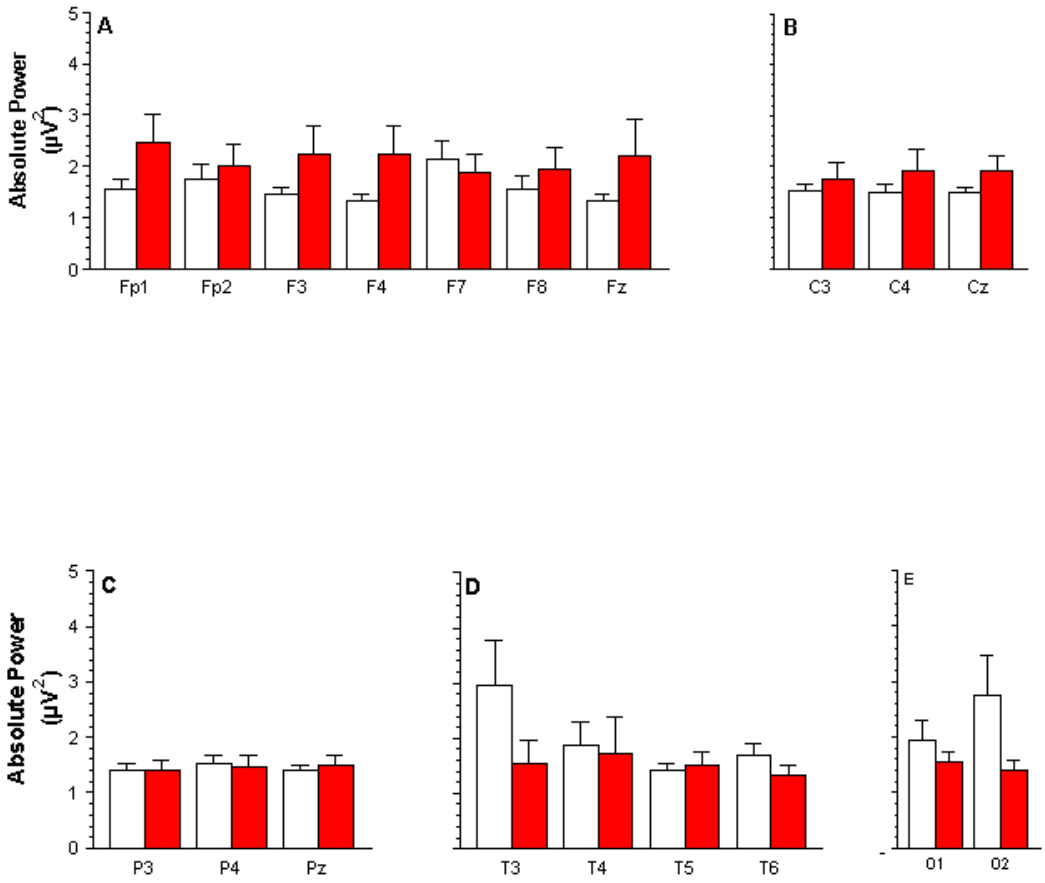

Figure 17: Absolute power of γ frequency in patients with opioid use disorder. (A) The γ power comparisons between opioid patients versus controls measured at the frontal electrodes, Fp1, Fp2, F3, F4, F7, F8, and Fz. (B) The γ power comparisons measured at the central electrodes, C3, C4, and Cz. (C) The γ power comparisons measured at the parietal electrodes, P3, P4, and Pz. (D) The γ power comparisons measured at the temporal electrodes, T3, T4, T5, and T6. (E) The γ power comparisons measured at the occipital electrodes, O1 and O2. Open columns denote the healthy control group and solid red columns denote the opioid group. All data are expressed in mean ± SEM. NS, P > 0.05 vs. healthy control determined by repeated measures ANOVA.

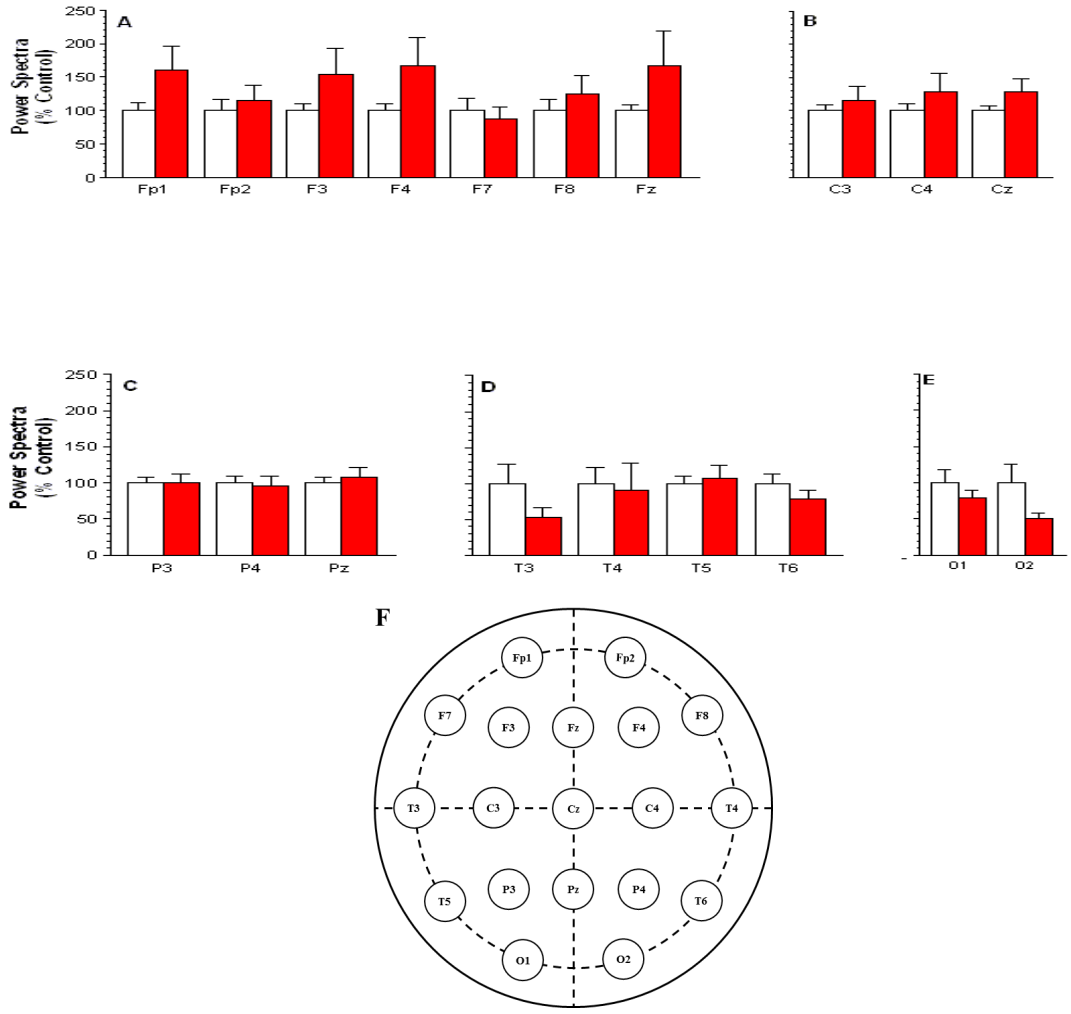

Figure 18: Topographic changes of γ power in patients with opioid use disorder. (A) The γ power percentage change measured at the frontal electrodes, Fp1, Fp2, F3, F4, F7, F8, and Fz. (B) The γ power percentage change measured at the central electrodes, C3, C4, and Cz. (C) The γ power percentage change measured at the parietal electrodes, P3, P4, and Pz. (D) The γ power percentage change measured at the temporal electrodes, T3, T4, T5, and T6. (E) The γ power percentage change measured at the occipital electrodes, O1 and O2. Open columns denote the healthy control group and solid red columns denote the opioid group. All data are expressed in mean ± SEM. NS, P > 0.05 vs. healthy control determined by repeated measures ANOVA. (F) The topographic distribution of percentage power differences between opioid users and healthy controls. The clear electrodes represent no change (<15%) in activity.

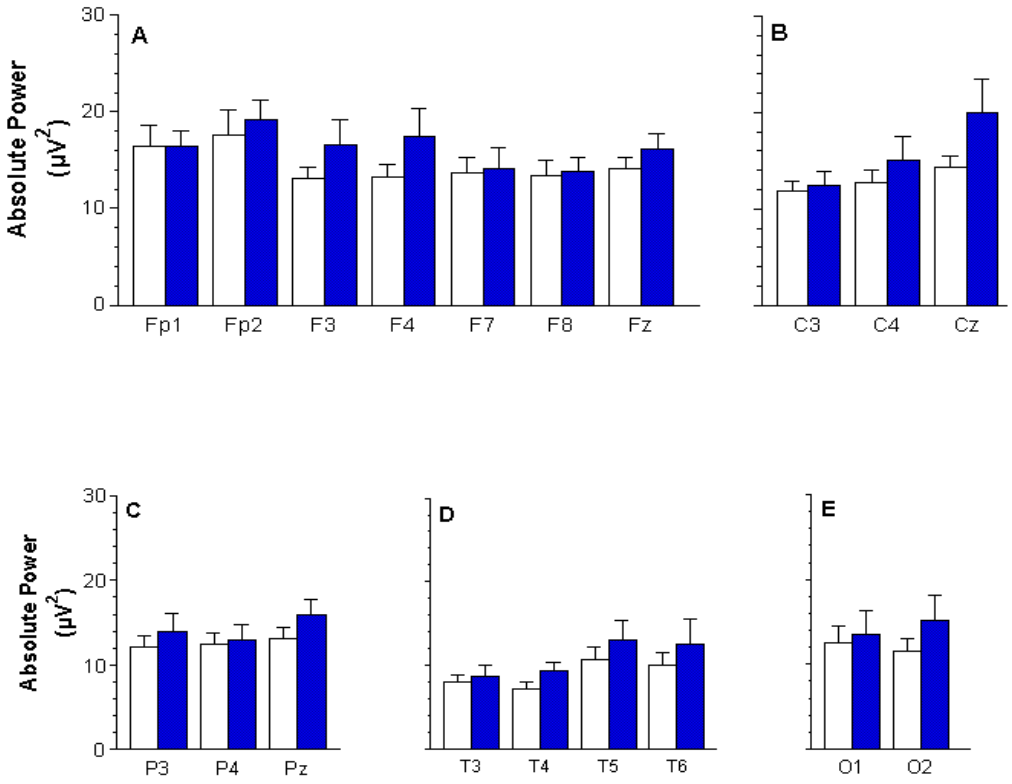

Figure 19: Absolute power of δ frequency in patients with methamphetamine use disorder. (A) The δ power comparisons between methamphetamine patients versus controls measured at the frontal electrodes, Fp1, Fp2, F3, F4, F7, F8, and Fz. (B) The δ power comparisons measured at the central electrodes, C3, C4, and Cz. (C) The δ power comparisons measured at the parietal electrodes, P3, P4, and Pz. (D) The δ power comparisons measured at the temporal electrodes, T3, T4, T5, and T6. (E) The δ power comparisons measured at the occipital electrodes, O1 and O2. Open columns denote the healthy control group and solid blue columns denote the methamphetamine group. All data are expressed in mean ± SEM. NS, P > 0.05 vs. healthy control determined by repeated measures ANOVA.

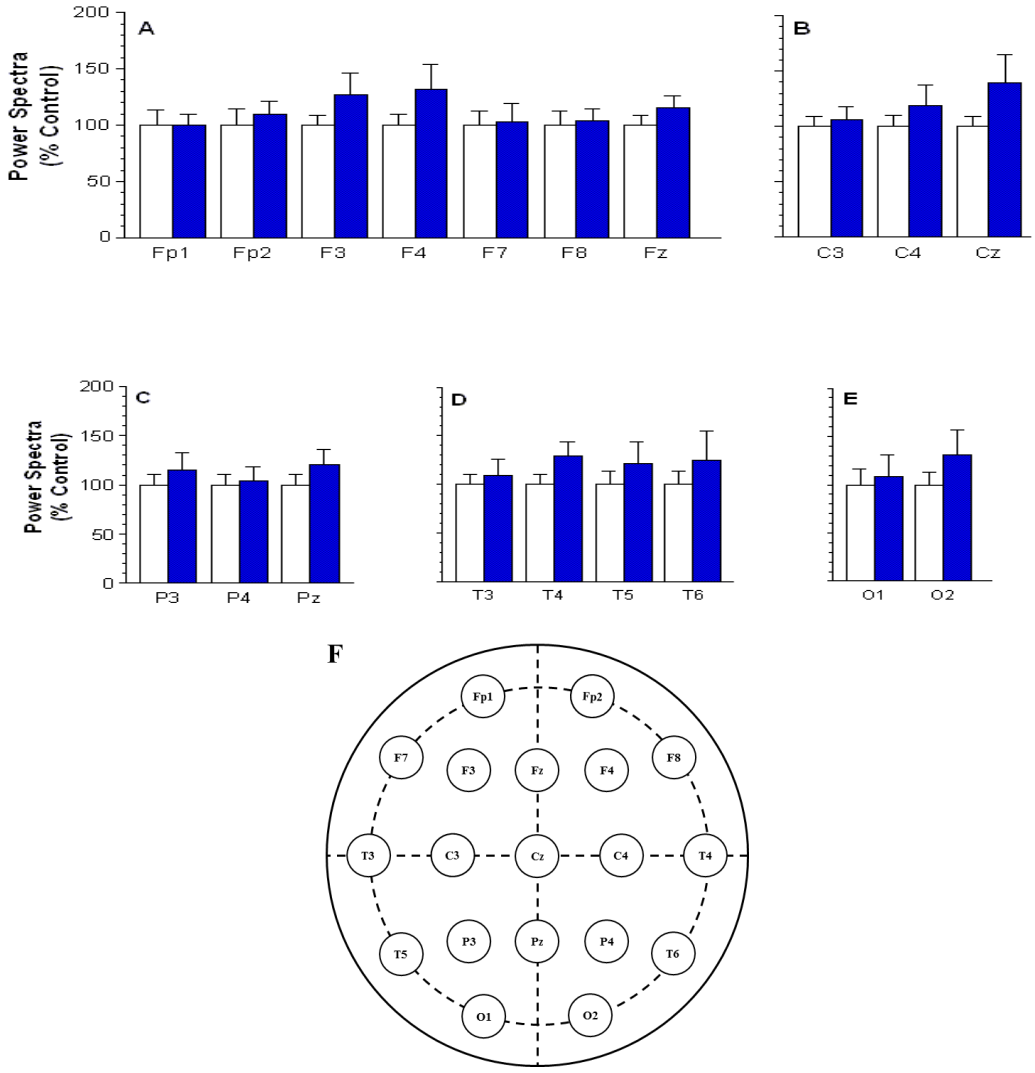

Figure 20: Topographic changes of δ power in patients with methamphetamine use disorder. (A) The δ power percentage change measured at the frontal electrodes, Fp1, Fp2, F3, F4, F7, F8, and Fz. (B) The δ power percentage change measured at the central electrodes, C3, C4, and Cz. (C) The δ power percentage change measured at the parietal electrodes, P3, P4, and Pz. (D) The δ power percentage change measured at the temporal electrodes, T3, T4, T5, and T6. (E) The δ power percentage change measured at the occipital electrodes, O1 and O2. Open columns denote the healthy control group and solid blue columns denote the methamphetamine group. All data are expressed in mean ± SEM. NS, P > 0.05 vs. healthy control determined by repeated measures ANOVA. (F) The topographic distribution of percentage power differences between meth users and healthy controls. The clear electrodes represent no change (<15%) in activity.

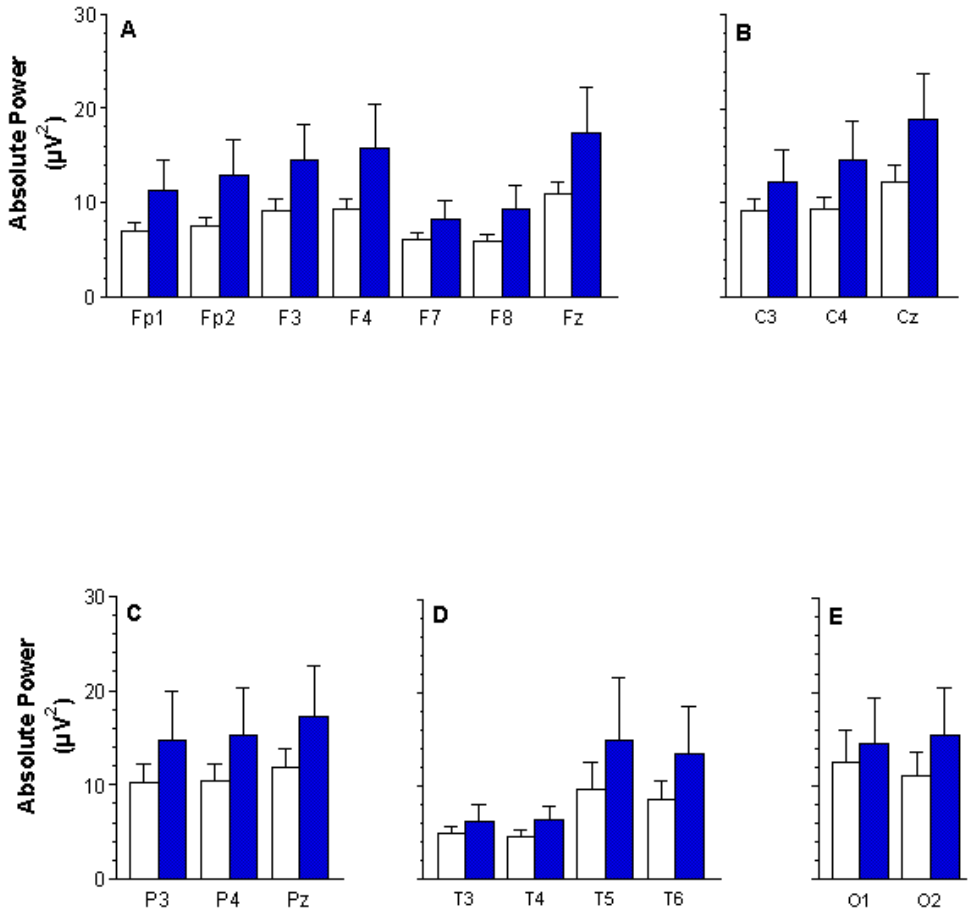

Figure 21: Absolute power of θ frequency in patients with methamphetamine use disorder. (A) The θ power comparisons between methamphetamine patients versus controls measured at the frontal electrodes, Fp1, Fp2, F3, F4, F7, F8, and Fz. (B) The θ power comparisons measured at the central electrodes, C3, C4, and Cz. (C) The θ power comparisons measured at the parietal electrodes, P3, P4, and Pz. (D) The θ power comparisons measured at the temporal electrodes, T3, T4, T5, and T6. (E) The θ power comparisons measured at the occipital electrodes, O1 and O2. Open columns denote the healthy control group and solid blue columns denote the methamphetamine group. All data are expressed in mean ± SEM. NS, P > 0.05 vs. healthy control determined by repeated measures ANOVA.

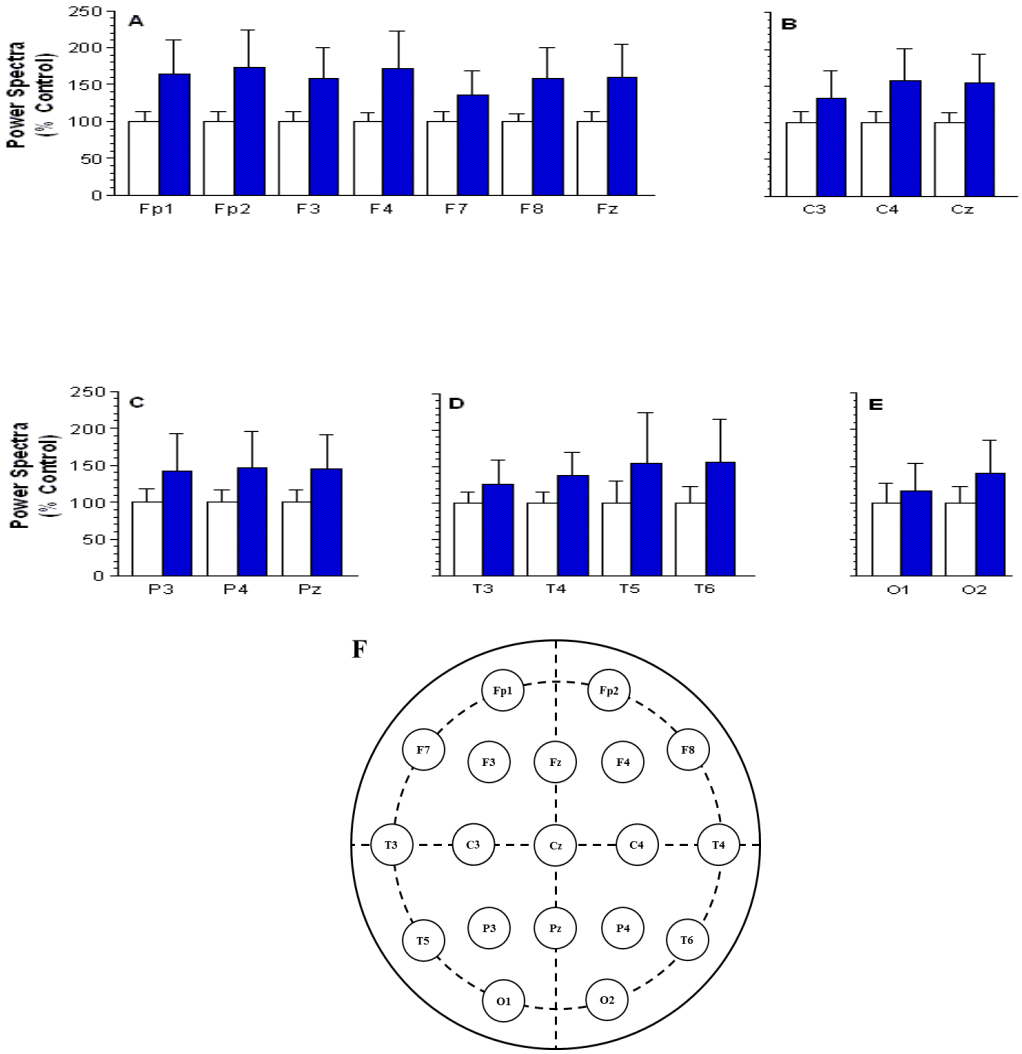

Figure 22: Topographic changes of θ power in patients with methamphetamine use disorder. (A) The θ power percentage change measured at the frontal electrodes, Fp1, Fp2, F3, F4, F7, F8, and Fz. (B) The θ power percentage change measured at the central electrodes, C3, C4, and Cz. (C) The θ power percentage change measured at the parietal electrodes, P3, P4, and Pz. (D) The θ power percentage change measured at the temporal electrodes, T3, T4, T5, and T6. (E) The θ power percentage change measured at the occipital electrodes, O1 and O2. Open columns denote the healthy control group and solid blue columns denote the methamphetamine group. All data are expressed in mean ± SEM. NS, P > 0.05 vs. healthy control determined by repeated measures ANOVA. (F) The topographic distribution of percentage power differences between meth users and healthy controls. The clear electrodes represent no change (<15%) in activity.

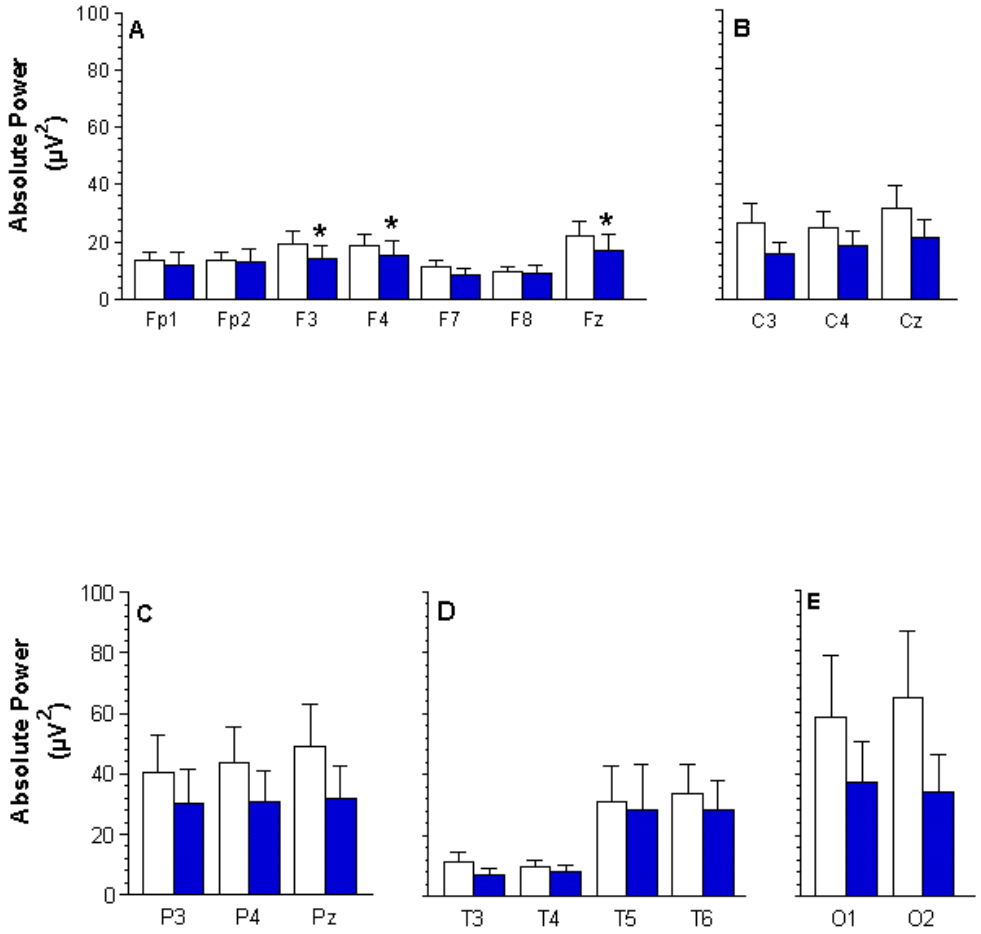

Figure 23: Absolute power of α frequency in patients with methamphetamine use disorder. (A) The α power comparisons between methamphetamine patients versus controls measured at the frontal electrodes, Fp1, Fp2, F3, F4, F7, F8, and Fz. (B) The α power comparisons measured at the central electrodes, C3, C4, and Cz. (C) The α power comparisons measured at the parietal electrodes, P3, P4, and Pz. (D) The α power comparisons measured at the temporal electrodes, T3, T4, T5, and T6. (E) The α power comparisons measured at the occipital electrodes, O1 and O2. Open columns denote the healthy control group and solid blue columns denote the methamphetamine group All data are expressed in mean ± SEM. ∗P < 0.05 vs. healthy controls determined by repeated measures ANOVA followed by post hoc Fisher's test. NS, P > 0.05 vs. healthy control determined by repeated measures ANOVA.

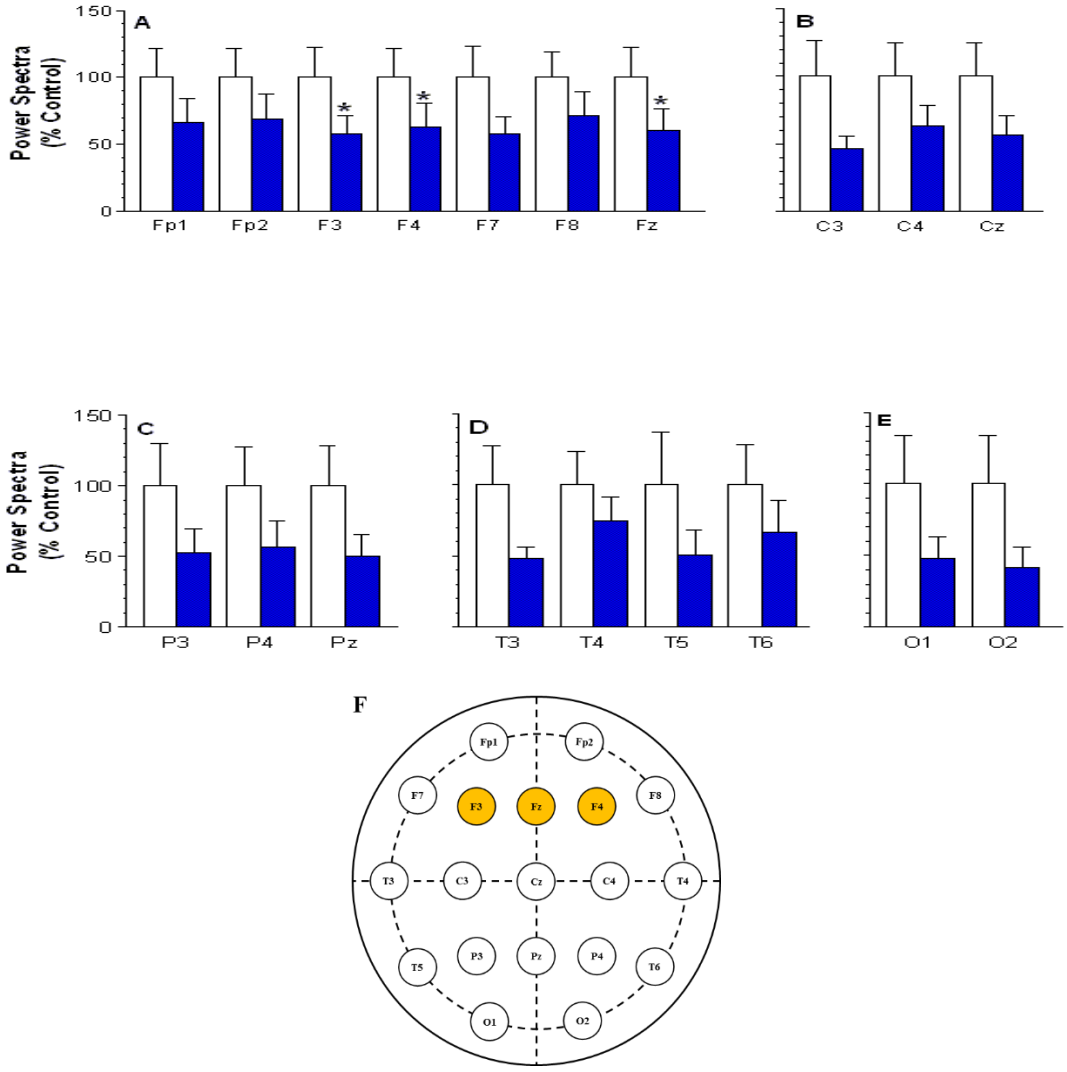

Figure 24: Topographic changes of α power in patients with methamphetamine use disorder. (A) The α power percentage change measured at the frontal electrodes, Fp1, Fp2, F3, F4, F7, F8, and Fz. (B) The α power percentage change measured at the central electrodes, C3, C4, and Cz. (C) The α power percentage change measured at the parietal electrodes, P3, P4, and Pz. (D) The α power percentage change measured at the temporal electrodes, T3, T4, T5, and T6. (E) The α power percentage change measured at the occipital electrodes, O1 and O2. Open columns denote the healthy control group and solid blue columns denote the methamphetamine group. All data are expressed in mean ± SEM. ∗P < 0.05 vs. healthy controls determined by repeated measures ANOVA followed by post hoc Fisher's test. NS, P > 0.05 vs. healthy control determined by repeated measures ANOVA. (F) The topographic distribution of percentage power differences between meth users and healthy controls. The orange electrodes represent medium decreases (36-60%) in activity; and the clear electrodes represent no change (<15%) in activity.

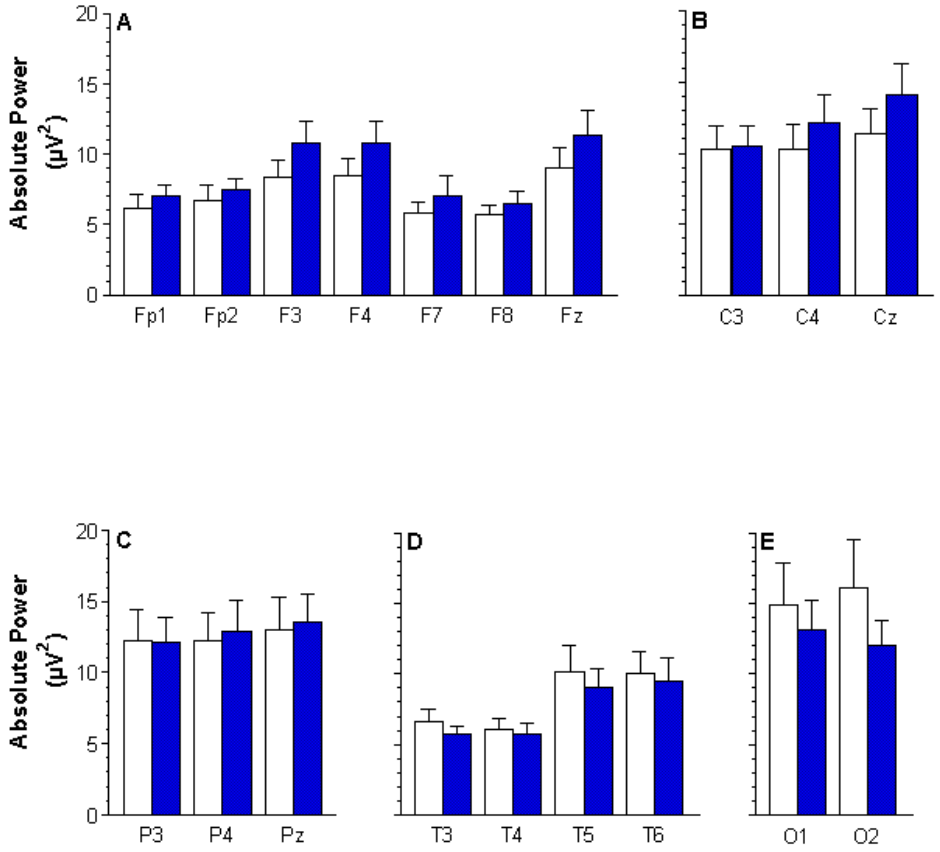

Figure 25: Absolute power of β frequency in patients with methamphetamine use disorder. (A) The β power comparisons between methamphetamine patients versus controls measured at the frontal electrodes, Fp1, Fp2, F3, F4, F7, F8, and Fz. (B) The β power comparisons measured at the central electrodes, C3, C4, and Cz. (C) The β power comparisons measured at the parietal electrodes, P3, P4, and Pz. (D) The β power comparisons measured at the temporal electrodes, T3, T4, T5, and T6. (E) The β power comparisons measured at the occipital electrodes, O1 and O2. Open columns denote the healthy control group and solid blue columns denote the methamphetamine group. All data are expressed in mean ± SEM. NS, P > 0.05 vs. healthy control determined by repeated measures ANOVA.

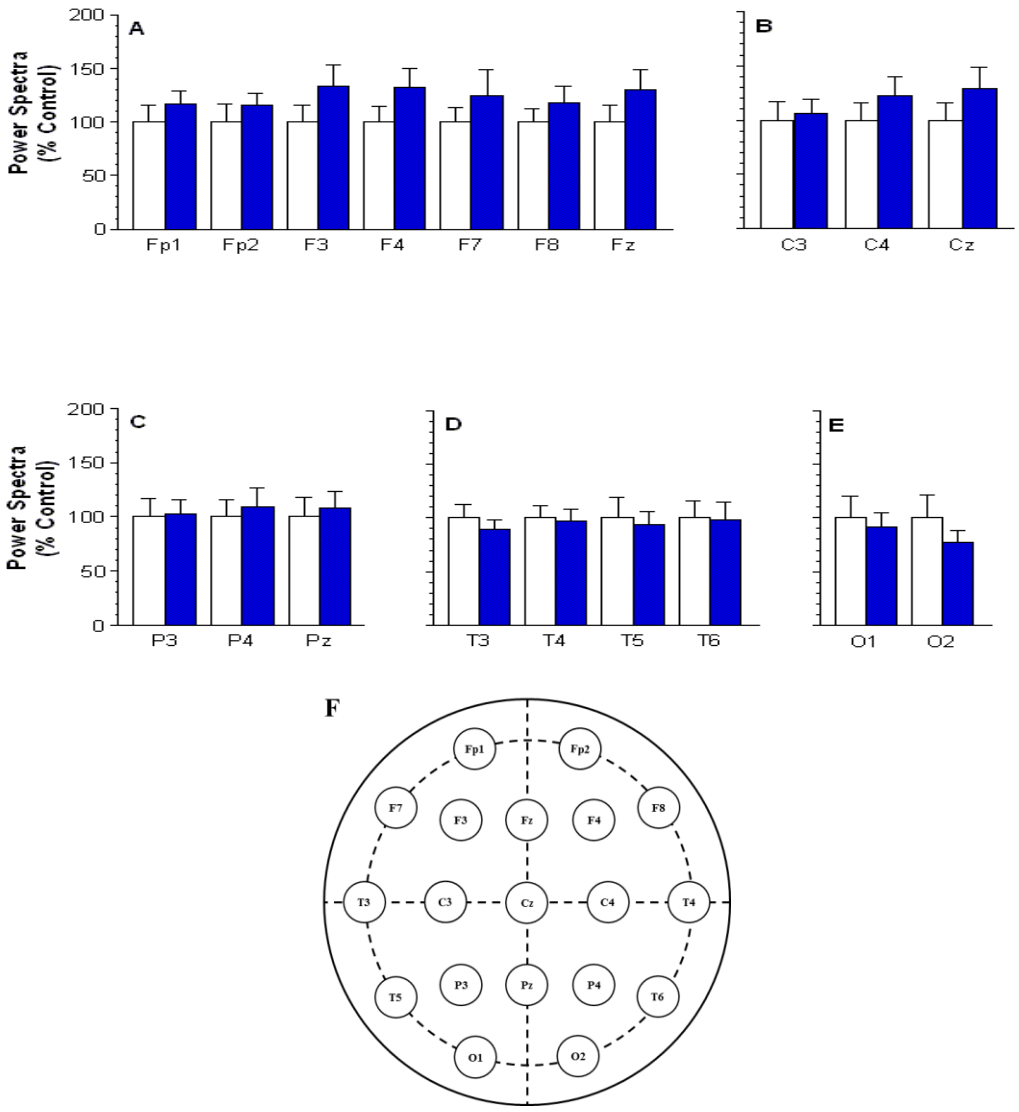

Figure 26: Topographic changes of β power in patients with methamphetamine use disorder. (A) The β power percentage change measured at the frontal electrodes, Fp1, Fp2, F3, F4, F7, F8, and Fz. (B) The β power percentage change measured at the central electrodes, C3, C4, and Cz. (C) The β power percentage change measured at the parietal electrodes, P3, P4, and Pz. (D) The β power percentage change measured at the temporal electrodes, T3, T4, T5, and T6. (E) The β power percentage change measured at the occipital electrodes, O1 and O2. Open columns denote the healthy control group and solid blue columns denote the methamphetamine group. All data are expressed in mean ± SEM. NS, P > 0.05 vs. healthy control determined by repeated measures ANOVA. (F) The topographic distribution of percentage power differences between meth users and healthy controls. The clear electrodes represent no change (<15%) in activity.

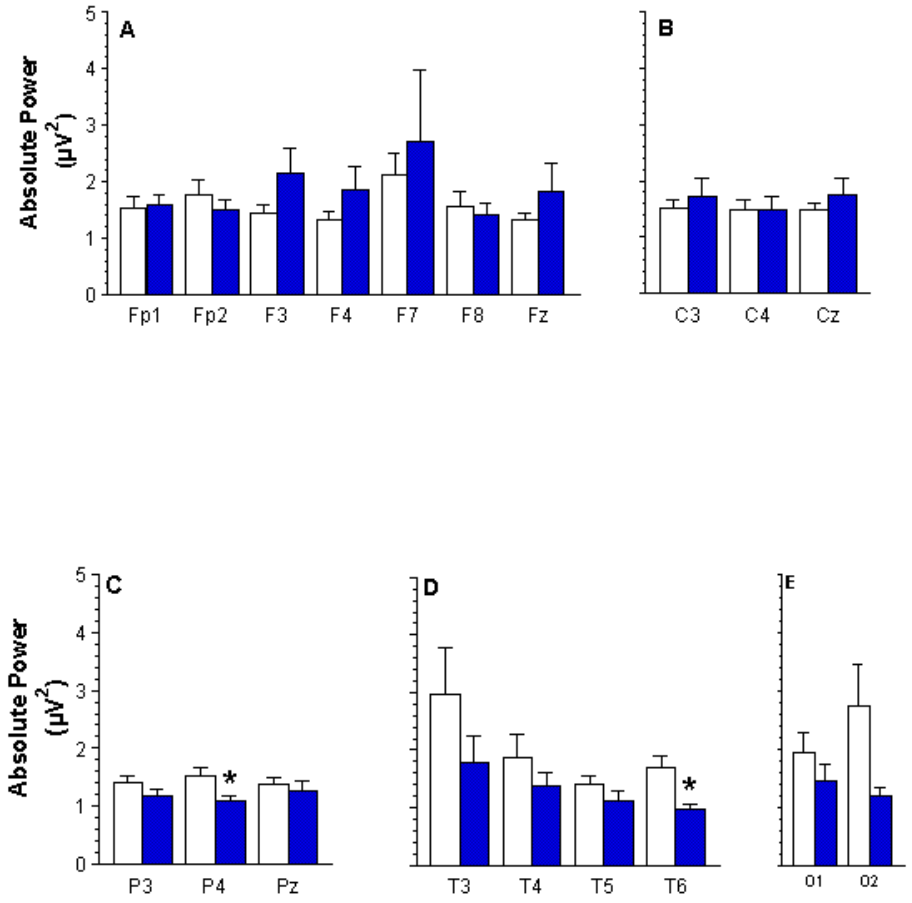

Figure 27: Absolute power of γ frequency in patients with methamphetamine use disorder. (A) The γ power comparisons between methamphetamine patients versus controls measured at the frontal electrodes, Fp1, Fp2, F3, F4, F7, F8, and Fz. (B) The γ power comparisons measured at the central electrodes, C3, C4, and Cz. (C) The γ power comparisons measured at the parietal electrodes, P3, P4, and Pz. (D) The γ power comparisons measured at the temporal electrodes, T3, T4, T5, and T6. (E) The γ power comparisons measured at the occipital electrodes, O1 and O2. Open columns denote the healthy control group and solid blue columns denote the methamphetamine group All data are expressed in mean ± SEM. ∗P < 0.05 vs. healthy controls determined by repeated measures ANOVA followed by post hoc Fisher's test. NS, P > 0.05 vs. healthy control determined by repeated measures ANOVA.

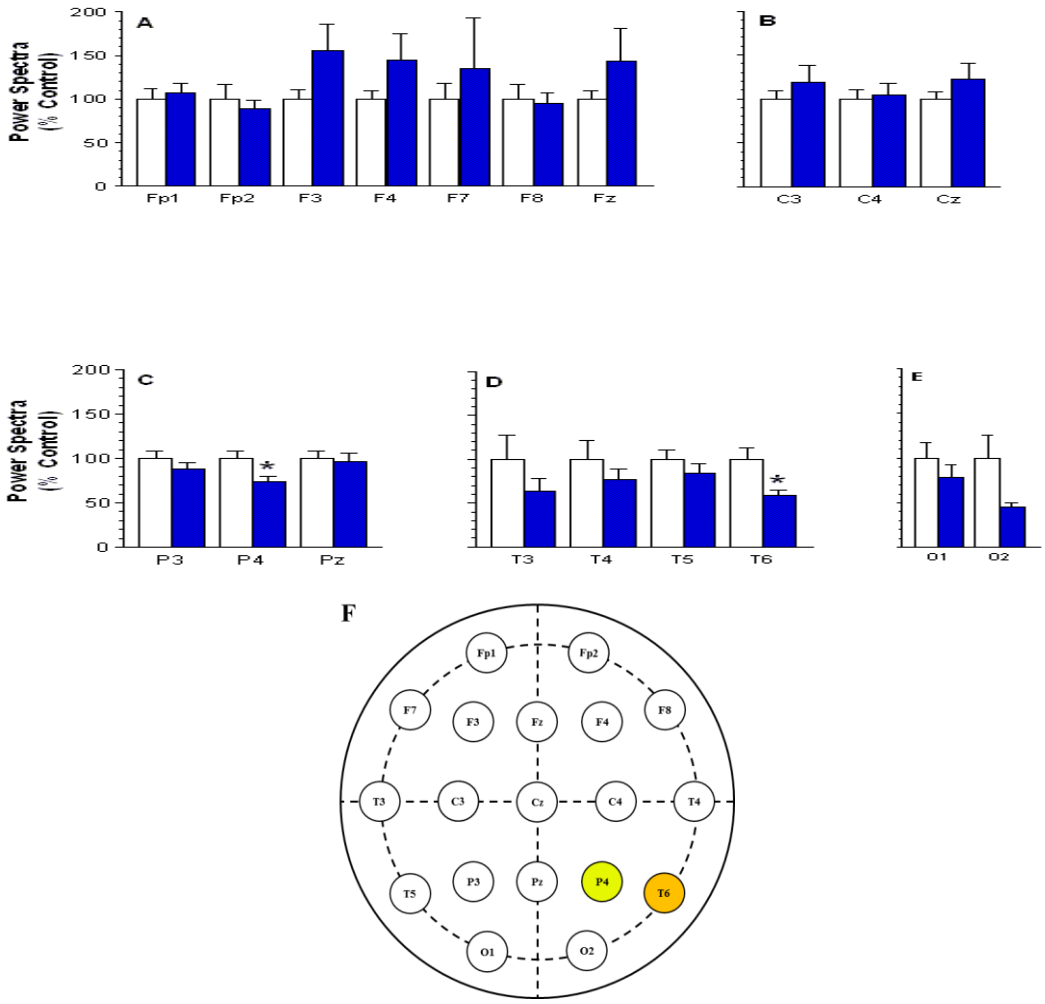

Figure 28: Topographic changes of γ power in patients with methamphetamine use disorder. (A) The γ power percentage change measured at the frontal electrodes, Fp1, Fp2, F3, F4, F7, F8, and Fz. (B) The γ power percentage change measured at the central electrodes, C3, C4, and Cz. (C) The γ power percentage change measured at the parietal electrodes, P3, P4, and Pz. (D) The γ power percentage change measured at the temporal electrodes, T3, T4, T5, and T6. (E) The γ power percentage change measured at the occipital electrodes, O1 and O2. Open columns denote the healthy control group and solid blue columns denote the methamphetamine group. All data are expressed in mean ± SEM. ∗P < 0.05 vs. healthy controls determined by repeated measures ANOVA followed by post hoc Fisher's test. NS, P > 0.05 vs. healthy control determined by repeated measures ANOVA. (F) The topographic distribution of percentage power differences between meth users and healthy controls. The yellow electrodes represent low decreases (16-35%) in activity; the orange electrodes represent medium decreases (36-60%) in activity; and the clear electrodes represent no change (<15%) in activity.

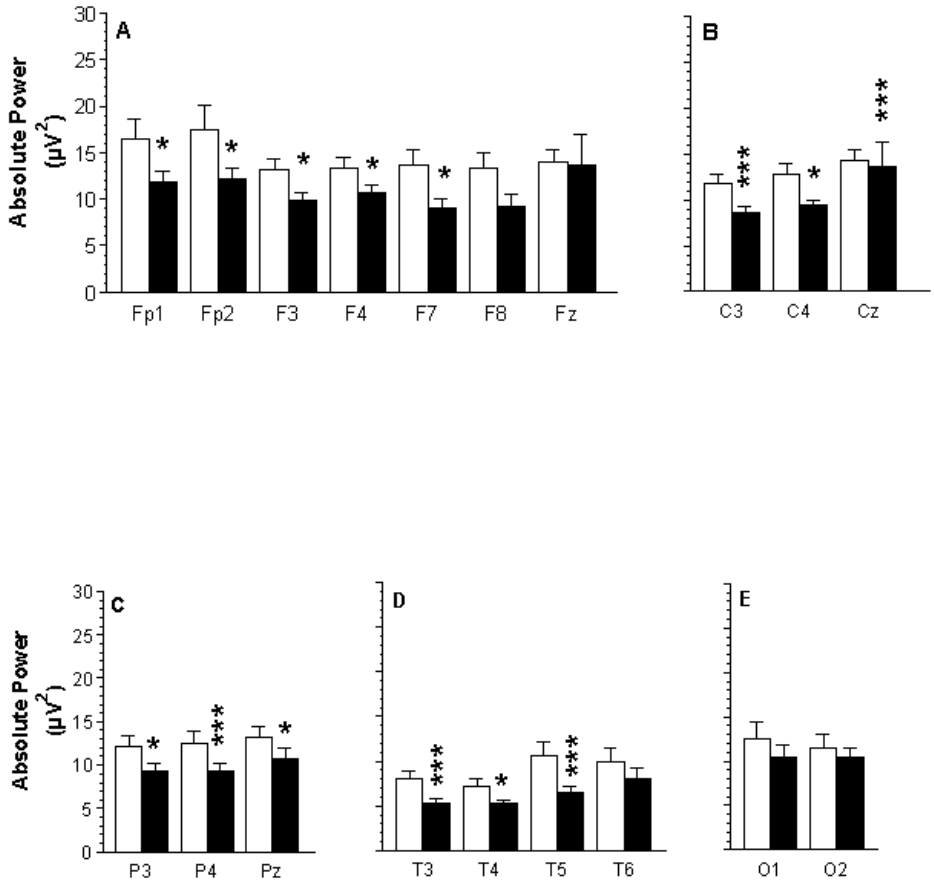

Figure 29: Absolute power of δ frequency in patients with alcohol use disorder. (A) The δ power comparisons between alcohol patients versus controls measured at the frontal electrodes, Fp1, Fp2, F3, F4, F7, F8, and Fz. (B) The δ power comparisons measured at the central electrodes, C3, C4, and Cz. (C) The δ power comparisons measured at the parietal electrodes, P3, P4, and Pz. (D) The δ power comparisons measured at the temporal electrodes, T3, T4, T5, and T6. (E) The δ power comparisons measured at the occipital electrodes, O1 and O2. Open columns denote the healthy control group and solid black columns denote the alcohol group. All data are expressed in mean ± SEM. ∗P < 0.05, ∗∗∗P < 0.001 vs. healthy controls determined by repeated measures ANOVA followed by post hoc Fisher's test. NS, P > 0.05 vs. healthy control determined by repeated measures ANOVA.

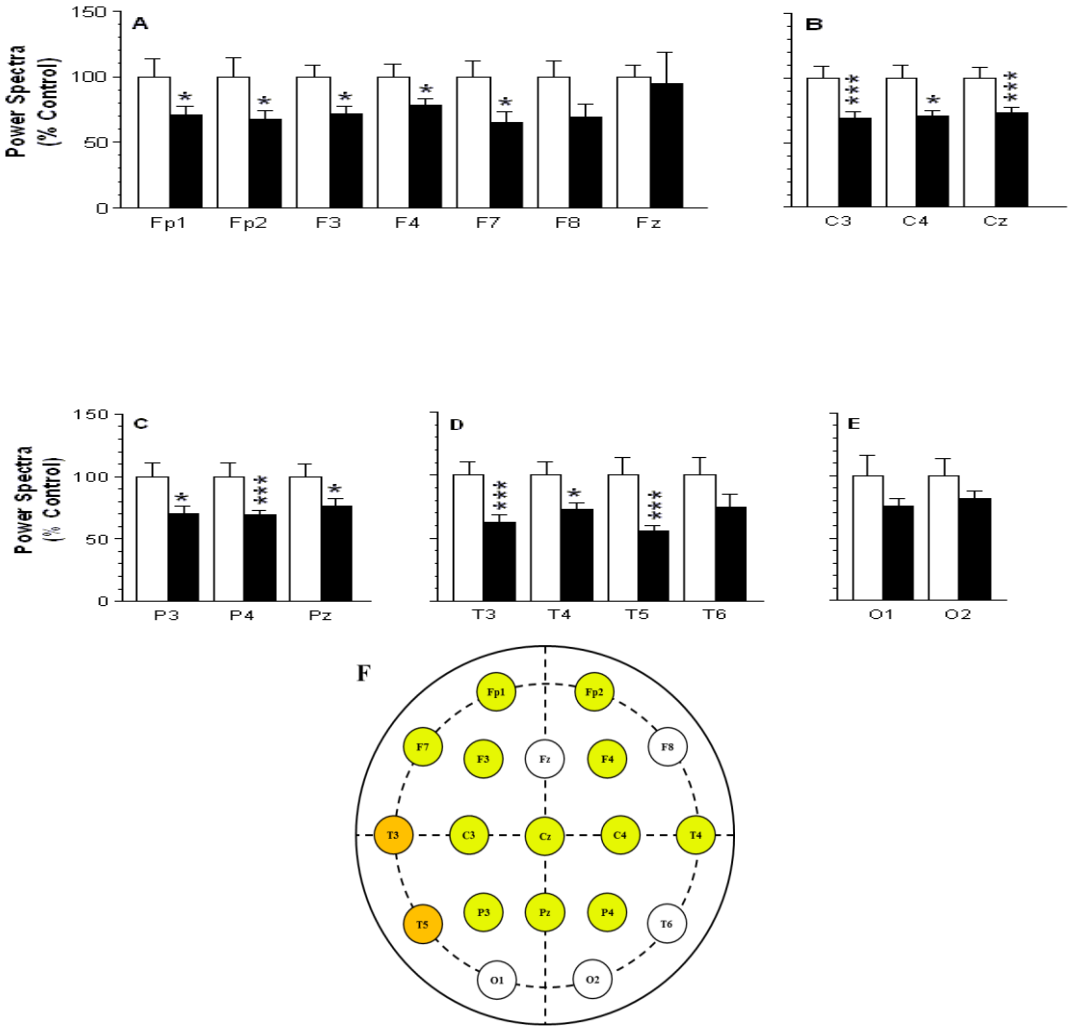

Figure 30: Topographic changes of δ power in patients with alcohol use disorder. (A) The δ power percentage change measured at the frontal electrodes, Fp1, Fp2, F3, F4, F7, F8, and Fz. (B) The δ power percentage change measured at the central electrodes, C3, C4, and Cz. (C) The δ power percentage change measured at the parietal electrodes, P3, P4, and Pz. (D) The δ power percentage change measured at the temporal electrodes, T3, T4, T5, and T6. (E) The δ power percentage change measured at the occipital electrodes, O1 and O2. Open columns denote the healthy control group and solid black columns denote the alcohol group. All data are expressed in mean ± SEM. ⁎P < 0.05, ⁎⁎⁎P < 0.001 vs. healthy controls determined by repeated measures ANOVA followed by post hoc Fisher's test. NS, P > 0.05 vs. healthy control determined by repeated measures ANOVA. (F) The topographic distribution of percentage power differences between alcohol users and healthy controls. The yellow electrodes represent low decreases (16-35%) in activity; the orange electrodes represent medium decreases (36-60%) in activity; and the clear electrodes represent no change (<15%) in activity.

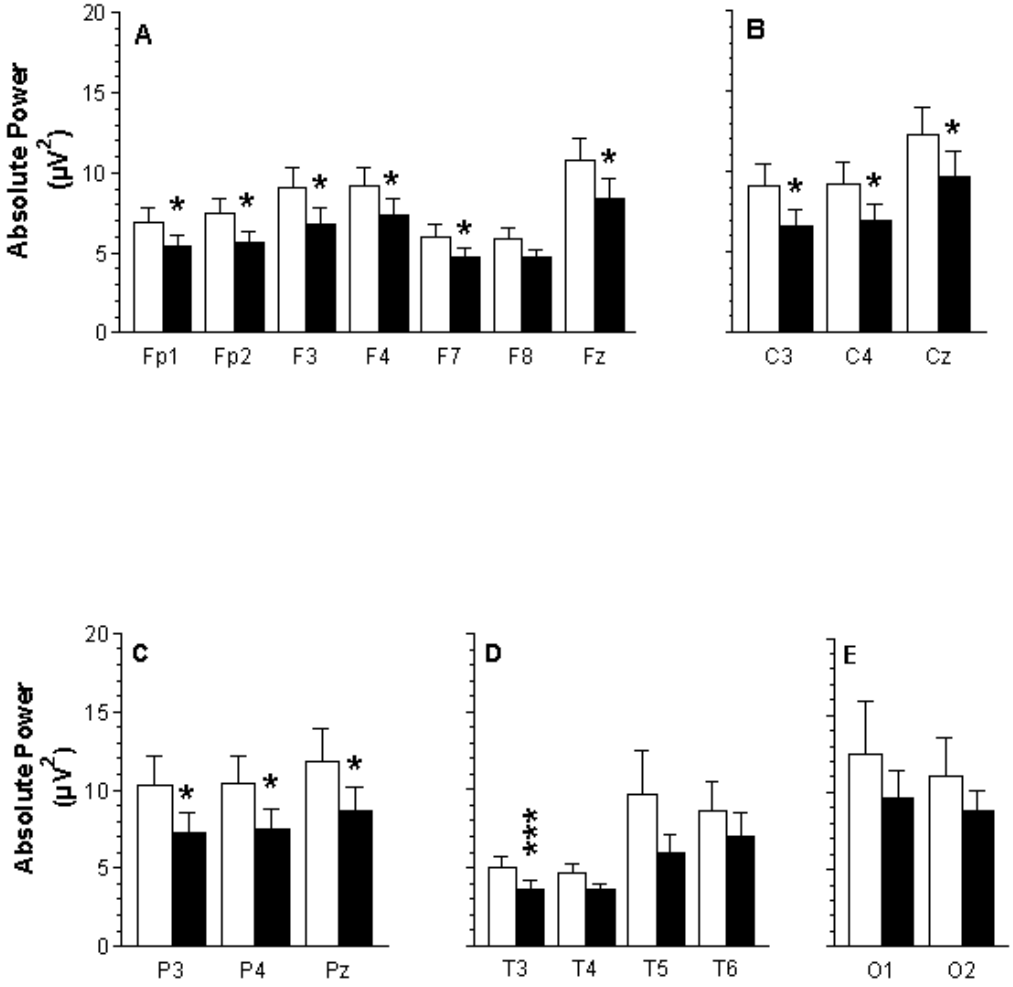

Figure 31: Absolute power of θ frequency in patients with alcohol use disorder. (A) The δ power comparisons between alcohol patients versus controls measured at the frontal electrodes, Fp1, Fp2, F3, F4, F7, F8, and Fz. (B) The δ power comparisons measured at the central electrodes, C3, C4, and Cz. (C) The δ power comparisons measured at the parietal electrodes, P3, P4, and Pz. (D) The δ power comparisons measured at the temporal electrodes, T3, T4, T5, and T6. (E) The δ power comparisons measured at the occipital electrodes, O1 and O2. Open columns denote the healthy control group and solid black columns denote the alcohol group. All data are expressed in mean ± SEM. ⁎P < 0.05, ⁎⁎⁎P < 0.001 vs. healthy controls determined by repeated measures ANOVA followed by post hoc Fisher's test. NS, P > 0.05 vs. healthy control determined by repeated measures ANOVA.

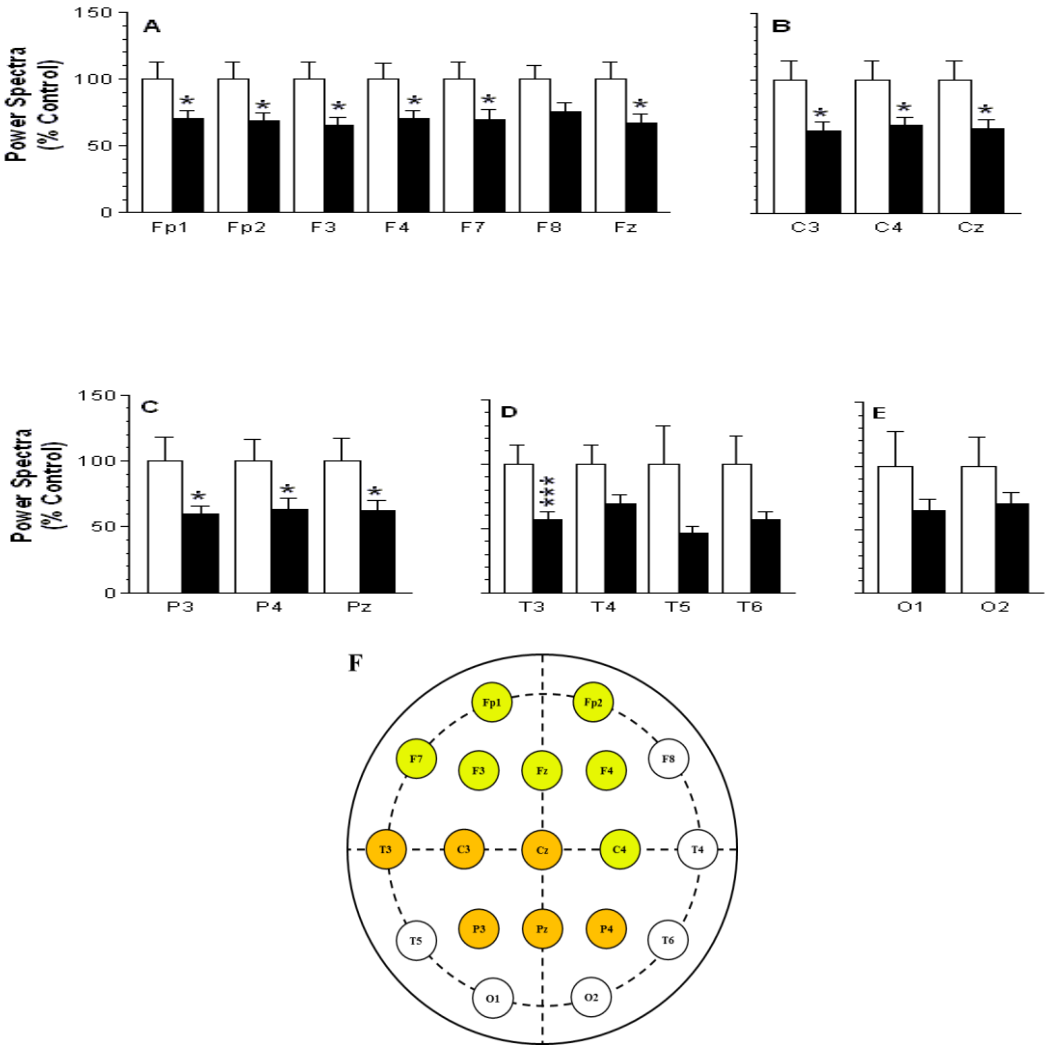

Figure 32: Topographic changes of θ power in patients with alcohol use disorder. (A) The θ power percentage change measured at the frontal electrodes, Fp1, Fp2, F3, F4, F7, F8, and Fz. (B) The θ power percentage change measured at the central electrodes, C3, C4, and Cz. (C) The θ power percentage change measured at the parietal electrodes, P3, P4, and Pz. (D) The θ power percentage change measured at the temporal electrodes, T3, T4, T5, and T6. (E) The θ power percentage change measured at the occipital electrodes, O1 and O2. Open columns denote the healthy control group and solid black columns denote the alcohol group. All data are expressed in mean ± SEM. ∗P < 0.05, ∗∗∗P < 0.001 vs. healthy controls determined by repeated measures ANOVA followed by post hoc Fisher's test. NS, P > 0.05 vs. healthy control determined by repeated measures ANOVA. (F) The topographic distribution of percentage power differences between alcohol users and healthy controls. The yellow electrodes represent low decreases (16-35%) in activity; the orange electrodes represent medium decreases (36-60%) in activity; and the clear electrodes represent no change (<15%) in activity.

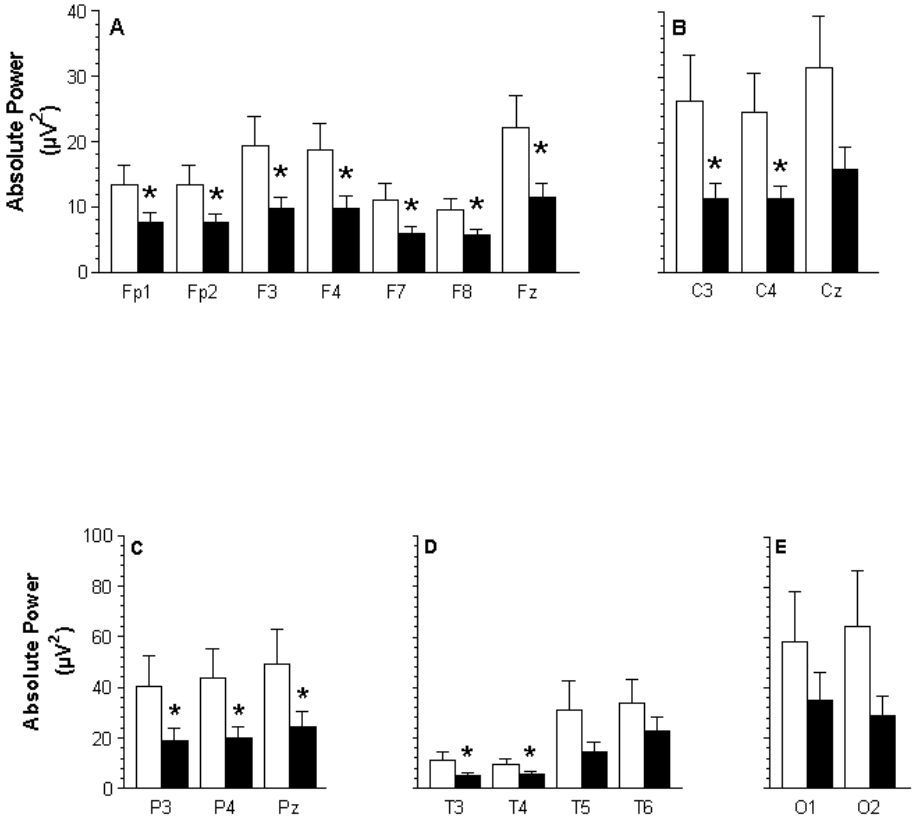

Figure 33: Absolute power of α frequency in patients with alcohol use disorder. (A) The α power comparisons between alcohol patients versus controls measured at the frontal electrodes, Fp1, Fp2, F3, F4, F7, F8, and Fz. (B) The α power comparisons measured at the central electrodes, C3, C4, and Cz. (C) The α power comparisons measured at the parietal electrodes, P3, P4, and Pz. (D) The α power comparisons measured at the temporal electrodes, T3, T4, T5, and T6. (E) The α power comparisons measured at the occipital electrodes, O1 and O2. Open columns denote the healthy control group and solid black columns denote the alcohol group. All data are expressed in mean ± SEM. ∗P < 0.05 vs. healthy controls determined by repeated measures ANOVA followed by post hoc Fisher's test. NS, P > 0.05 vs. healthy control determined by repeated measures ANOVA.

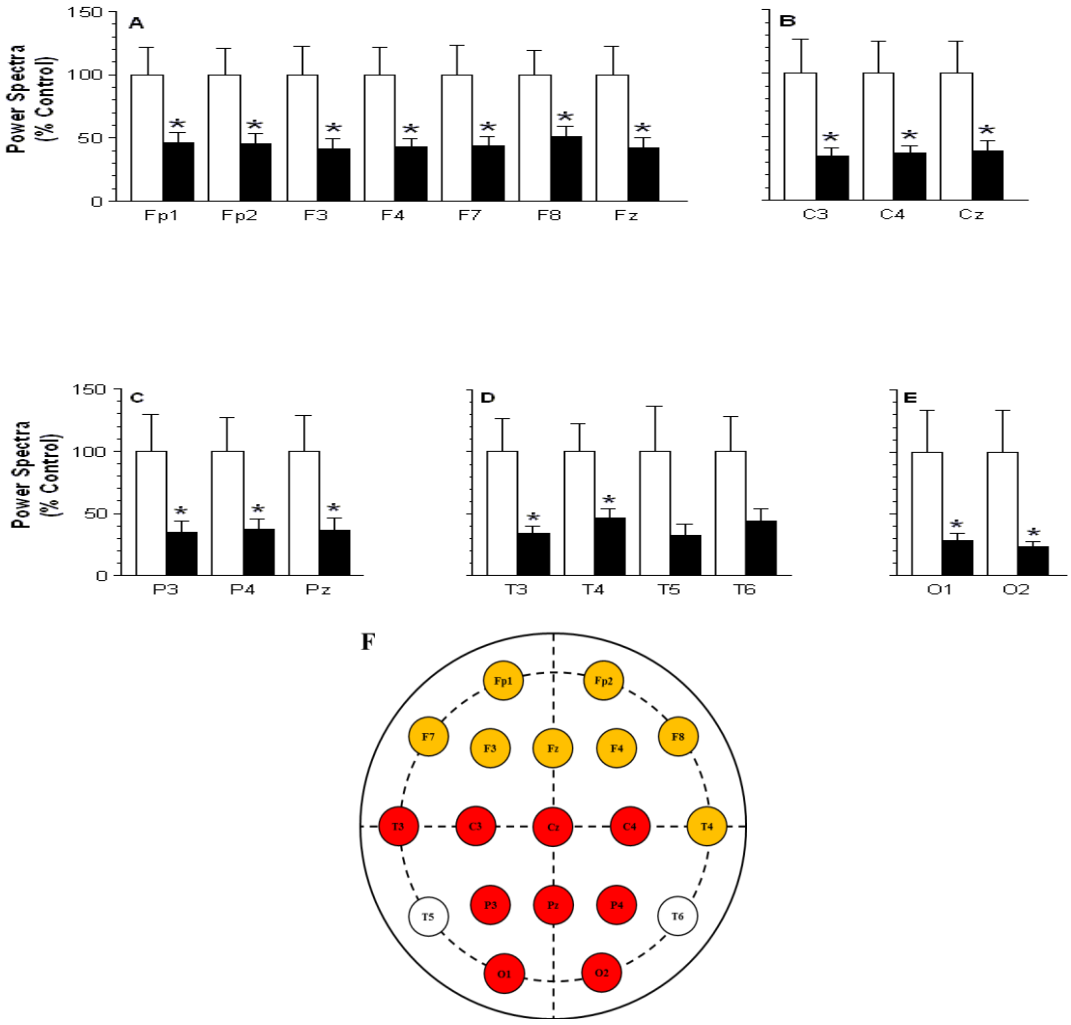

Figure 34: Topographic changes of α power in patients with alcohol use disorder. (A) The α power percentage change measured at the frontal electrodes, Fp1, Fp2, F3, F4, F7, F8, and Fz. (B) The α power percentage change measured at the central electrodes, C3, C4, and Cz. (C) The α power percentage change measured at the parietal electrodes, P3, P4, and Pz. (D) The α power percentage change measured at the temporal electrodes, T3, T4, T5, and T6. (E) The α power percentage change measured at the occipital electrodes, O1 and O2. Open columns denote the healthy control group and solid black columns denote the alcohol group. All data are expressed in mean ± SEM. ∗P < 0.05 vs. healthy controls determined by repeated measures ANOVA followed by post hoc Fisher's test. NS, P > 0.05 vs. healthy control determined by repeated measures ANOVA. (F) The topographic distribution of percentage power differences between alcohol users and healthy controls. The orange electrodes represent medium decreases (36-60%) in activity; the red electrodes represent high decreases (>60%) in activity; and the clear electrodes represent no change (<15%) in activity.

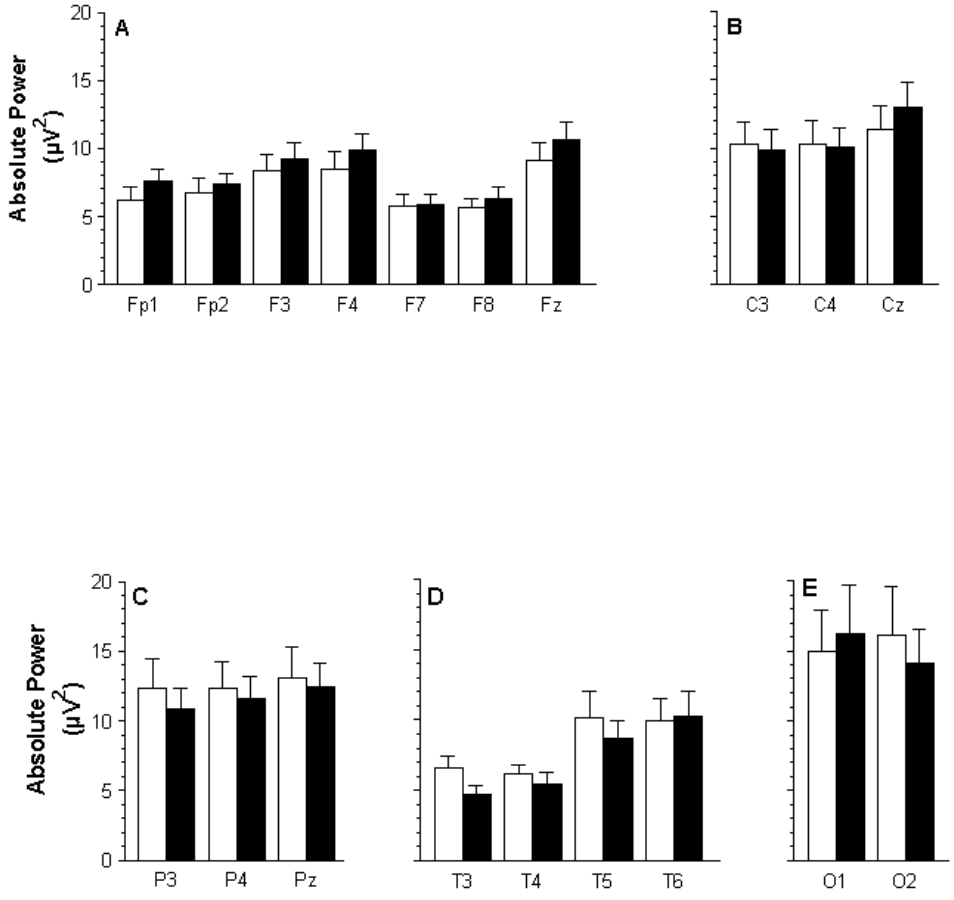

Figure 35: Absolute power of β frequency in patients with alcohol use disorder. (A) The β power comparisons between alcohol patients versus controls measured at the frontal electrodes, Fp1, Fp2, F3, F4, F7, F8, and Fz. (B) The β power comparisons measured at the central electrodes, C3, C4, and Cz. (C) The β power comparisons measured at the parietal electrodes, P3, P4, and Pz. (D) The β power comparisons measured at the temporal electrodes, T3, T4, T5, and T6. (E) The β power comparisons measured at the occipital electrodes, O1 and O2. Open columns denote the healthy control group and solid black columns denote the alcohol group. All data are expressed in mean ± SEM. NS, P > 0.05 vs. healthy control determined by repeated measures ANOVA.

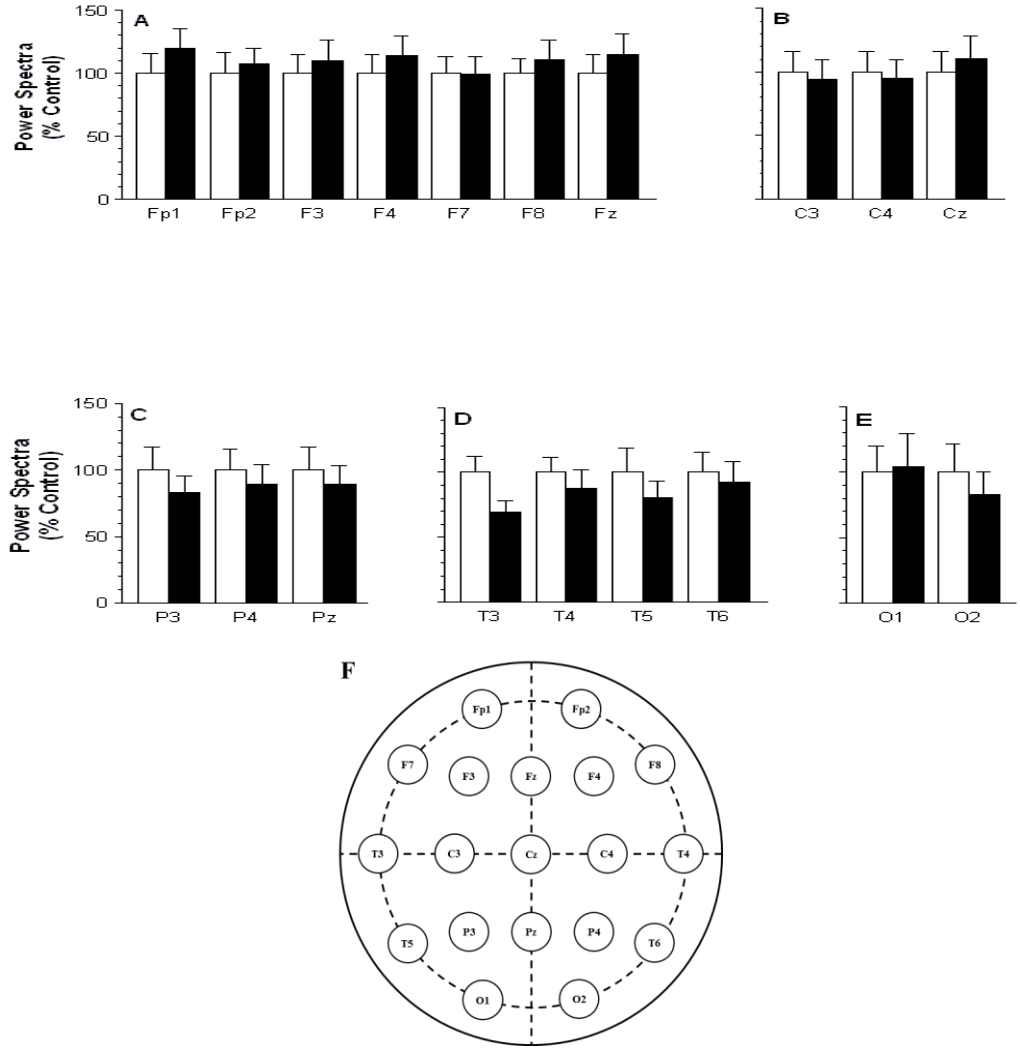

Figure 36: Topographic changes of β power in patients with alcohol use disorder. (A) The β power percentage change measured at the frontal electrodes, Fp1, Fp2, F3, F4, F7, F8, and Fz. (B) The β power percentage change measured at the central electrodes, C3, C4, and Cz. (C) The β power percentage change measured at the parietal electrodes, P3, P4, and Pz. (D) The β power percentage change measured at the temporal electrodes, T3, T4, T5, and T6. (E) The β power percentage change measured at the occipital electrodes, O1 and O2. Open columns denote the healthy control group and solid black columns denote the alcohol group. All data are expressed in mean ± SEM. NS, P > 0.05 vs. healthy control determined by repeated measures ANOVA. (F) The topographic distribution of percentage power differences between alcohol users and healthy controls. The clear electrodes represent no change (<15%) in activity.

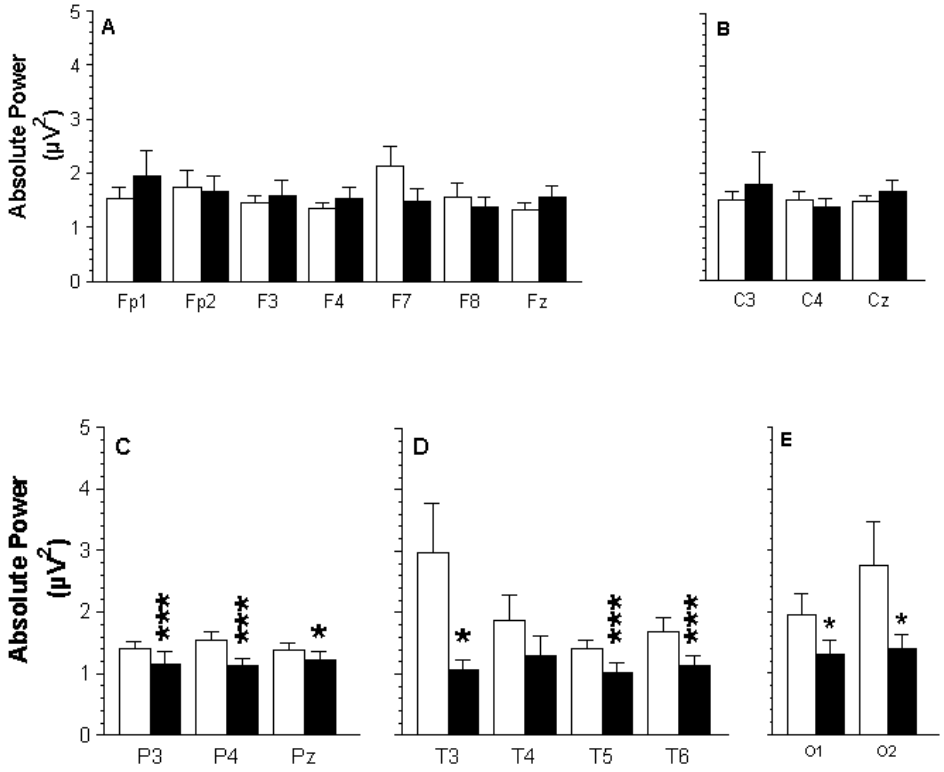

Figure 37: Absolute power of γ frequency in patients with alcohol use disorder. (A) The γ power comparisons between alcohol patients versus controls measured at the frontal electrodes, Fp1, Fp2, F3, F4, F7, F8, and Fz. (B) The γ power comparisons measured at the central electrodes, C3, C4, and Cz. (C) The γ power comparisons measured at the parietal electrodes, P3, P4, and Pz. (D) The γ power comparisons measured at the temporal electrodes, T3, T4, T5, and T6. (E) The γ power comparisons measured at the occipital electrodes, O1 and O2. Open columns denote the healthy control group and solid black columns denote the alcohol group. All data are expressed in mean ± SEM. ∗P < 0.05, ∗∗∗P < 0.001 vs. healthy controls determined by repeated measures ANOVA followed by post hoc Fisher's test. NS, P > 0.05 vs. healthy control determined by repeated measures ANOVA.

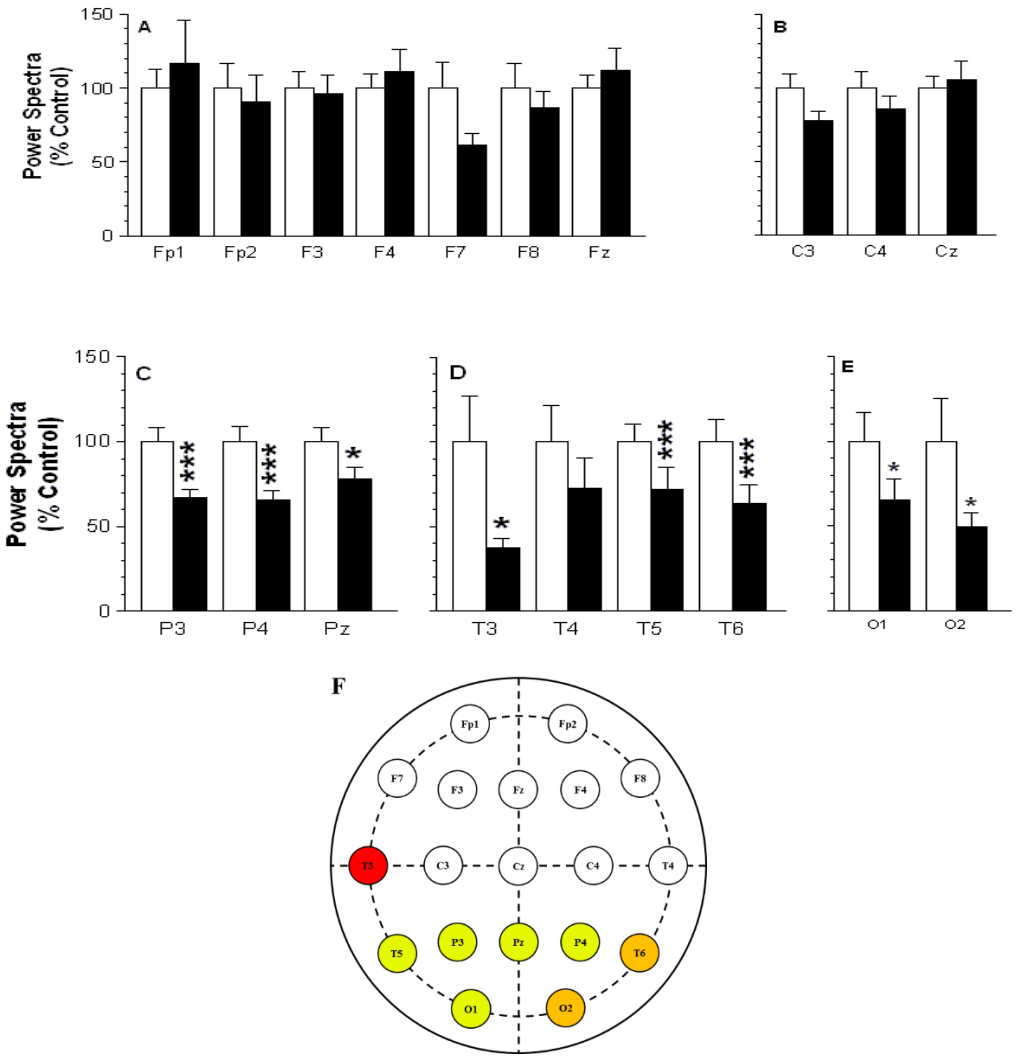

Figure 38: Topographic changes of γ power in patients with alcohol use disorder. (A) The γ power percentage change measured at the frontal electrodes, Fp1, Fp2, F3, F4, F7, F8, and Fz. (B) The γ power percentage change measured at the central electrodes, C3, C4, and Cz. (C) The γ power percentage change measured at the parietal electrodes, P3, P4, and Pz. (D) The γ power percentage change measured at the temporal electrodes, T3, T4, T5, and T6. (E) The γ power percentage change measured at the occipital electrodes, O1 and O2. Open columns denote the healthy control group and solid black columns denote the alcohol group. All data are expressed in mean ± SEM. ⁎P < 0.05, ⁎⁎⁎P < 0.001 vs. healthy controls determined by repeated measures ANOVA followed by post hoc Fisher's test. NS, P > 0.05 vs. healthy control determined by repeated measures ANOVA. (F) The topographic distribution of percentage power differences between alcohol users and healthy controls. The yellow electrodes represent low decreases (16-35%) in activity; orange electrodes represent medium decreases (36-60%) in activity; the red electrodes represent high decreases (>60%) in activity; The clear electrodes represent no change (<15%) in activity.

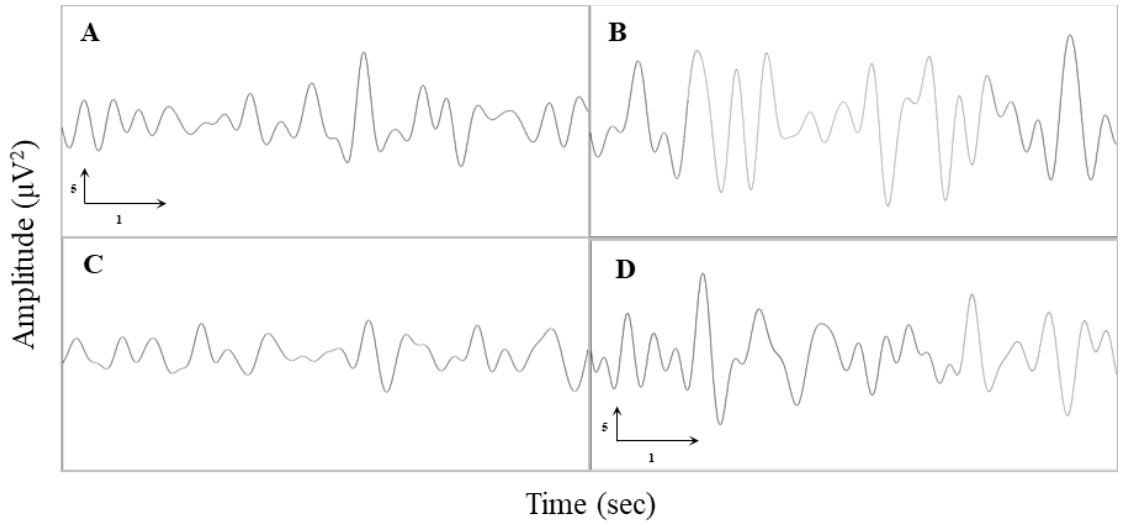

Figure 39: Absolute power of δ frequency across all groups. (A) A δ wave recorded from F3 electrode in a healthy control. (B) A δ wave recorded from F3 electrode in an opioid use disorder patient. (C) A δ wave recorded from F3 electrode in an alcohol use disorder patient. (D) A δ wave recorded from F3 electrode in a methamphetamine use disorder patient. Each panel displays 30 μV^2 on the vertical axis and 6 seconds on the horizontal axis.

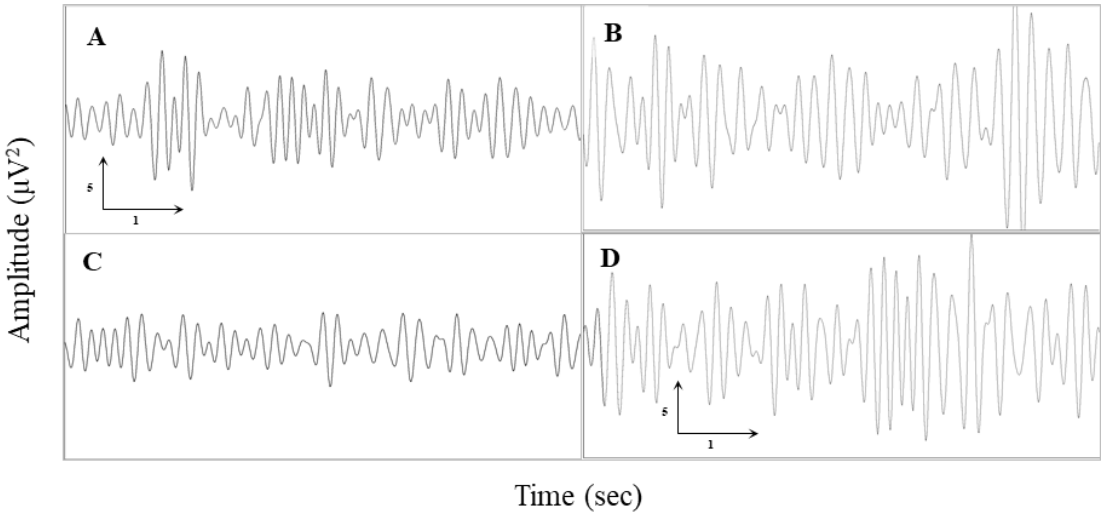

Figure 40: Absolute power of θ frequency across all groups. (A) A θ wave recorded from Cz electrode in a healthy control. (B) A θ wave recorded from Cz electrode in an opioid use disorder patient. (C) A θ wave recorded from Cz electrode in an alcohol use disorder patient. (D) A θ wave recorded from Cz electrode in a methamphetamine use disorder patient. Each panel displays 20 μV^2 on the vertical axis and 6 seconds on the horizontal axis.

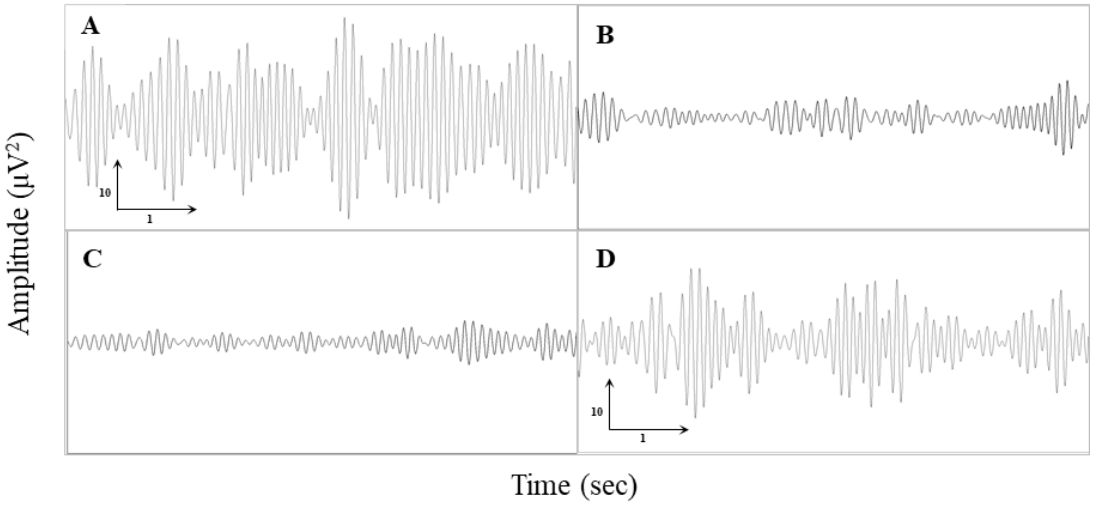

Figure 41: Absolute power of α frequency across all groups. (A) An α wave recorded from O2 electrode in a healthy control. (B) An α wave recorded from O2 electrode in an opioid use disorder patient. (C) An α wave recorded from O2 electrode in an alcohol use disorder patient. (D) An α wave recorded from O2 electrode in a methamphetamine use disorder patient. Each panel displays 40 μV^2 on the vertical axis and 6 seconds on the horizontal axis.

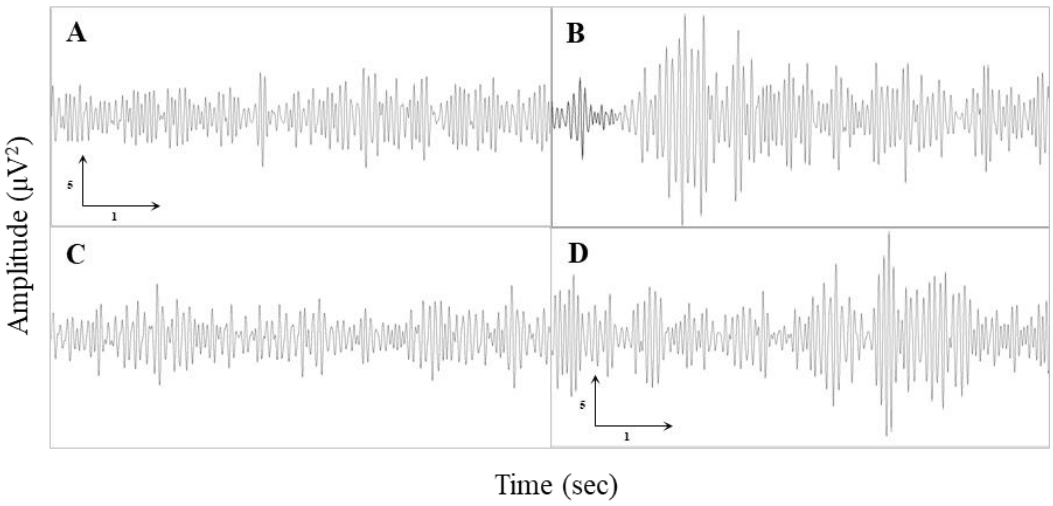

Figure 42: Absolute power of β frequency across all groups. (A) A β wave recorded from Fz electrode in a healthy control. (B) A β wave recorded from F4 electrode in an opioid use disorder patient. (C) A β wave recorded from F4 electrode in an alcohol use disorder patient. (D) A β wave recorded from F4 electrode in a methamphetamine use disorder patient. Each panel displays 20 μV^2 on the vertical axis and 6 seconds on the horizontal axis.

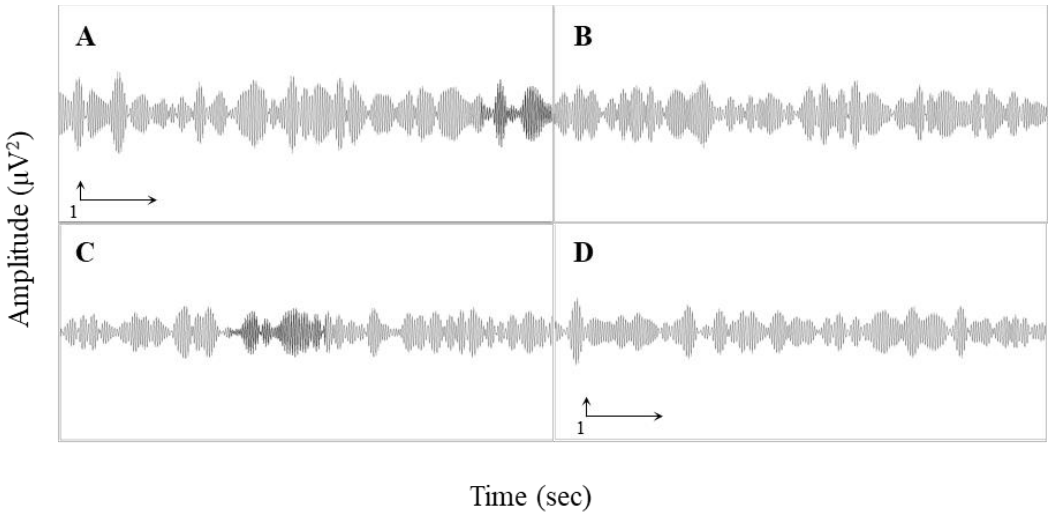

Figure 43: Absolute power of γ frequency across all groups. (A) A γ wave recorded from P4 electrode in a healthy control. (B) A γ wave recorded from C4 electrode in an opioid use disorder patient. (C) A γ wave recorded from C4 electrode in an alcohol use disorder patient. (D) A γ wave recorded from C4 electrode in a methamphetamine use disorder patient. Each panel displays 10 μV^2 on the vertical axis and 6 seconds on the horizontal axis.

4. Discussion and conclusion

The current study compared the eyes-closed resting state EEG power spectra of five major frequencies (δ, θ, α, β, and γ) in OUD against three separate groups, including MUD, AUD, and healthy controls. The overall goal was to determine how each frequency is altered during OUD, as well as whether the findings were attributed solely to OUD by validating the data against the other groups. To elaborate the implications of these comparisons, the distribution of absolute power in the healthy control group will be discussed first.

4.1 Power distribution in healthy controls

The first analysis conducted herein revealed the power distribution in healthy individuals as measured across 19 scalp electrodes. The electrodes were grouped as follows: frontal region (Fp1, Fp2, F3, F4, F7, F8, and Fz); central region (C3, C4, Cz, T3, and T4); and rear region (T5, T6, P3, P4, Pz, O1, and O2). As seen in Table 5, δ power was significantly larger in the frontal region as compared to the rear region. Apart from γ (no significant difference), the remaining frequencies (θ, α, and β) produced larger power in the rear region as compared to the frontal region. Excluding δ and γ, the central region in θ, α, and β frequencies produced power levels between the frontal and rear regions, displaying a gradual transition between the regions of the cortex.

The second analysis conducted was a comparison of the left and right hemispheres in the brain across five frequencies (δ, θ, α, β, and γ) across 16 electrodes as

measured at the scalp. The electrodes were grouped as follows: left (FP1, F3, F7, C3, T3, T5, P3, and O1) and right (Fp2, F4, F8, C4, T4, T6, P4, and O2). The midline electrodes (Fz, Cz, and Pz) were excluded in this analysis. As seen in Table 6, the left and right hemispheres produced the same power levels across each of the frequencies. This indicates the hemispheres are as equally active (or inactive, if you will) during the resting state and the recording apparatuses are of good quality.

Extracting the data from Table 5, it is apparent that the δ frequency was largest in the frontal lobes, while α frequency produced the largest power in the rear region (most notably the occipital lobes), which is comparable to previous studies (Acosta-Urquidi, 2015; Kim et al., 2017). The reason for the observed frequency power differences, may be due to the microcircuitry within each region of the brain. For example, the pyramidal cells in the frontal cortex appear to have more dendritic branching than their counterparts found in the occipital cortex (Elston, 2003). Additionally, the frontal cortex receives more deep brain connections from structures such as the hippocampus (Jin & Maren, 2015) and VTA (Buchta et al., 2017). Likewise, the occipital cortex receives more connections from the thalamus than other cortical regions (Sun et al., 2016).

Further, studies have revealed the functional roles of oscillations across cortical microcircuits. δ frequency may act globally across the cortex during slow-wave sleep (Vijayan et al., 2015) or regionally in the frontal cortex during motor activity (Liang et al., 2018). The θ band is also implicated with movement in the frontal cortex (Liang et al, 2018), as well as its role in memory processing in the frontal cortex (Khader & Rösler, 2011) and hippocampus (Klausberger et al., 2003). α frequency appears to be involved in nearly everything. In addition to its role in the occipital cortex with motor movement

(Liang et al., 2018), frontal α is involved with memory retrieval (Khader & Rösler, 2011), parietal α with memory retention (Von Stein & Sarnthein, 2000), and thalamic α with sleep (Vijayan et al., 2015). β frequency has long been known for its role in motor functions, occurring throughout the primary motor and primary somatosensory cortices (Romei et al., 2016; Espenhahn et al., 2019). γ frequency has been implicated in visual processing in the occipital cortex (Von Stein & Sarnthein, 2000) and memory processing in the hippocampus (Klausberger et al., 2003).

Interestingly, these frequencies appear in certain regions more so than others. For example, faster frequencies such as β and γ, interact locally more often than globally, whereas the slower frequencies, δ and θ, tend to interact long-range (Von Stein & Sarnthein, 2000; Canolty et al., 2010). Intuitively, this makes sense. Slower frequencies have longer wavelengths and faster frequencies have shorter wavelengths.

4.2 Advantages of the current study and diagnostic potential

Previous EEG power spectra studies on OUD have revealed mixed findings (see review by Ieong & Yuan, 2017). The present study sought to outline the power changes of OUD by using three comparative groups, including MUD, AUD, and healthy controls. Unlike previous studies, the setup and acquisition methods utilized in the current study were consistent with the standards set by the American Clinical Neurophysiology Society (ACNS; Sinha et al., 2016) and the International Federation of Clinical Neurophysiology (IFCN, Nuwer et al., 1998). Thus, the methods employed may serve as a template for future studies using resting-state EEG recordings for use with OUD.

Due to the clinical nature of these findings, EEG may be used for diagnostic evaluation of OUD. According to a survey study conducted by Wakeman and his team in

2016, primary care practitioners reported feeling "ill-prepared" to diagnose substance use disorders (such as OUD) and additionally felt they were not well trained to treat such disorders (Wakeman, Pham-Kanter, & Donelan, 2016). It has recently been estimated that nearly ¾ of all chronic pain relief opioid users may go undiagnosed for OUD, causing further strain on their physical health and financial well-being (Charumilind et al., 2018). In fact, the Council of Economic Advisers reported in 2017 that the OUD's Economic burden was estimated to be $500 billion in 2015 (CEA-US, 2017).

4.3 EEG power changes in opioid use disorder

Analyses across all 19 electrodes and the five frequencies, found interesting patterns of activity in OUD. The δ frequency was most significantly altered in OUD. Power increased in 14 of the 19 electrodes (74%) in this frequency. The θ frequency power was also significantly increased across 9 of the 19 electrodes (47%), with the frontal lobes being mostly affected. The β frequency power was also increased, but only significantly in 5 of the frontal electrodes (26% of total). Interestingly, α frequency power was reduced across the cortex, but only significantly in 3 rear electrodes (16% of the total). Although not significant, γ frequency displayed a pattern of increased power in the frontal lobes and reductions in the occipital lobes, with the remaining regions unaffected. The increases across the δ, θ, and β frequencies are consistent with some reports (Wang et al., 2015) but the decrease in α frequency is not. Likewise, the increases across the δ, θ, and β frequencies is not consistent with this report (Fingelkurts et al., 2008) but the decrease in α frequency is.

Due to the significant changes across most of the frequencies, EEG may be an effective tool for the evaluation of OUD in the clinical setting, especially when measuring cortical activity in the frontal region.

4.3 EEG power changes in methamphetamine use disorder

Analyses across all 19 electrodes and the five frequencies, found very little change in MUD. Although not significant, the δ, θ, and β frequencies revealed slight increases in power across the cortex, most notably in the frontal lobe. The α frequency power was reduced across the entire cortex, but only significantly in 3 frontal electrodes (16% of the total). Like OUD, γ frequency power appeared increased in the frontal regions but reduced in the rear regions, although only significant in 2 of the rear electrodes (11% of the total). The changes seen herein are in line with at least one report (Zannetti et al., 2018).

4.4 EEG power changes in alcohol use disorder

Our analyses across all 19 electrodes and the five frequencies, found significant changes in AUD. The activity across all frequencies appeared to be reduced globally. The δ frequency was reduced in 14 of the 19 electrodes (74%) and were distributed across most of the cortex. The θ frequency was reduced in 13 of the 19 electrodes (68%). These changes are in line with one report (Saletu-Zyhlarz et al., 2004). The α frequency power was the most significantly altered frequency, having large reductions across 17 of the 19 electrodes (89%), which is consistent with Courtney & Polich's work (2010). γ frequency power was significantly reduced in 8 of 19 electrodes (42%), mostly in the rear of the cortex. β frequency power revealed no change in activity across the cortex.

Given the significant alterations seen across the cortex in AUD, EEG may prove to be a sensitive tool for diagnostic purposes. Any of the slower frequencies (δ and θ) and especially α frequency, may yield promising results in terms of quantifying AUD.

4.5 Mechanisms underlying EEG power changes

When inspecting the differences seen across OUD, MUD, and AUD, it is abundantly clear that OUD and AUD have significantly altered cortical frequency power. MUD on the other hand, did not change much at all. The underlying microcircuit changes may be cause for the observed differences.

It is now generally accepted that the human brain contains approximately 100 billion neuronal cells throughout (Herculano-Houzel, 2009). Of these, GABAergic cells account for approximately 20% of the total neuronal population (Grillner & Graybiel, 2006; Hendry et al., 1987). Dopaminergic cells only account for <1% of the total neuronal population in the brain (Björklund & Dunnett, 2007; Schultz, 2007). Based on the mechanisms of action of each substance (opioid vs. alcohol vs. methamphetamine), it may be reasonable to conclude that opioids and alcohol produced significant changes due to the alterations of GABAergic cells in the brain. Methamphetamine primarily acts upon dopaminergic cells, thus the contribution to the EEG is less robust than the other substances herein.

Due to the above-noted power changes, chronic opioid use appears to affect the slower frequencies (δ and θ) more so than the other frequencies. In addition, the frontal cortex was most affected across several frequencies. When considering the EEG recordings were done during an "idling" state with participants fully awake, the observations do not appear to be related to motor functioning nor sleep. Taking this in

relation to the observed changes, this suggests long-range (ie., deep brain afferents) interactions to the uniquely structured frontal lobe are significantly altered in OUD. This increase in slow frequency power may be the representative signature of the preoccupation/anticipation stage of addiction (Koob & Volkow, 2016) brought on by intrinsic stimuli to opioids that are commonly referred to as "cravings" (Stewart et al., 2019).

4.6 Conclusion

To conclude, the study here revealed unique topographic distribution of power changes across five major frequency bands in OUD. Using MUD, AUD, and healthy controls as comparative groups, OUD revealed increases across several frequency bands, while MUD revealed almost no significant changes, and AUD revealed significant reductions across almost all frequencies. These changes can be attributed to the differences in underlying microcircuitry within each region of the brain, as well as due to the characteristic mechanisms of action by each substance of abuse.

Due to the non-invasive nature of EEG recording, relative ease of setup, and cost-effectiveness, the use of EEG in clinical diagnostic procedures for OUD may be of great societal benefit. Further, given the results obtained herein, EEG may be a great tool for diagnostics of AUD but not MUD. With the on-going opioid epidemic still plaguing the nation, new tools and ideas need to be implemented to help combat this debilitating disease.

References

Acosta-Urquidi, J. (2015). QEEG studies of the acute effects of the visionary tryptamine DMT. *Cosmos and History: The Journal of Natural and Social Philosophy, 11*(2), 115-129.

Al-Hasani, R., & Bruchas, M. R. (2011). Molecular mechanisms of opioid receptor-dependent signaling and behavior. *The Journal of the American Society of Anesthesiologists, 115*(6), 1363-1381.

American Psychiatric Association [APA]. (2013). *Diagnostic and statistical manual of mental disorders (DSM-5®)*. American Psychiatric Pub.

Angelopoulos E, Koutsoukos E, Maillis A, Papadimitriou GN, Stefanis C (2011). Cortical interactions during the experience of auditory verbal hallucinations. The Journal of neuropsychiatry and clinical neurosciences 23:287-293.

Askitopoulou, H., Ramoutsaki, I. A., & Konsolaki, E. (2002). Archaeological evidence on the use of opium in the Minoan world. In *International Congress Series* (Vol. 1242, pp. 23-29). Elsevier.

Assadi SM, Radgoodarzi R, Ahmadi-Abhari SA (2003). Baclofen for maintenance treatment of opioid dependence: a randomized double-blind placebo-controlled clinical trial [ISRCTN32121581]. BMC psychiatry 3:16.

Babiloni, C., Del Percio, C., Boccardi, M., Lizio, R., Lopez, S., Carducci, F., ... & Prestia, A. (2015). Occipital sources of resting-state alpha rhythms are related to

local gray matter density in subjects with amnesic mild cognitive impairment and Alzheimer's disease. Neurobiology of aging, 36(2), 556-570.

Bajo M, Madamba SG, Roberto M, Siggins GR (2014). Acute morphine alters GABAergic transmission in the central amygdala during naloxone-precipitated morphine withdrawal: role of cyclic AMP. Frontiers in integrative neuroscience 8:45.

Beaulieu, J. M., & Gainetdinov, R. R. (2011). The physiology, signaling, and pharmacology of dopamine receptors. *Pharmacological reviews*, *63*(1), 182-217.

Björklund, A., & Dunnett, S. B. (2007). Dopamine neuron systems in the brain: an update. *Trends in neurosciences*, *30*(5), 194-202.

Blackwell, J. M., & Geffen, M. N. (2017). Progress and challenges for understanding the function of cortical microcircuits in auditory processing. *Nature communications*, *8*(1), 2165.

Bonci A, Williams JT (1997). Increased probability of GABA release during withdrawal from morphine. The Journal of neuroscience: the official journal of the Society for Neuroscience 17:796-803.

Brooner, R. K., King, V. L., Kidorf, M., Schmidt, C. W., & Bigelow, G. E. (1997). Psychiatric and substance use comorbidity among treatment-seeking opioid abusers. *Archives of General psychiatry*, *54*(1), 71-80.

Buchta, W. C., Mahler, S. V., Harlan, B., Aston-Jones, G. S., & Riegel, A. C. (2017). Dopamine terminals from the ventral tegmental area gate intrinsic inhibition in the prefrontal cortex. *Physiological reports*, *5*(6), e13198.

Buzsaki G, Wang XJ (2012). Mechanisms of gamma oscillations. Annual review of neuroscience 35:203-225.

Cabrera, E. A., Wiers, C. E., Lindgren, E., Miller, G., Volkow, N. D., & Wang, G. J. (2016). Neuroimaging the effectiveness of substance use disorder treatments. *Journal of Neuroimmune Pharmacology*, *11*(3), 408-433.

Camprodon, J. A., & Stern, T. A. (2013). Selecting neuroimaging techniques: a review for the clinician. *The primary care companion for CNS disorders*, *15*(4).

Canolty, R. T., Ganguly, K., Kennerley, S. W., Cadieu, C. F., Koepsell, K., Wallis, J. D., & Carmena, J. M. (2010). Oscillatory phase coupling coordinates anatomically dispersed functional cell assemblies. *Proceedings of the National Academy of Sciences*, *107*(40), 17356-17361.

Charbogne, P., Gardon, O., Martín-García, E., Keyworth, H. L., Matsui, A., Mechling, A. E., ... & Darcq, E. (2017). Mu opioid receptors in gamma-aminobutyric acidergic forebrain neurons moderate motivation for heroin and palatable food. *Biological psychiatry*, *81*(9), 778-788.

Charumilind, S., Latkovic, T., Lewis, R., & Mendez-Escobar, E. (2018). Why we need bolder action to combat the opioid epidemic. In *Healthcare Systems and Services Practice*. McKinsey & Company.

Chavkin, C., & Koob, G. F. (2016). Dynorphin, dysphoria, and dependence: the stress of addiction. *Neuropsychopharmacology*, *41*(1), 373.

Chen X, Marrero HG, Murphy R, Lin YJ, Freedman JE (2000). Altered gating of opiate receptor-modulated K+ channels on amygdala neurons of morphine-dependent

rats. Proceedings of the National Academy of Sciences of the United States of America 97:14692-14696.

Connor, J. P., Gullo, M. J., White, A., & Kelly, A. B. (2014). Polysubstance use: diagnostic challenges, patterns of use and health. *Current opinion in psychiatry*, *27*(4), 269-275.

Council of Economic Advisers (CEA-US). (2017). *The underestimated cost of the opioid crisis*. Executive Office of the President of the United States, Council of Economic Advisers.

Courtney, K. E., & Polich, J. (2010). Binge drinking effects on EEG in young adult humans. *International journal of environmental research and public health*, *7*(5), 2325-2336.

Dascal, N., & Kahanovitch, U. (2015). The Roles of Gβγ and Gα in Gating and Regulation of GIRK Channels. In *International review of neurobiology* (Vol. 123, pp. 27-85). Academic Press.

Dildy-Mayfield, J. E., & Harris, R. A. (1995). Ethanol inhibits kainate responses of glutamate receptors expressed in Xenopus oocytes: role of calcium and protein kinase C. *Journal of Neuroscience*, *15*(4), 3162-3171.

Elston, G. N. (2003). Cortex, cognition and the cell: new insights into the pyramidal neuron and prefrontal function. *Cerebral Cortex*, *13*(11), 1124-1138.

Espenhahn, S., van Wijk, B. C., Rossiter, H. E., de Berker, A. O., Redman, N. D., Rondina, J., ... & Ward, N. S. (2019). Cortical beta oscillations are associated with motor performance following visuomotor learning. *NeuroImage*, *195*, 340-353.

Federici, M., Nisticò, R., Giustizieri, M., Bernardi, G., & Mercuri, N. B. (2009). Ethanol enhances GABAB-mediated inhibitory postsynaptic transmission on rat midbrain dopaminergic neurons by facilitating GIRK currents. *European Journal of Neuroscience*, *29*(7), 1369-1377.

Fingelkurts, A. A., Fingelkurts, A. A., Kivisaari, R., Autti, T., Borisov, S., Puuskari, V., ... & Kähkönen, S. (2007). Opioid withdrawal results in an increased local and remote functional connectivity at EEG alpha and beta frequency bands. *Neuroscience research*, *58*(1), 40-49.

Fingelkurts, A., Kähkönen, S., Fingelkurts, A., Kivisaari, R., Borisov, S., Puuskari, V., ... & Autti, T. (2008). Reorganization of the composition of brain oscillations and their temporal characteristics during opioid withdrawal. *Journal of Psychopharmacology*, *22*(3), 270-284.

Fleckenstein, A. E., & Hanson, G. R. (2003). Impact of psychostimulants on vesicular monoamine transporter function. *European journal of pharmacology*, *479*(1-3), 283-289.

Frisoni, P., Bacchio, E., Bilel, S., Talarico, A., Gaudio, R., Barbieri, M., ... & Marti, M. (2018). Novel Synthetic Opioids: The Pathologist's Point of View. *Brain sciences*, *8*(9), 170.

Frye, G. D., Taylor, L., Trzeciakowski, J. P., & Griffith, W. H. (1991). Effects of acute and chronic ethanol treatment on pre-and postsynaptic responses to baclofen in rat hippocampus. *Brain research*, *560*(1-2), 84-91.

Gatley, S. J., Volkow, N. D., Wang, G. J., Fowler, J. S., Logan, J., Ding, Y. S., & Gerasimov, M. (2005). PET imaging in clinical drug abuse research. *Current pharmaceutical design, 11*(25), 3203-3219.

Grillner, S., & Graybiel, A. M. (Eds.). (2006). *Microcircuits: the interface between neurons and global brain function* (Vol. 93). MIT Press.

Hari, R., & Parkkonen, L. (2015). The brain timewise: how timing shapes and supports brain function. *Phil. Trans. R. Soc. B*, 370(1668), 20140170.

Harquel, S., Bacle, T., Beynel, L., Marendaz, C., Chauvin, A., & David, O. (2016). Mapping dynamical properties of cortical microcircuits using robotized TMS and EEG: Towards functional cytoarchitectonics. *Neuroimage, 135*, 115-124.

Hedegaard, H., Warner, M., & Miniño, A. M. (2018). *Drug overdose deaths in the United States, 1999-2017* (pp. 1-8). US Department of Health and Human Services, Centers for Disease Control and Prevention, National Center for Health Statistics.

Hendry, S. H., Schwark, H. D., Jones, E. G., & Yan, J. (1987). Numbers and proportions of GABA-immunoreactive neurons in different areas of monkey cerebral cortex. *Journal of Neuroscience, 7*(5), 1503-1519.

Herculano-Houzel, S. (2009). The human brain in numbers: a linearly scaled-up primate brain. *Frontiers in human neuroscience, 3*, 31.

Heshmati, M., & Russo, S. J. (2015). Anhedonia and the brain reward circuitry in depression. *Current behavioral neuroscience reports*, *2*(3), 146-153.

Ieong, H. F. H., & Yuan, Z. (2017). Resting-state neuroimaging and neuropsychological findings in opioid use disorder during abstinence: a review. *Frontiers in human neuroscience*, *11*, 169.

Jackson, D. M., & Westlind-Danielsson, A. (1994). Dopamine receptors: molecular biology, biochemistry and behavioural aspects. *Pharmacology & therapeutics*, *64*(2), 291-370.

Jalabert, M., Bourdy, R., Courtin, J., Veinante, P., Manzoni, O. J., Barrot, M., & Georges, F. (2011). Neuronal circuits underlying acute morphine action on dopamine neurons. *Proceedings of the National Academy of Sciences*, *108*(39), 16446-16450.

Jang, H. S., Kim, J. Y., Kim, S. H., & Lee, M. G. (2009). Role of dopamine receptors on electroencephalographic changes produced by repetitive apomorphine treatments in rats. *The Korean Journal of Physiology & Pharmacology*, *13*(3), 147-151.

Jiang, X., Shen, S., Cadwell, C. R., Berens, P., Sinz, F., Ecker, A. S., ... & Tolias, A. S. (2015). Principles of connectivity among morphologically defined cell types in adult neocortex. *Science*, *350*(6264), aac9462.

Jin, J., & Maren, S. (2015). Prefrontal-hippocampal interactions in memory and emotion. *Frontiers in systems neuroscience*, *9*, 170.

Johanson, C. E., Frey, K. A., Lundahl, L. H., Keenan, P., Lockhart, N., Roll, J., ... & Schuster, C. R. (2006). Cognitive function and nigrostriatal markers in abstinent methamphetamine abusers. *Psychopharmacology*, *185*(3), 327-338.

Johnson, S. W., & North, R. A. (1992). Opioids excite dopamine neurons by hyperpolarization of local interneurons. *Journal of neuroscience*, *12*(2), 483-488.

Jones, M. R., Viswanath, O., Peck, J., Kaye, A. D., Gill, J. S., & Simopoulos, T. T. (2018). A brief history of the opioid epidemic and strategies for pain medicine. *Pain and therapy*, *7*, 13-21.

Jones, S. R., Gainetdinov, R. R., Wightman, R. M., & Caron, M. G. (1998). Mechanisms of amphetamine action revealed in mice lacking the dopamine transporter. *Journal of Neuroscience*, *18*(6), 1979-1986.

Karila, L., Marillier, M., Chaumette, B., Billieux, J., Nicolas, F., & Amine, B. (2018). New synthetic opioids: Part of a new addiction landscape. *Neuroscience & Biobehavioral Reviews*.

Kepecs, A., & Fishell, G. (2014). Interneuron cell types are fit to function. *Nature*, *505*(7483), 318.

Khader, P. H., & Rösler, F. (2011). EEG power changes reflect distinct mechanisms during long-term memory retrieval. *Psychophysiology*, *48*(3), 362-369.

Kim, M., Sowndhararajan, K., Kim, T., Kim, J., Yang, J., & Kim, S. (2017). Gender differences in electroencephalographic activity in response to the earthy odorants geosmin and 2-methylisoborneol. *Applied Sciences*, *7*(9), 876.

Klausberger, T., Magill, P. J., Márton, L. F., Roberts, J. D. B., Cobden, P. M., Buzsáki, G., & Somogyi, P. (2003). Brain-state-and cell-type-specific firing of hippocampal interneurons in vivo. *Nature*, *421*(6925), 844.

Ko, H., Cossell, L., Baragli, C., Antolik, J., Clopath, C., Hofer, S. B., & Mrsic-Flogel, T. D. (2013). The emergence of functional microcircuits in visual cortex. *Nature*, *496*(7443), 96.

Koob, G. F., & Volkow, N. D. (2010). Neurocircuitry of addiction. *Neuropsychopharmacology*, *35*(1), 217.

Koob, G. F., & Volkow, N. D. (2016). Neurobiology of addiction: a neurocircuitry analysis. *The Lancet Psychiatry*, *3*(8), 760-773.

Kvitsiani, D., Ranade, S., Hangya, B., Taniguchi, H., Huang, J. Z., & Kepecs, A. (2013). Distinct behavioural and network correlates of two interneuron types in prefrontal cortex. *Nature*, *498*(7454), 363.

Lay, J., Carbone, S. E., DiCello, J. J., Bunnett, N. W., Canals, M., & Poole, D. P. (2016). Distribution and trafficking of the μ-opioid receptor in enteric neurons of the guinea pig. *American Journal of Physiology-Gastrointestinal and Liver Physiology*, *311*(2), G252-G266.

Lewohl, J. M., Crane, D. I., & Dodd, P. R. (1997). Expression of the α1, α2 and α3 isoforms of the GABAA receptor in human alcoholic brain. *Brain research*, *751*(1), 102-112.

Levashova, A. I., & Myagkova, M. A. (2018). Mechanism of action of anti-opioid peptides at pain syndrome. *Russian Chemical Bulletin*, *67*(4), 624-635.

Liang, M., Starrett, M. J., & Ekstrom, A. D. (2018). Dissociation of frontal-midline delta-theta and posterior alpha oscillations: A mobile EEG study. *Psychophysiology*, *55*(9), e13090.

Lobo, I. A., & Harris, R. A. (2008). GABAA receptors and alcohol. *Pharmacology Biochemistry and Behavior*, *90*(1), 90-94.

Lud Cadet, J., Jayanthi, S., T McCoy, M., Beauvais, G., & Sheng Cai, N. (2010). Dopamine D1 receptors, regulation of gene expression in the brain, and neurodegeneration. *CNS & Neurological Disorders-Drug Targets (Formerly Current Drug Targets-CNS & Neurological Disorders)*, *9*(5), 526-538.

Madhavan, A., Bonci, A., & Whistler, J. L. (2010). Opioid-Induced GABA potentiation after chronic morphine attenuates the rewarding effects of opioids in the ventral tegmental area. *Journal of Neuroscience, 30*(42), 14029-14035.

Markram, H., Toledo-Rodriguez, M., Wang, Y., Gupta, A., Silberberg, G., & Wu, C. (2004). Interneurons of the neocortical inhibitory system. *Nature reviews neuroscience, 5*(10), 793.

McCann, U. D., Kuwabara, H., Kumar, A., Palermo, M., Abbey, R., Brasic, J., ... & Ricaurte, G. A. (2008). Persistent cognitive and dopamine transporter deficits in abstinent methamphetamine users. *Synapse*, *62*(2), 91-100.

Meldrum, M. L. (2016). The ongoing opioid prescription epidemic: historical context. *American Journal of Public Health*, *106*(8), 1365.

Mena, J. C., Cuellar, H., Vargas, D., & Riascos, R. (2005). PET and SPECT in drug and substance abuse. *Topics in Magnetic Resonance Imaging*, *16*(3), 253-256.

Meunier, J. C., Mollereau, C., Toll, L., Suaudeau, C., Moisand, C., Alvinerie, P., ... & Mazarguil, H. (1995). Isolation and structure of the endogenous agonist of opioid receptor-like ORL1 receptor. *Nature*, *377*(6549), 532.

Motlagh, F., Ibrahim, F., Rashid, R., Shafiabady, N., Seghatoleslam, T., Habil, H. (2018). Acute effects of methadone on EEG power spectrum and event-related potentials among heroin dependents. *Psychopharmacology 235*:3273-3288.

Münch, M., Knoblauch, V., Blatter, K., Schröder, C., Schnitzler, C., Kräuchi, K., ... & Cajochen, C. (2004). The frontal predominance in human EEG delta activity after sleep loss decreases with age. *European Journal of Neuroscience*, *20*(5), 1402-1410.

National Institute on Drug Abuse [NIDA]. (2019, January 22). *Opioid Overdose Crisis*. Retrieved from https://www.drugabuse.gov/drugs-abuse/opioids/opioid-overdose-crisis

Nelson, S. B. (2002). Cortical microcircuits. *Neuron, 36*(1), 19-27.

Newton, T. F., Cook, I. A., Kalechstein, A. D., Duran, S., Monroy, F., Ling, W., & Leuchter, A. F. (2003). Quantitative EEG abnormalities in recently abstinent methamphetamine dependent individuals. *Clinical Neurophysiology*, *114*(3), 410-415.

Nuwer, M. R., Comi, G., Emerson, R., Fuglsang-Frederiksen, A., Guérit, J. M., Hinrichs, H., ... & Rappelsburger, P. (1998). IFCN standards for digital recording of clinical EEG. *Electroencephalography and clinical Neurophysiology*, *106*(3), 259-261.

Park, S. W., Shen, X., Tien, L. T., Roman, R., & Ma, T. (2011). Methamphetamine-induced changes in the striatal dopamine pathway in μ-opioid receptor knockout mice. *Journal of biomedical science, 18*(1), 83.

Patestas, M. A., & Gartner, L. P. (2016). *A Textbook of Neuroanatomy* (2nd ed.). Hoboken, NJ: Wiley-Blackwell.

Peng, J., Sarkar, S., & Chang, S. L. (2012). Opioid receptor expression in human brain and peripheral tissues using absolute quantitative real-time RT-PCR. *Drug and alcohol dependence*, *124*(3), 223-228.

Pfeffer, C. K., Xue, M., He, M., Huang, Z. J., & Scanziani, M. (2013). Inhibition of inhibition in visual cortex: the logic of connections between molecularly distinct interneurons. *Nature neuroscience*, *16*(8), 1068.

Pifl, C., Drobny, H., Reither, H., Hornykiewicz, O., & Singer, E. A. (1995). Mechanism of the dopamine-releasing actions of amphetamine and cocaine: plasmalemmal dopamine transporter versus vesicular monoamine transporter. *Molecular Pharmacology*, *47*(2), 368-373.

Pradhan, A. A., Befort, K., Nozaki, C., Gavériaux-Ruff, C., & Kieffer, B. L. (2011). The delta opioid receptor: an evolving target for the treatment of brain disorders. *Trends in pharmacological sciences*, *32*(10), 581-590.

Purves, D., Augustine, G. J., & Fitzpatrick, D. (2001). *Neuroscience* (2nd ed.). Sunderland, MA: Sinauer Associates, Inc.

Qiang, M., & Ticku, M. K. (2005). Role of AP-1 in ethanol-induced N-methyl-d-aspartate receptor 2B subunit gene up-regulation in mouse cortical neurons. *Journal of neurochemistry*, *95*(5), 1332-1341.

Radke, A. K., Jury, N. J., Delpire, E., Nakazawa, K., & Holmes, A. (2017). Reduced ethanol drinking following selective cortical interneuron deletion of the GluN2B NMDA receptors subunit. *Alcohol*, *58*, 47-51.

Rangaswamy, M., Porjesz, B., Chorlian, D. B., Wang, K., Jones, K. A., Bauer, L. O., ... & Begleiter, H. (2002). Beta power in the EEG of alcoholics. *Biological psychiatry*, *52*(8), 831-842.

Reinscheid, R. K., Nothacker, H. P., Bourson, A., Ardati, A., Henningsen, R. A., Bunzow, J. R., ... & Civelli, O. (1995). Orphanin FQ: a neuropeptide that activates an opioidlike G protein-coupled receptor. *Science*, *270*(5237), 792-794.

Rexed, B. (1954). A cytoarchitectonic atlas of the spinal cord in the cat. *Journal of comparative neurology*, *100*(2), 297-379.

Romei, V., Bauer, M., Brooks, J. L., Economides, M., Penny, W., Thut, G., ... & Bestmann, S. (2016). Causal evidence that intrinsic beta-frequency is relevant for enhanced signal propagation in the motor system as shown through rhythmic TMS. *Neuroimage*, *126*, 120-130.

Rosenblatt, R. A., Andrilla, C. H. A., Catlin, M., & Larson, E. H. (2015). Geographic and specialty distribution of US physicians trained to treat opioid use disorder. *The Annals of Family Medicine*, *13*(1), 23-26.

Rosenblum, A., Marsch, L. A., Joseph, H., & Portenoy, R. K. (2008). Opioids and the treatment of chronic pain: controversies, current status, and future directions. *Experimental and clinical psychopharmacology*, *16*(5), 405.

Rothblat, D. S., Rubin, E., & Schneider, J. S. (2001). Effects of chronic alcohol ingestion on the mesostriatal dopamine system in the rat. *Neuroscience letters*, *300*(2), 63-66.

Russo, S. J., & Nestler, E. J. (2013). The brain reward circuitry in mood disorders. *Nature Reviews Neuroscience*, *14*(9), 609.

Saletu-Zyhlarz, G. M., Arnold, O., Anderer, P., Oberndorfer, S., Walter, H., Lesch, O. M., ... & Saletu, B. (2004). Differences in brain function between relapsing and abstaining alcohol-dependent patients, evaluated by EEG mapping. *Alcohol and Alcoholism*, *39*(3), 233-240.

Substance Abuse and Mental Health Services Administration [SAMHSA]. (2019). *Key Substance Use and Mental Health Indicators in the United States: Results from the 2016 National Survey on Drug Use and Health* (HHS Publication No. SMA 17-5044, NSDUH Series H-5052). Rockville, MD: Center for Behavioral Health

Statistics and Quality, Substance Abuse and Mental Health Services Administration.

Schultz, W. (2007). Multiple dopamine functions at different time courses. *Annu. Rev. Neurosci.*, *30*, 259-288.

Sekine, Y., Ouchi, Y., Sugihara, G., Takei, N., Yoshikawa, E., Nakamura, K., ... & Kawai, M. (2008). Methamphetamine causes microglial activation in the brains of human abusers. *Journal of Neuroscience*, *28*(22), 5756-5761.

Sinha, S. R., Sullivan, L. R., Sabau, D., Orta, D. S. J., Dombrowski, K. E., Halford, J. J., ... & Stecker, M. M. (2016). American clinical neurophysiology society guideline 1: minimum technical requirements for performing clinical electroencephalography. *The Neurodiagnostic Journal*, *56*(4), 235-244.

Stewart, J. L., May, A. C., Aupperle, R. L., & Bodurka, J. (2019). Forging neuroimaging targets for recovery in opioid use disorder. *Frontiers in psychiatry*, *10*, 117.

Sulzer, D., Sonders, M. S., Poulsen, N. W., & Galli, A. (2005). Mechanisms of neurotransmitter release by amphetamines: a review. *Progress in neurobiology*, *75*(6), 406-433.

Sun, W., Tan, Z., Mensh, B. D., & Ji, N. (2016). Thalamus provides layer 4 of primary visual cortex with orientation-and direction-tuned inputs. *Nature neuroscience*, *19*(2), 308.

Tatum IV, W. O. (2014). Handbook of EEG interpretation. Demos Medical Publishing.

Thatcher, R. W. (2010). Validity and reliability of quantitative electroencephalography. *Journal of Neurotherapy*, *14*(2), 122-152.

Thompson, M., & Thompson, L. (2015). *The neurofeedback book*. Wheat Ridge, CO: Association for Applied Psychophysiology and Biofeedback.

Toscani, M., Marzi, T., Righi, S., Viggiano, M. P., & Baldassi, S. (2010). Alpha waves: a neural signature of visual suppression. *Experimental brain research*, *207*(3-4), 213-219.

Vallone, D., Picetti, R., & Borrelli, E. (2000). Structure and function of dopamine receptors. *Neuroscience & biobehavioral reviews*, *24*(1), 125-132.

Vardanyan, R. S., & Hruby, V. J. (2014). Fentanyl-related compounds and derivatives: current status and future prospects for pharmaceutical applications. *Future medicinal chemistry*, *6*(4), 385-412.

Vegue, M., Perin, R., & Roxin, A. (2017). On the structure of cortical micro-circuits inferred from small sample sizes. *Journal of Neuroscience*, 0984-17.

Vijayan, S., Klerman, E. B., Adler, G. K., & Kopell, N. J. (2015). Thalamic mechanisms underlying alpha-delta sleep with implications for fibromyalgia. *Journal of neurophysiology*, *114*(3), 1923-1930.

Volkow, N. D., Chang, L., Wang, G. J., Fowler, J. S., Franceschi, D., Sedler, M., ... & Logan, J. (2001). Loss of dopamine transporters in methamphetamine abusers recovers with protracted abstinence. *Journal of Neuroscience*, *21*(23), 9414-9418.

Volkow, N. D., Wang, G. J., Telang, F., Fowler, J. S., Logan, J., Jayne, M., ... & Wong, C. (2007). Profound decreases in dopamine release in striatum in detoxified alcoholics: possible orbitofrontal involvement. *Journal of Neuroscience*, *27*(46), 12700-12706.

Von Stein, A., & Sarnthein, J. (2000). Different frequencies for different scales of cortical integration: from local gamma to long range alpha/theta synchronization. *International journal of psychophysiology*, *38*(3), 301-313.

Wakeman, S. E., Pham-Kanter, G., & Donelan, K. (2016). Attitudes, practices, and preparedness to care for patients with substance use disorder: results from a survey of general internists. *Substance abuse*, *37*(4), 635-641.

Wang, G. Y., Kydd, R., Wouldes, T. A., Jensen, M., & Russell, B. R. (2015). Changes in resting EEG following methadone treatment in opiate addicts. *Clinical Neurophysiology*, *126*(5), 943-950.

Yang, G. R., Murray, J. D., & Wang, X. J. (2016). A dendritic disinhibitory circuit mechanism for pathway-specific gating. *Nature communications*, *7*, 12815.

Zanettini, C., Scaglione, A., Keighron, J. D., Giancola, J. B., Lin, S. C., Newman, A. H., & Tanda, G. (2018). Pharmacological classification of centrally acting drugs using EEG in freely moving rats: An old tool to identify new atypical dopamine uptake inhibitors. *Neuropharmacology*.